

# Durham E-Theses

---

## *Protein Crystallisation using Microemulsions*

FRENCH, JANET,ELIZABETH

---

### How to cite:

FRENCH, JANET,ELIZABETH (2013) *Protein Crystallisation using Microemulsions*, Durham theses, Durham University. Available at Durham E-Theses Online: <http://etheses.dur.ac.uk/8454/>

---

### Use policy

The full-text may be used and/or reproduced, and given to third parties in any format or medium, without prior permission or charge, for personal research or study, educational, or not-for-profit purposes provided that:

- a full bibliographic reference is made to the original source
- a [link](#) is made to the metadata record in Durham E-Theses
- the full-text is not changed in any way

The full-text must not be sold in any format or medium without the formal permission of the copyright holders.

Please consult the [full Durham E-Theses policy](#) for further details.



# Protein Crystallisation using Microemulsions

Author: Janet French

Thesis for Postgraduate Master of Science by Research

Chemistry Department

Supervisors: Dr Sharon Cooper and Dr Ehmke Pohl

2011-2012

## *Acknowledgements*

Primarily, my thanks and appreciation goes to my supervisors, Dr Sharon Copper and Dr Ehmke Pohl. It has been thoroughly enjoyable and an honour to partake in this MSc under your excellent guidance and support.

Thank you to Dr Steven Cobb and members of his research group, Sam Lear and Alex Hudson, for providing compounds for chemical crystallisation.

For their training on equipment, support and expert advice, I would like to thank Helen Riggs, Dr Olga Chetina, Natalie Tatum and Ian Edwards.

Thank you to members of Dr Sharon Cooper and Dr Ehmke Pohl's research groups, with particular mention to Cen Chen, Natasha Loines, Dr Catherine Nicholson and Helen Ramsey. Your friendship, endless cups of tea and cake, and encouragement is truly valued.

Finally, I must thank my family, friends and fiancé for keeping me going.

*"The copyright of this thesis rests with the author. No quotation from it should be published without the author's prior written consent and information derived from it should be acknowledged."*

# *Abstract*

X-ray crystallography is the most powerful technique for structural determination of proteins, a vital research tool, enabling insight at the atomic level, of the three dimensional structure of key protein receptors for potential drug compounds. To be successful, single, high quality crystals of the compound in question are required. Current methods to produce crystals involve frustratingly long timescales, extensive trial and error using large amounts of material, and have no guarantee of success. Polymorphic compounds add another level of frustration, requiring the thermodynamic control of crystallisation in order to overcome Ostwald's rule of stages, which considers crystallisation from bulk solution to be under kinetic control with metastable polymorphs often crystallising initially. These factors have led to what is currently referred to as the "bottle-neck" of protein crystallisation, an acute problem<sup>1</sup> motivating the rapid development of protein crystallisation techniques<sup>2</sup>.

This thesis aims to alleviate the bottle-neck found in protein crystallisation by exploring protein crystallisation using microemulsions; a technique, which until now, has only been successfully applied to the thermodynamic control of crystallisation for small compounds, such as 5-methyl-2-[(2-nitrophenyl)amino]-3-thiophenecarbonitrile (commonly known as ROY)<sup>3</sup> and glycine<sup>4</sup>. Through the application of several different surfactant systems for the crystallisation of model protein, Lysozyme, this thesis explores the use of microemulsions with the aim of producing high quality single crystals suitable for X-ray diffraction experiments.

Numerous, large, high quality, single crystals of Lysozyme were successfully grown using a TritonX-100/1-hexanol surfactant system in which an anti-solvent, mixed microemulsion method was applied. Small angle X-ray scattering (SAXS) was effectively used to confirm formation of microemulsions and led to the determination of droplet sizes using generalised indirect Fourier Transform (GIFT) analysis. X-ray diffraction experiments showed single crystals grown from microemulsions to have a high internal order, with the resultant data sets of a publishable quality and of a comparative quality to data sets collected from crystals grown using standard vapour diffusion crystallisation techniques.

This thesis demonstrates, for the first time, that microemulsions can be successfully used to produce high quality, single crystals of the protein, Lysozyme, shining light on this novel technique as a potential means of relieving the bottle-neck of protein crystallisation. Future directions of this work include exploring the robustness of the microemulsion

crystallisation technique with other proteins such as insulin, glucose isomerase and albumin. Expanding this novel technique to the crystallisation of membrane proteins may be initially explored through the crystallisation of a 25 residue, membrane spanning part of the M2 protein of the influenza virus. This would provide an interesting starting point due to the proteins' biological importance as a target of anti-influenza drugs.

# Contents

	<b>Page</b>
<b>Chapter One Introduction</b>	<b>1</b>
<b>Chapter Two Background</b>	<b>4</b>
2.1 Surfactants	4
2.1.1 Classification	5
2.1.2 Interfacial Tension	6
2.1.3 Properties: Efficiency and Effectiveness	6
2.1.4 Micellisation	7
2.1.5 The Krafft Point	10
2.1.6 The Cloud Point	11
2.2 Emulsions	12
2.2.1 Hydrophilic-lipophilic Balance (HLB)	14
2.2.2 Phase Inversion Temperature (PIT)	15
2.2.3 Nano-emulsions	16
2.2.4 Microemulsions	17
2.2.5 Microemulsions: Microstructure and Classification	18
2.2.6 Co-surfactant	19
2.2.7 Surfactant Film Spontaneous Curvature	20
2.2.8 Bending Elasticity of the Surfactant Film	21
2.2.9 Phase Behaviour	21
2.2.10 Microemulsions: Droplet Polydispersity	23
2.2.11 Applications of Microemulsions	24
2.3 Crystallisation	24
2.3.1 Nucleation and Supersaturation	25
2.3.2 Homogeneous Nucleation	26
2.3.3 Heterogeneous Nucleation	27
2.3.4 Chemical Crystallisation	29
2.3.5 Protein Crystallisation	30
2.3.6 Vapour Diffusion methods	30
2.3.7 Batch Methods	33
2.3.8 Polymorphism	33
2.3.9 The Microemulsion Method: Thermodynamic Control of Crystallisation	34
2.3.10 Lysozyme: A model Protein for Crystallisation Studies	37
2.3.11 Membrane Proteins: A Crystallisation Challenge	38
2.4 X-ray Crystallography	40
2.4.1 Crystal Structure	41
2.4.2 The Reciprocal Lattice	42
2.4.3 Miller Indices	42
2.4.4 X-ray Scattering	44
2.4.5 The Phase Problem	45
2.4.6 Small Angle X-ray Scattering (SAXS)	46
<b>Chapter Three Experimental Methods</b>	<b>48</b>
3.1 Chemical Crystallisation	48
3.1.1 Initial Solubility Screens	48
3.1.2 Crystallisation by Evaporation	49
3.1.3 Crystallisation by Liquid Diffusion	49
3.1.4 Crystallisation by Vapour Diffusion	50

3.1.5	Selecting and Harvesting a Crystal	51
3.2	Protein Crystallisation	51
3.2.1	Preparation of Hanging Drop Vapour Diffusion Trays	52
3.2.2	Microemulsion Preparation	52
3.2.2.1	Phase Diagrams	53
3.2.2.2	Ionic Surfactant Systems	54
3.2.2.3	Non-ionic Surfactant Systems	55
3.2.2.4	Methods for Further Facilitating Crystallisation in Microemulsions	55
3.3	Microemulsion Droplet Size Determination	57
3.3.1	Geometric Calculations	57
3.3.2	X-ray Scattering Experiments for Microemulsions: SAXS	57
3.3.3	Generalised Indirect Fourier Transform (GIFT)	58
3.4	Optical Microscopy	59
3.5	X-ray Diffraction Experiments for Single Crystals: X-ray Crystallography	60
3.5.1	Harvesting a Crystal	60
3.5.2	Screening a Crystal	61
3.5.3	Data Collection and Processing	63
<b>Chapter</b>	<b>Results</b>	64
<b>Four</b>		
4.1	Chemical Crystallisation	64
4.1.1	Crystallisation of ASH89	64
4.1.2	Crystallisation of ASH81/87	66
4.1.3	Crystallisation of ASH82	68
4.1.4	Crystallisation of ASH90	68
4.1.5	Crystallisation of ASH93	69
4.1.6	Crystallisation of ASH91	69
4.1.7	Crystallisation of ASH59	70
4.1.8	Crystallisation of GDL02, GDL38 and GDL39	70
4.2	Proteins Crystallisation from Hanging Drop Vapour Diffusion Trays	71
4.3	Bulk Anti-solvent Experiments	73
4.4	Protein Crystallisation from Microemulsions	74
4.4.1	AOT Surfactant System	74
4.4.2	AOT Surfactant System: SAXS/GIFT Analysis	78
4.4.3	Span80/Brij30 Surfactant System	79
4.4.4	Span80/Tween80 Surfactant System	80
4.4.5	TX-100/1-hexanol and TX-114 Surfactant Systems: Phase Diagrams	83
4.4.6	TritonX-114 Surfactant System	86
4.4.7	TritonX-100/1-hexanol Surfactant System	86
4.4.8	TritonX-100/1-hexanol Surfactant System: Mixed Microemulsions	88
4.5	TritonX-100/1-hexanol Surfactant System: Droplet Size Analysis	94
4.5.1	Varying Lysozyme Concentration in Single Microemulsions	94
4.5.2	Varying Composition Ratio of Single Anti-solvent Microemulsions	96
4.5.3	Droplet Sizes of Mixed Microemulsions	99
4.6	Single Crystal X-ray Diffraction Experiments	103
<b>Chapter Five</b>	<b>Conclusions</b>	108
<b>Appendix</b>		112
A1	Crystallisation Conditions for Different Crystal Forms of Lysozyme and Lysozyme Nitrate	112
A2	Preparation of Compounds Subjected to Chemical Crystallisation	114
<b>References</b>		115

## *List of Abbreviations*

% (wt)	Percentage by mass
2D	Two Dimensional
3D	Three Dimensional
AOT	Dioctyl sulfosuccinate sodium salt
API	active pharmaceutical ingredient
Brij30	Dodecyl tetraethylene glycol ether
CMC	Critical Micelle Concentration
CSD	Cambridge Structural Database
CTAB	Hexadecyltrimethylammonium bromide
DMSO	Dimethyl sulfoxide
DNA	Deoxyribonucleic acid
EMIGEN	N,N-Dimethyl-N-dodecylglycine betaine
FT	Fourier Transform
GEWL	Guinea Fowl egg-white Lysozyme
GIFT	General indirect fourier transform
GPCR	G-Protein Coupled Receptors
HEWL	Hen egg-white Lysozyme
HLB	Hydrophilic-lipophilic balance
LCP	Lipidic cubic phase
LSP	Lipidic sponge phase
mRNA	Messenger ribonucleic acid
NaAc	Sodium Acetate
NaCl	Sodium Chloride
o/w	Oil-in-water
PDB	Protein Data Bank
PEG	Polyethylene glycol
PGSE-NMR	pulsed gradient spin-echo nuclear magnetic resonance
PIT	Phase Inversion Temperature
ROY	5-methyl-2-[(2-nitrophenyl) amino]-3-thiophenecarbonitrile
SAXS	Small Angle X-ray Scattering
SGC	Structural Genomics Consortium
SNR	Signal to noise ratio
Span80	Sorbitane monooleate
Surfactant	Surface Active Agent
TEWL	Turkey egg-white Lysozyme
TritonX-100 or TX-100	<i>t</i> -Octylphenoxypolyethoxyethanol
TritonX-114 or TX-114	Polyethylene glycol <i>tert</i> -octylphenyl ether
tRNA	transfer ribonucleic acid
Tween80	polyoxyethylenesorbitan monooleate
V/V	volume/volume percentage
w/o	water-in-oil
w/V	weight/volume percentage
w/w	weight/weight percentage



## *List of Figures*

Figure	Page
2.1 Chemical Structure of Span80	4
2.2 Plot showing how conductivity of a solution changes with surfactant concentration.	8
2.3 Shapes of surfactant aggregates	9
2.4 Changes in the solubility and the CMC as temperature is increased	11
2.5 The physical appearance of macro-emulsions, nano-emulsions and microemulsions	12
2.6 Schematic of mechanisms of emulsion degradation	13
2.7 The effect of temperature, oil polarity and electrolyte concentration on the PIT	15
2.8 Schematic of Winsor classification of microemulsions	18
2.9 Schematic defining spontaneous curvature of a surfactant film	20
2.10 Phase diagrams	23
2.11 Crystallisation phase diagram	26
2.12 Schematic of heterogeneous nucleation of a liquid droplet on a smooth, structureless substrate	28
2.13 Schematic of chemical crystallisation methods	29
2.14 Schematic of vapour diffusion, protein crystallisation methods	31
2.15 Crystallisation phase diagram highlighting nucleation and crystal growth	32
2.16 Schematic of batch crystallisation method	33
2.17 Helmholtz free energy plots	35
2.18 Schematic of transient dimmer formation between microemulsion droplets	37
2.19 Schematic of a unit cell	41
2.20 Schematic of regularly arranged crystal lattice points	43
2.21 Schematic of Miller Indices assignment	43
2.22 Scattering diagram	44
2.23 Schematic of Bragg's Law	45
3.1 Ternary phase diagram	53
3.2 Single crystal mounted and centred on goniometer	61
3.3 Diffraction image	62
4.1 Clusters of ASH89 crystals	64
4.2 Separated cluster of Ash89 crystals	65
4.3 Cluster of ASH81/87 crystals	67
4.4 Isolate needle ASH81/87 crystal	67
4.5 Multiple crystallisation events in one hanging drop	72
4.6 Single crystal grown from hanging drop vapour diffusion tray	73
4.7 Ternary phase diagram for AOT surfactant system	75
4.8 $I(q)$ against $q$ plot for microemulsion of the AOT surfactant system	78
4.9 Pair distribution plot for microemulsions of the AOT surfactant system	79
4.10 Pseudo ternary phase diagram for Span80/Tween80 surfactant system	81
4.11 Pseudo ternary phase diagrams for TX-100/1-hexanol surfactant system	84
4.12 Ternary phase diagram for TX-114 surfactant system	85
4.13 Crystals grown from mixed microemulsion	90
4.14 Single crystals grown from mixed microemulsion	91
4.15 Crystallisation outcome of several different mixed microemulsions	92
4.16 $I(q)$ against $q$ plot for single Lysozyme microemulsions	94
4.17 Pair distribution plot for single Lysozyme microemulsions	95

4.18	$I(q)$ against $q$ plot for single anti-solvent microemulsions	97
4.19	Pair distribution plot for single anti-solvent microemulsions	97
4.20	$I(q)$ against $q$ plot for mixed microemulsions, anti-solvent microemulsion composition ratio 1:3:6, varying Lysozyme concentration	99
4.21	$I(q)$ against $q$ plot for mixed microemulsions, anti-solvent microemulsion composition ratio 2:3:5, varying Lysozyme concentration	100
4.22	Pair distribution plot for mixed microemulsions, anti-solvent microemulsion composition ratio 1:3:6, varying Lysozyme concentration	101
4.23	Pair distribution plot for mixed microemulsions, anti-solvent microemulsion composition ratio 2:3:5, varying Lysozyme concentration	101
4.24	Single crystal mounted and centred on goniometer	104
4.25	Spatial distribution of $(I-\langle I \rangle)/s_u$	106

# Chapter One

---

## *Introduction*

The structural characterisation of proteins and small chemical compounds (including peptides composed of less than twenty-four amino acids) is deemed highly valuable research within both the academic and industrial communities. From a single crystal of the compound in question, it is possible to determine the compound's physical attributes; bond length and angles, as well as torsion angles, electrostatic potential and a very good idea about intermolecular interactions can be deciphered. The benefits of such knowledge are manifold. For a drug molecule to be effective, it must be able to bind to a protein receptor site, and hence the protein's tertiary structure must be known for successful design of drug molecules. It is also highly advantageous to obtain structural characterisation of pharmaceutical active ingredients (API) as it is important in both drug application and the patenting process. The importance is highlighted by the large investment made by pharmaceutical companies, which extensively fund research into new drug molecules. The importance of obtaining structural information for these molecules is manifold, including being able to make predictions of protein ligand interactions through the use of molecular modelling<sup>5-7</sup>.

Single crystal X-ray crystallography is by far the most powerful method of structural characterisation; enabling the compound's three dimensional structure to be solved, and ideally to a high resolution. This valuable method has led to four Nobel prizes in the last twelve years and will be celebrated in the International Year of Crystallography in 2014<sup>8</sup>. The three dimensional structure of a compound can be determined provided diffraction-quality single crystals can be produced. Unfortunately, current methods to produce crystals involve frustratingly long timescales with no guarantee of success. Additionally, with polymorphic compounds, careful selection of the appropriate crystallisation conditions has to be considered in order to obtain a particular polymorph (often the most thermodynamically stable form). Failure to crystallise the required crystal form can have serious repercussions, as was the case for a marketed anti-HIV drug, Ritonavir<sup>9</sup>, in 1998. Naively, a metastable form of the compound was initially marketed; however, over time, the active ingredient transformed to a more stable form which had a reduced bioavailability, making the drug less effective. This resulted in Ritonavir being removed from the market at a substantial financial cost<sup>10</sup>.

This thesis will address both chemical and protein crystallisation. For chemical crystallisation, commonly used methods of crystallisation will be applied, with the aim of using single crystal X-ray diffraction experiments to characterise the structure of the crystals produced. This will rely upon successful crystallisation of the compounds, which in some cases, is not always guaranteed and often hindered by the small amount of crystallisable material available. For protein crystallisation, this thesis pioneers the use of microemulsions to determine whether a generic improvement in the protein crystallisation methodology is possible.

Interest in the application of microemulsions to protein crystallisation stems from successful related work, showing an improved quality and stability of small molecule crystals can be obtained directly from microemulsions. It has recently been illustrated that microemulsion systems can impart thermodynamic control on the crystallisation process. Crystallisation from bulk solutions is typically under kinetic control, hence metastable polymorphs tend to crystallise first (in accordance with Ostwald's 1897 rule of stages<sup>11, 12</sup> described in Section 2.3.8). However, in the 3D-nanoconfinement of microemulsion droplets, a limited amount of crystallisable material within the droplets means that the controlling factor becomes the ability to form stable critical nuclei. Consequently, the more thermodynamically stable polymorphs are inherently favoured over higher energy, or less crystalline, forms<sup>3</sup>. This approach has been successfully demonstrated for the crystallisation of small molecules<sup>4</sup>. For this thesis it can be expected that protein crystallisation could be enhanced in a similar manner.

To show that crystallisation in microemulsions offers an improved methodology for protein crystallisation, the crystallisation of a commonly used standard protein from microemulsions will be compared to its crystallisation using conventional techniques. The standard test protein, Lysozyme, is known to crystallise easily. Hen egg-white Lysozyme can be crystallised in triclinic, monoclinic, tetragonal and hexagonal crystal forms<sup>13</sup>. The advantage using Lysozyme is all the different crystal forms have been extensively studied and hence comparative data is available. X-ray diffraction from crystals grown both by standard methods and using microemulsions will be used to draw conclusions with regards to the quality of the crystals grown from the two different mediums.

This thesis begins by detailing in Chapter Two the relevant background related to my research project on chemical crystallisation and the crystallisation of proteins from microemulsions. Chapter Three then continues to explain methods and experimental details used in the attempt to grow crystals for analysis, as well as the implications from the

data acquired by X-ray diffraction. Finally, conclusions (Chapter Five) will be drawn from the experimental results detailed in Chapter Four, which will be used to lead further research being conducted within these areas.

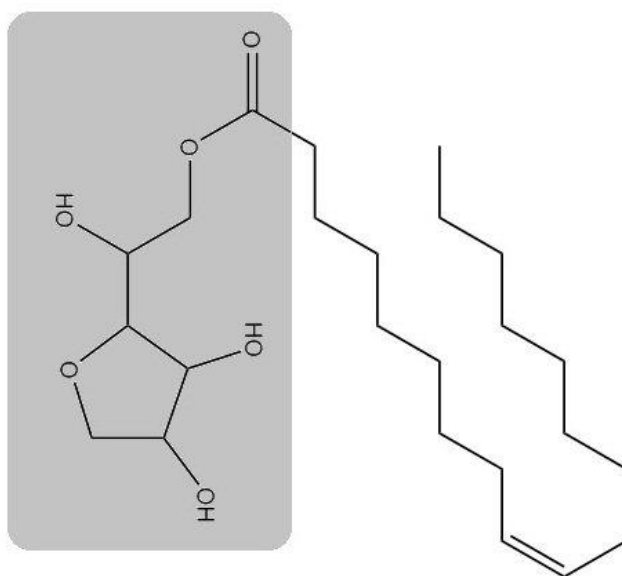
# Chapter Two

---

## *Background*

### 2.1| Surfactants

Surface active agents, commonly known as surfactants, are amphiphilic in nature. Amphiphilic molecules or ions simultaneously display lipophilic and hydrophilic affinities<sup>14</sup>. There are many substances that can act as surfactants; all share a characteristic molecular structure consisting of two distinct moieties: a hydrophilic head group and a hydrophobic alkyl chain group (Figure 2.1). Surfactants are of great interest due to their ability to reduce interfacial tension and their many potential applications such as detergents and wetting agents.


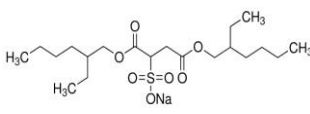
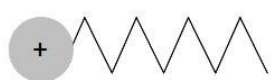
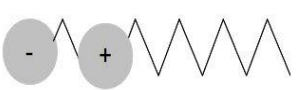
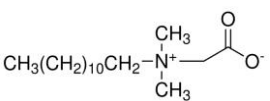

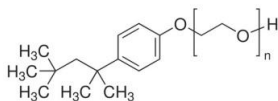


**Figure 2.1|** A single molecule of a non-ionic surfactant, Span 80, showing the hydrophobic tail group and the hydrophilic head group highlighted in grey.

### 2.1.1 | Classification

A primary classification of surfactants is made according to the charge of their hydrophilic head groups. There are two main classes: ionic (including anionic, cationic and zwitterionic head groups) and non-ionic (which have an uncharged head group) (Table 2.1). The hydrophilic head group of a particular surfactant facilitates an enhanced solubility in a range of aqueous solvents through hydrogen bonding and electrostatic interactions for non-ionic and ionic surfactants respectively<sup>15</sup>.

The nature of the hydrophobic tail group has a smaller influence on the qualitative behaviour of the surfactant compared to the head group despite the diversity among surfactants<sup>14</sup>. An extensive range of surfactants is available, and much research has been undertaken to improve preparation and optimise their physiochemical behaviour for specific applications<sup>16</sup>.

Class	Schematic structure	Example	
		Name	Structure
Ionic - <i>Anionic</i>		AOT	
Ionic - <i>Cationic</i>		CTAB	$\text{H}_3\text{C}(\text{H}_2\text{C})_{15}-\text{N}^+(\text{CH}_3)_3 \text{ Br}^-$
Ionic - <i>Zwitterionic</i>		EMPIGEN <sup>17</sup>	
Non-ionic		Triton X-100	

**Table 2.1 |** Classification of surfactants based on the charge of the hydrophilic head groups.

### 2.1.2| Interfacial Tension

An interface is the boundary between two immiscible phases<sup>18</sup>. The potential energies of molecules at the interface are greater than that for the same molecules within the respective bulk phases. This is due to the interaction energies at the interface between the dissimilar molecules of the two phases. Further, the equivalent difference in potential energies requires work to bring a molecule from the bulk phase to the interface. Interfacial tension,  $\gamma$ , is a measure of this work; it is the minimum amount of work required to create a unit area of interface.

The change in Gibbs free energy associated with interfacial tension is given by Equation 2.1<sup>19</sup>,

$$dG = VdP - SdT + \sum \mu_i dn_i + \gamma dA \quad (2.1)$$

where  $G$  is the Gibbs free energy of the system,  $P$ ,  $V$ , and  $T$  are the pressure, volume and temperature of the system respectively,  $\mu_i$  is the chemical potential of component  $i$ ,  $n_i$  is the number of moles of component  $i$ ,  $\gamma$  is the interfacial tension and  $A$  is the interfacial area. In a system of fixed composition, at constant temperature and pressure, interfacial tension can be described as the Gibbs energy change per unit area of interfacial tension (Equation 2.2)<sup>19</sup>.

$$\gamma = \left( \frac{dG}{dA} \right)_{T,P,n_i} \quad (2.2)$$

High interfacial tension is found between dissimilar phases; however, the application of surfactant can be used to reduce interfacial tension. This is a primary application of surfactants and is made possible by their amphiphilic nature.

### 2.1.3| Properties: Efficiency and Effectiveness

Surfactants are able to reduce interfacial tension by adsorbing at the interface as a result of their amphiphilic nature. When added to two immiscible phases, the surfactant molecules will arrange so that the hydrophilic head groups are orientated towards the polar, aqueous phase and the hydrophobic tails groups towards the non-polar, oil phase. The interactions between the hydrophilic and hydrophobic moieties of the surfactant with the respective



phases are more favourable compared to the interaction between molecules of the two immiscible phases; thus surfactants significantly reduce interfacial tension.

The tendency to accumulate at interfaces and as a result, the extent of reduction in the interfacial tension, differs from surfactant to surfactant. Therefore, choice of surfactant is dependent on application. When comparing a particular surfactant's ability to reduce the interfacial tension of a given system, two parameters, efficiency and effectiveness, should be considered<sup>16, 18</sup>.

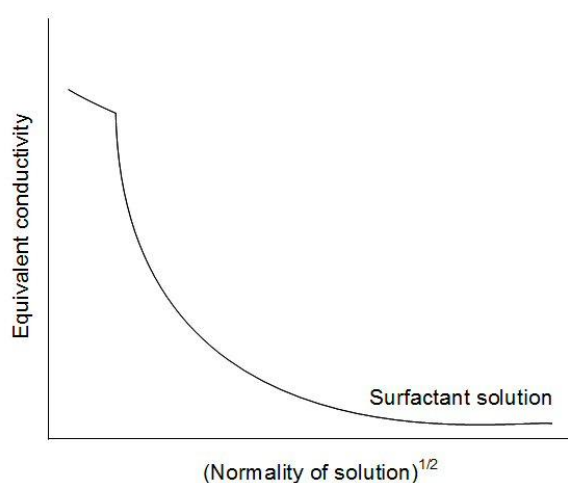
Efficiency is related to the bulk phase surfactant concentration required to reduce the interfacial tension by a given amount. Efficiency has been found to vary with length of hydrophobic alkyl chain length<sup>20, 21</sup> and degree of branching<sup>22-25</sup>. Surfactants with greater hydrophobic character and no branching are the most efficient in the reduction of interfacial tension<sup>26</sup>. For ionic surfactants, the use of a more strongly bound counter ion improves efficiency. Positioning of the hydrophilic head group also influences efficiency, with a terminal position being most efficient compared to a non-terminal position.

Effectiveness is the maximum reduction in interfacial tension that can be achieved by a particular surfactant irrespective of its concentration and to a large extent is dependent on the cohesiveness of the surfactant hydrophobic groups. Branched hydrophobic tail groups are therefore more effective as they have lower cohesive forces than straight chain hydrophobic tail groups. The effectiveness of surfactants increases when silicone or fluorocarbon-based hydrophobic groups are used instead of the more common alkyl chain tail groups<sup>18</sup>.

#### **2.1.4| Micellisation**

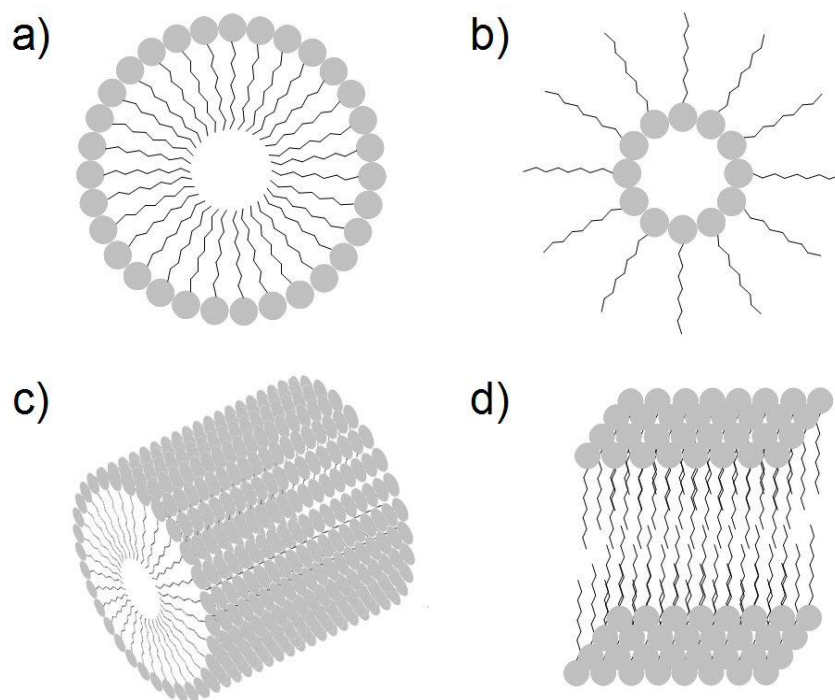
A characteristic property of surfactant molecules in solution is their ability to self-assemble into micelles, a process referred to as micellisation. Micelles are dynamic aggregates of surfactant molecules that form spontaneously at or above the critical micelle concentration (CMC). The CMC is the concentration, at a given temperature and pressure, above which micellisation can occur. The CMC may vary with temperature and pressure. For a solution of anionic surfactant, measurements of electrical conductance indicate the absence of aggregation when there is a low surfactant concentration. There is a sharp reduction in conductance (Figure 2.2) when surfactant concentration reaches a particular value, the CMC, indicating the formation of micelles<sup>16</sup>. Above the CMC, the surfactant concentration in solution is effectively constant; excess surfactant aggregates into micelles which are in

dynamic equilibrium with the monomer surfactant in solution<sup>27</sup>. Changes in other physical properties, such as turgidity and surface tension, can also be used to determine the CMC of a particular surfactant<sup>28</sup>.



**Figure 2.2** | Plot of equivalent conductivity (specific conductance per gram-equivalent of solute) against the square root of the normality of solution (gram equivalent weight of a solute per litre of solution). The sharp decline in conductance for the surfactant solution indicates the point of micelle formation. Adapted from Rosen<sup>16</sup>.

For spherical micelles (Figure 2.3a) in a polar solvent such as water, the hydrophobic tails of the surfactant molecules are contained within the interior of the micelle and the hydrophilic head groups are orientated towards the bulk aqueous solution<sup>29-31</sup>. Reverse micelles (Figure 2.3b) are formed in bulk oil solutions where the hydrophilic head groups are orientated away from the oil. Other structural forms of micelles include cylindrical micelles and bilayers (Figure 2.3c and d). Micellar shape can be predicted by the packing parameter (Table 2.2) of the particular surfactant<sup>32</sup>. The packing parameter is given by  $p_c = V/(a_0 l_c)$ , which is the ratio of the volume of the surfactants hydrophobic chain,  $V$ , to the product of effective surfactant length,  $l_c$ , and the effective head group surface area,  $a_0$ , which reflects the size and charge of the head group and its surrounding electrostatic environment<sup>33</sup>.



**Figure 2.3** | Shapes of surfactant aggregates: a) spherical micelle, b) spherical reverse micelle, c) cylindrical micelle, d) bilayer.

The free energy change of micelle formation,  $\Delta G_m$ , is given by Equation 2.3, where  $T$  is the temperature of the system and  $\Delta H_m$  and  $\Delta S_m$  are the enthalpy and entropy changes for micellisation respectively<sup>34</sup>.

$$\Delta G_m = \Delta H_m - \Delta S_m T \quad (2.3)$$

These parameters can be determined from the temperature dependence of the CMC or measured directly by using microcalorimetry. Micellisation is spontaneous and thermodynamically favoured when  $\Delta G_m$  is large and negative under the given conditions. At room temperature, hydrophobic interactions are the main driving force for micelle formation<sup>34</sup>. As surfactant concentration is increased above the CMC, the release of water molecules from ordered shells of hydration that surround the hydrophobic surfactant tails results in a large entropic gain. Other models such as 'Phase Separation' and 'Mass Action' can also be used to describe micelle formation<sup>31, 35</sup>.

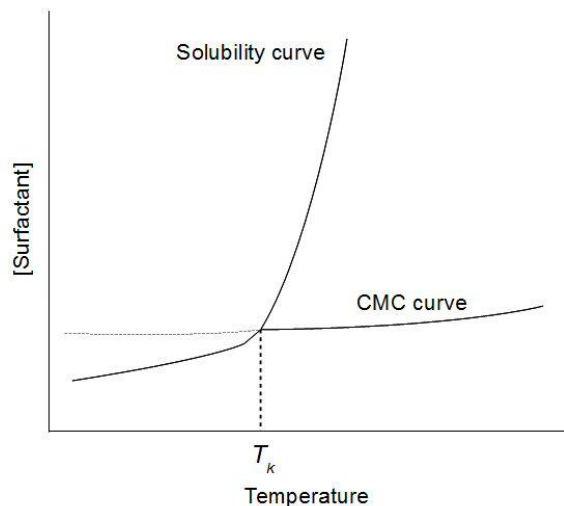
Packing Parameter	Micelle Shape
$p_c < \frac{1}{3}$	Spherical
$\frac{1}{3} < p_c < \frac{1}{2}$	Cylindrical
$\frac{1}{2} < p_c < 1$	Bilayer
$p_c > 1$	Reverse

**Table 2.2|** Typical shape of surfactant aggregates based on the packing parameter,  $p_c$ , of the surfactant. Adapted from Tolbert et al<sup>36</sup>.

### 2.1.5| The Krafft Point

The Krafft point, also known as the Krafft temperature,  $T_k$ , is commonly observed in ionic surfactants but rarely in non-ionic surfactants<sup>37</sup>. Philips defined the Krafft point as the temperature at which a surfactant's solubility is equal to its critical micelle concentration (CMC)<sup>38</sup>. Below the Krafft point, surfactants display a low solubility and tend not to form micelles. At, the Krafft point and above, there is a steep increase in the solubility of the surfactant due to the occurrence of surfactant micellisation<sup>39</sup>.

To determine the Krafft point of a particular surfactant, measurements of its CMC and solubility with changing temperature are required. The point of intersection between a solubility curve and CMC curve makes clear the concept of the Krafft point as shown in Figure 2.4.



**Figure 2.4** | Changes in the solubility and the CMC as temperature is increased. The point of intersection between the two curves is defined as the Krafft temperature,  $T_k$ . Adapted from<sup>27</sup>.

The Krafft point varies with surfactant hydrophobic chain length, extent of branching<sup>40</sup>, bulkiness of the hydrophilic head group and addition of a counter-ion<sup>31</sup>. When selecting a surfactant for a particular application it is important to consider its Krafft point, as below  $T_k$  a surfactant is significantly less effective and micellisation is not permitted.

#### 2.1.6 | The Cloud Point

Observed in non-ionic surfactants, the cloud point is the temperature at which a surfactant solution phase separates into surfactant-rich and surfactant-deficient phases. Clouding can affect solutions of ionic surfactants<sup>41, 42</sup>, but is predominantly observed for non-ionic surfactants. As the cloud point is approached, the hydrophilic head groups of micelles are dehydrated, and non-ionic surfactant micelles aggregate to form clusters<sup>43</sup> via an attractive potential, whose well-depth increases with temperature<sup>44</sup>. The cloudy appearance of a surfactant solution, at or above its cloud point, is due to the scattering of light by the micellar aggregates.

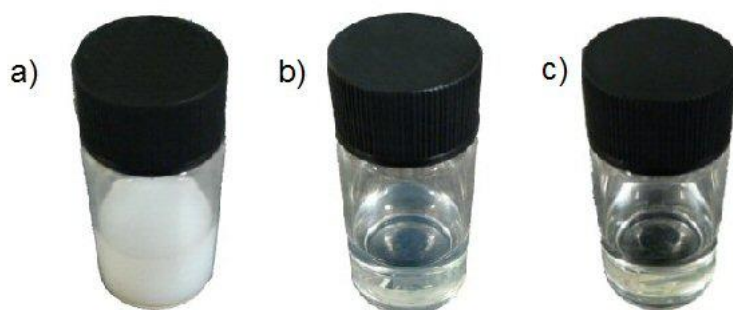
There is currently limited knowledge about the mechanism that results in the observed phase separation when the cloud point of a surfactant solution is reached. Initial explanations focused on a transition of micellar expansion from a globular shape to an enlarged rod-like shape<sup>45</sup>. However this remains a contentious explanation. More recently, A. Zliman and H. Bock attribute phase separation to the formation of a connected micellar

network or directional hydrogen bonding between surfactant head groups and molecules of water respectfully<sup>46, 47</sup>.

Variables such as structure and concentration of surfactant and the presence of additives, such as electrolytes or organic molecules, have been found to affect the cloud point of surfactants<sup>43</sup>. Fritz investigated the effect of surfactant chain length, and found the cloud point decreased with increasing carbon chain length<sup>48</sup>. Changes in pressure may also result in clouding<sup>49, 50</sup>.

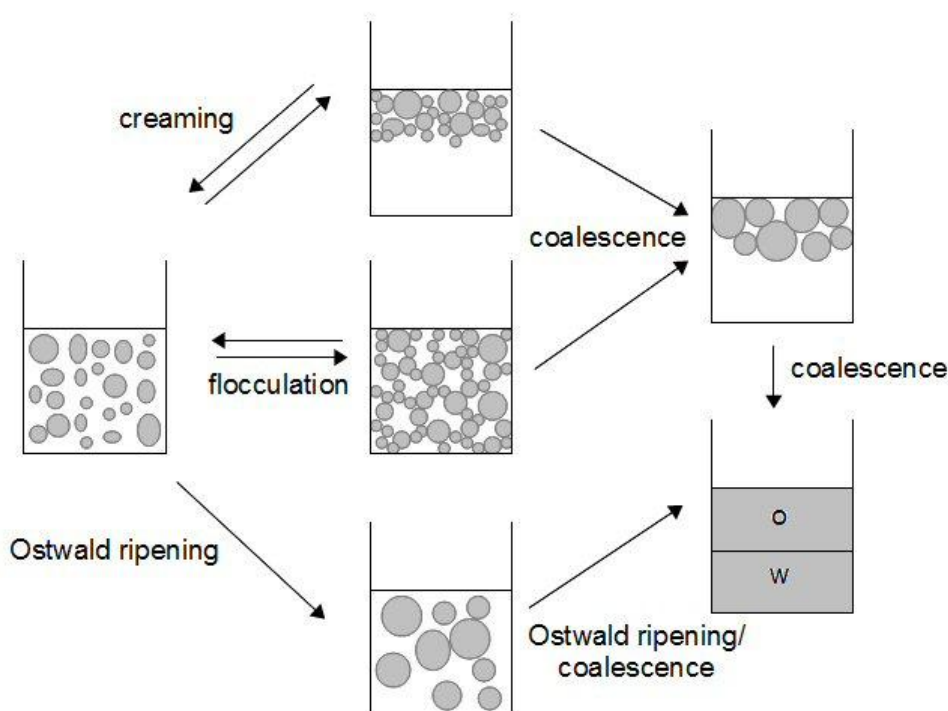
## 2.2| Emulsions

Emulsions are conventionally described as a dispersion of one liquid in another, where both liquids are either mutually immiscible with one another or poorly miscible<sup>51</sup>. Depending on the droplet size, three categories of emulsion can be defined. Macro-emulsions (Figure 2.5a) have a droplet size of approximately  $\geq 400$  nm and are white and cloudy in appearance, nano-emulsions (Figure 2.5b) have a droplet size of approximately 50-200 nm<sup>52, 53</sup> and appear blue and cloudy, and microemulsions (Figure 2.5c) have a droplet size of typically 2-1-100 nm<sup>54</sup> and are transparent.



**Figure 2.5|** The transparency of an emulsion depends on the size of the droplets. a) Macro-emulsion  
b) Nano-emulsion c) Microemulsion.

Macro-emulsions are thermodynamically unstable<sup>55</sup> due to an inherent positive free energy of formation. Thus, after a finite time, they will separate into two or more phases. Separation of emulsions, which are non-equilibrium systems, is due to the unfavourable high specific surface areas caused by the process of dispersion of one phase into another immiscible phase<sup>51</sup>. Emulsions may degrade into two or more phases via a number of different mechanisms<sup>56</sup> as summarised in Figure 2.6. Coalescence is the predominant mechanism of degradation for many emulsion systems; however, Ostwald ripening can be a significant factor, but is often neglected<sup>56</sup>. Ostwald ripening occurs due to the difference in chemical potentials of materials confined within small droplets compared to material within larger droplets. This causes emulsion droplets of a significant size to grow larger at the cost of the smaller droplets. Differences in chemical potentials arise due to the differences in the radius of curvature of the droplets.



**Figure 2.6|** Schematic representation of mechanisms of emulsion degradation. Adapted from Taylor<sup>56</sup>.

There have been extensive efforts to try and increase the stability, and thus lifetime of macro-emulsions. Such stability is required in macro-emulsions as they are used by industry for a broad range of applications including acting as carriers for drug molecules<sup>57, 58</sup> and pesticides<sup>59</sup>.

### 2.2.1| Hydrophilic-lipophilic Balance (HLB)

HLB, the hydrophilic-lipophilic balance, was first introduced in 1949 by Griffin<sup>60</sup>. HLB is an arbitrary scale that assigns a numerical value to individual surfactants indicating the balance of the strength and size of the surfactants' hydrophilic and hydrophobic moieties. For particular applications, considering the HLB of potential surfactants enables one to predict whether an oil-in-water emulsion or a water-in-oil emulsion will form in a given system<sup>60</sup>. Surfactants with HLB values of less than 10 typically form w/o-emulsions, whereas those with HLB values greater than 10 typically form o/w-emulsions. Table 2.3 summarizes expected functions of surfactants based on their HLB values<sup>61</sup>.

Surfactant HLB Number	Expected application of Surfactant
1.5-3	Anti-foaming agent
1-4	Emulsifier for w/o emulsions
6-8	Wetting agents
10-13	Emulsifier for o/w emulsions
13-15	Detergent
15-18	Solubiliser

**Table 2.3|** Expected application of surfactants given their assigned HLB value. Adapted from Kruglyakov<sup>61</sup>.

Griffin first developed an empirical formula (Equation 2.4) for calculating the HLB of non-ionic alkyl polyglycol ethers based on the weight percentages of ethylene oxide and hydroxide groups,  $E_j$  wt% and  $OH$  wt%, respectively.

$$HLB = \frac{E_j \text{wt\%} + OH \text{wt\%}}{5} \quad (2.4)$$

Davies and Rideal<sup>62</sup> further developed Griffin's initial concept to create a general empirical equation (Equation 2.5) to define HLB in terms of numerical values assigned to the chemical groupings present in the surfactant molecule.

$$HLB = 7 + \sum(\text{hydrophilic number}) - \sum(\text{hydrophobic number}) \quad (2.5)$$

If more than one surfactant is used, the HLB of the blend can easily be calculated using an additive approach<sup>60</sup>. For example, a surfactant blend composed of 25% surfactant A with HLB 4 and 75% surfactant B with HLB 14 would have an overall HLB value of 11.5. HLB values

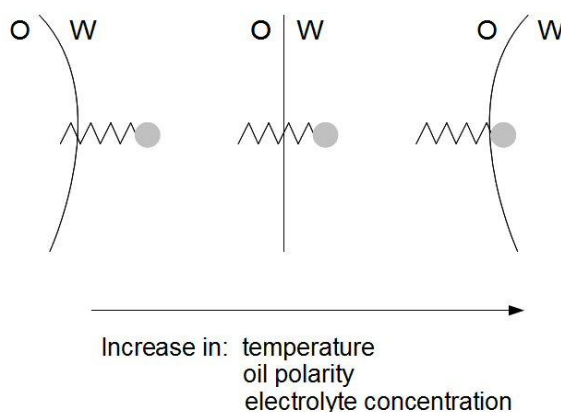


(along with other influencing factors) of the surfactants used in thesis have been considered in order to obtain water in oil microemulsion systems.

### 2.2.2| Phase Inversion Temperature (PIT)

The stability of emulsions formed from a surfactant system, are highly temperature dependent. Water-continuous emulsions are most stable at a low temperature, and oil-continuous emulsions are most stable at higher temperatures. This is because the extent of hydration around the hydrophilic surfactant head groups decreases as temperature is increased. Consequently, the hydrophilic nature of a surfactant decreases as temperature increases<sup>16</sup>. PIT, the phase inversion temperature, is defined as the temperature at which a particular non-ionic surfactant system switches from an o/w emulsion to a w/o emulsion. Unlike HLB, which is a parameter regarding an individual surfactant independent of the system, PIT is a parameter concerning the whole system. There is an approximately linear relationship between PIT and HLB; increasing the chain length on a surfactant results in both a higher HLB and PIT value.

The nature of the oil used, the ratio of oil to water, and the use of additives (such as salts) all influence the PIT<sup>31</sup>. Oil additives such as fatty acids or alcohols, which increase the polarity of the oil, result in a significant reduction in the PIT. Figure 2.7 demonstrates the effect that such factors have on an emulsion system, highlighting the change in curvature at the oil-water interface and the change in position of the surfactants tail group across the interface. At the PIT, the interfacial tension between oil and water is found to be at a minimum.



**Figure 2.7|** Schematic representation of the effect of temperature, oil polarity and electrolyte concentration on the PIT, where 'o' and 'w' indicate oil and water phases respectively. Adapted from Jönsson et al<sup>31</sup>.

### 2.2.3| Nano-emulsions

Emulsions with droplet sizes of approximately 50-200 nm are commonly and most favourably known as nano-emulsions<sup>53, 63</sup> but they are also referred to as mini-emulsions<sup>64</sup> or sometimes submicron emulsions<sup>65</sup>. Due to their small droplet size, nano-emulsions appear translucent or transparent with a blue tint (due to scattering of light) (Figure 2.5b) and present stability towards creaming. They are more kinetically stable than macro-emulsions; however, they are not thermodynamically stable.

Nano-emulsions are non-equilibrium systems and do not form spontaneously under ambient conditions<sup>63</sup>. To form small droplets, energy and/or large amounts of surfactant are required. The Laplace pressure,  $p$ , which is the difference in pressure between the inside and outside of a nano-emulsion droplet, can aid understanding when considering the large amount of energy required to form nano-emulsions compared to macro-emulsions<sup>53</sup>. The Laplace pressure  $p$ , is given by Equation 2.6, where  $R_1$  and  $R_2$  are the droplet radii of curvature and  $\gamma$  is interfacial tension.  $R_1 = R_2 = R$  for spherical drops, reducing to Equation 2.7.

$$p = \gamma \left( \frac{1}{R_1} + \frac{1}{R_2} \right) \quad (2.6)$$

$$p = \frac{2\gamma}{R} \quad (2.7)$$

Considering the inverse relationship, it is apparent that the Laplace pressure increases as a droplet is deformed to create smaller droplets; this can be demonstrated when a spherical droplet deforms to form a prolate ellipsoid. The stress needed to deform a drop is greater for smaller drops due to a spherical drop having one radius of curvature and a prolate ellipsoid having two radii of curvature. More energy is required to produce smaller drops as more vigorous agitation from the surrounding liquid is required when the stress is greater<sup>66</sup>. As previously mentioned in Section 2.1.2 addition of surfactants will lower the interfacial tension, thus facilitating the formation of nano-emulsions as  $p$  is reduced with a decrease in  $\gamma$ . To assist the preparation of nano-emulsions, numerous methods have been developed including application of the PIT concept, high pressure homogenisers and the employment of the low energy emulsification method at constant temperature<sup>53</sup>.

Nano-emulsions have many diverse applications; including the provision of an encapsulation medium for delivery of antimicrobial essential oils<sup>67</sup>, as a medium for the

production of polymeric nano-particles, and a method known as the mini-emulsion polymerisation, which considers nano-emulsion droplets as nano-reactors<sup>68</sup>. The appeal of nano-emulsions in such applications is manifold, including their stability against sedimentation or creaming and their ability to remain a dispersed system due to their small droplet sizes preventing flocculation.

#### 2.2.4| Microemulsions

Microemulsions are thermodynamically stable<sup>69</sup>, self-aggregated systems. Macroscopically, they are homogeneous mixtures of water, oil and surfactant. However, at a microscopic level, microemulsions consist of a colloidal dispersion of water-rich or oil-rich domains separated by a film of amphiphilic molecules<sup>70</sup>. In some systems a co-surfactant is also used. Microemulsions form spontaneously and, at equilibrium, will have droplet sizes of 1-100 nm<sup>54</sup>. Small droplet sizes reduces scattering of visible light, leading to their transparent appearance. Microemulsions are of great interest due to their chemical and physical stability, enabling long-lived stability of mixed oil and water systems which cannot be achieved through the use of macro-emulsions.

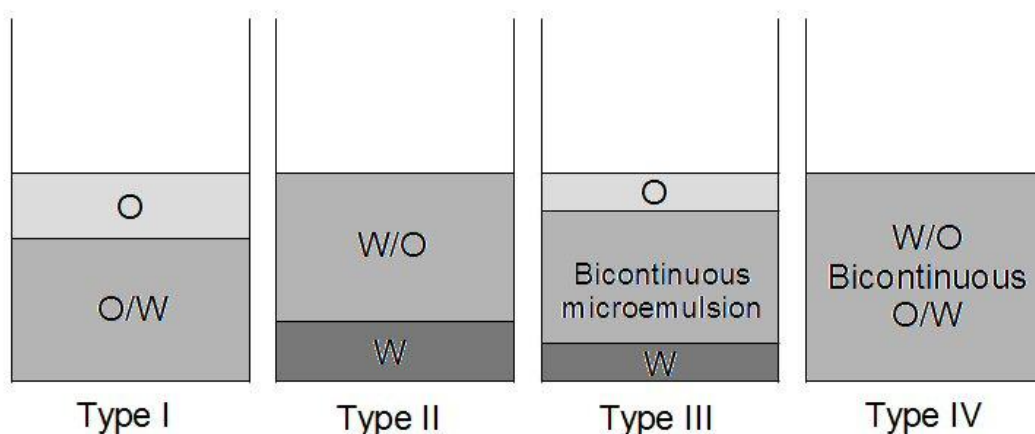
The micellisation process during the formation of microemulsions can be described using Equation 2.8<sup>71</sup>, where  $\Delta G_f$  is the free energy of formation,  $\gamma$  is the interfacial tension,  $\Delta A$  is the change in interfacial area, temperature is denoted  $T$  and  $\Delta S$  the change in entropy. Formation is favourable when  $T\Delta S > \gamma\Delta A$ ; therefore, microemulsions will form when an ultra-low interfacial tension is achieved which compensates for the large change in interfacial area that occurs due to the formation of droplets.

$$\Delta G = \gamma\Delta A - T\Delta S \quad (2.8)$$

Since microemulsions were first described in 1943 by Schulman<sup>72</sup>, extensive research has been facilitated by the development of experimental characterisation techniques such as small-angle X-ray scattering (SAXS), small-angle neutron scattering (SANS) and electron microscopy<sup>73</sup>. As a result, an extensive knowledge of microemulsion structure has been established and today work continues to explore the potential applications of microemulsions<sup>74</sup>.

### 2.2.5| Microemulsions: Microstructure and Classification

In 1948, Winsor first described four classifications of equilibrium microemulsion systems composed of water (or aqueous salt solution), oil (a mixture of single organic liquid) and approximately 5-25% of surfactant<sup>75</sup>. Figure 2.8 depicts these four classes which he described as: Winsor I, a phase separated system with an upper excess oil phase and a lower o/w microemulsion; Winsor II, a phase separated system with an upper w/o microemulsion and a lower excess water phase; Winsor III, a triple layer system with an upper excess oil phase, a lower excess water phase and a middle biscontinuous microemulsion phase; and Winsor IV, a homogeneous system consisting of one microemulsion phase<sup>70</sup>. Depending on the conditions, this single phase can be an o/w microemulsion consisting of normal micelles or a w/o microemulsion consisting of reverse micelles. The four Winsor equilibrium systems described can interconvert between one another depending on the conditions.



**Figure 2.8|** Schematic representation of the four Winsor classifications of microemulsions. Different phases are highlighted in different shades of grey; pale grey indicates an Oil (O) phase, dark grey indicates a Water (W) phase, medium grey indicates a microemulsion phase. The type of microemulsion phase varies depending on the Winsor type; O/W indicates oil-in-water microemulsion, W/O indicates a water-in-oil microemulsion. Winsor type IV could be each of the different microemulsion forms, W/O, bicontinuous or O/W.

### 2.2.6| Co-surfactant

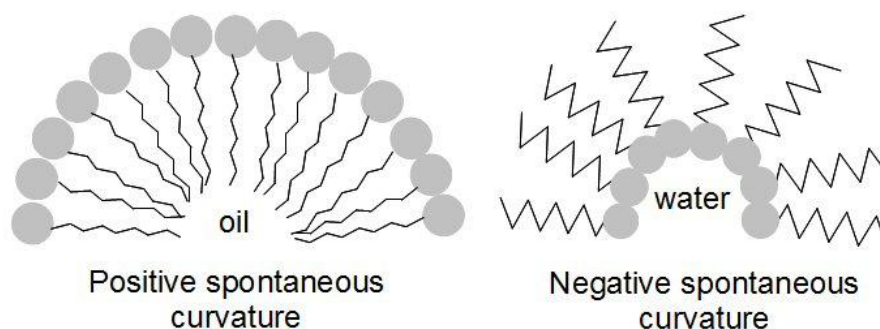
A co-surfactant is often used to aid stability of microemulsions and support the dispersion of surfactant molecules at the interface between the oil and water phases<sup>76</sup>. Weakly amphiphilic molecules such as medium and long chain alcohols are typically used as co-surfactants alongside the primary surfactant to lower the interfacial tension. However, in some circumstances short chain alcohols such as methanol also prove effective<sup>4</sup>.

For ternary microemulsions (those without a co-surfactant) extensive investigations exploring their microstructures have shown good agreement between theory and experiments when considering changes in parameters such as salinity of the aqueous phase or temperature. However, there is limited understanding for quaternary microemulsions in which the co-surfactant may partition among the oil, aqueous and interface domains instead of exclusively residing at the interface as seen in ternary microemulsion systems. A quantitative description of the dependence of a quaternary systems composition on the partition equilibria is crucial to gaining a greater understanding of quaternary microemulsions. Palozo et al in 2003 investigated the interfacial composition of CTAB/water/*n*-pentanol/*n*-hexane microemulsions, and quantitatively discussed the w/o droplet size in terms of surface composition and water content for a wide range of system compositions<sup>77</sup>. Using PGSE-NMR experiments, it was found that *n*-pentanol partitions strongly at the interface. The composition of the interface could be described to be dependent on the overall composition using a simple partition equilibrium. The total interface area was found to increase and the film thickness to decrease as the amount of *n*-pentanol was increased. The amount of water in the quaternary microemulsions was also found to have an effect, resulting in an increase of reverse micellar radii as more water was added. Over the experimental composition range used only inverse micellar structures were observed.

Within this investigation, a co-surfactant of 1-hexanol will be used with surfactant TritonX-100, to create a surfactant system which will support the formation of reverse micelles in a stable microemulsion system for the crystallisation of Lysozyme (Section 3.2.2.3 and 4.4.7).

### 2.2.7| Surfactant Film Spontaneous Curvature

Aggregates of surfactant within microemulsions can be considered to be composed of surfactant films. The curvature of such films influences the structures of the resultant aggregates. Alongside spontaneous curvature,  $c_0$ , the volume fractions of oil and water also govern whether a w/o or o/w microemulsion is formed<sup>78</sup>. Spontaneous curvature is the inverse of the radius of curvature and is defined to be negative if the surfactant film is curved around the hydrophilic domain or positive if it is curved towards the hydrophobic domain<sup>31</sup>, as demonstrated in Figure 2.9. Overall a surfactant film is flexible, displaying regions of both positive and negative curvature. A spontaneous curvature close to zero shows that the film has little curvature towards either of the aqueous or non-polar phases. Planar films such as lamellar, bicontinuous phases and sponge-like phases all exhibit zero spontaneous curvature. Droplet microemulsions are the most common structure observed in microemulsions<sup>78</sup>. Normal micelles formed in o/w microemulsions will have a positive film curvature and reverse micelles in w/o microemulsions will have a negative film curvature.



**Figure 2.9|** Spontaneous curvature is defined to be positive or negative depending on which way the surfactant film curves around the hydrophilic domain.

The type of microemulsion formed can be manipulated by varying the spontaneous curvature. By lowering the repulsions between surfactant head groups, which can be achieved for ionic surfactants by using electrolyte additives, spontaneous curvature can be decreased. Spontaneous curvature can be more readily controlled in ternary microemulsion systems compared to quaternary systems which incorporate a co-surfactant. In such systems  $c_0$  depends on the surfactant/co-surfactant ratio at the interface which can be varied by altering the surfactant/co-surfactant ratio in the overall mixture with the aqueous

and non-polar phases. However, as previously mentioned in Section 2.2.6, co-surfactants can partition in both immiscible phases thus resulting in little to no control.

### 2.2.8| Bending Elasticity of the Surfactant Film

Understanding the phase behaviour of surfactant systems, and trying to select a particular micellar structure from, requires consideration of numerous parameters including simple packing and energy considerations. The bending elastic energy of a surfactant film contributes to the free energy of the surfactant systems. The contribution of the surfactant film to the free energy (per unit area) is given in Equation 2.9<sup>78</sup>, where  $C_1$  and  $C_2$  are the principal curvatures of the surfactant films,  $C_0$  is the spontaneous curvature, and  $K$  and  $\bar{K}$  are the mean and Gaussian bending elastic constants. To describe the elastic properties of a surfactant film the two elastic constants,  $K$  and  $\bar{K}$  are required.

$$F = \frac{1}{2}K(C_1 + C_2 - 2C_0)^2 + \bar{K}C_1C_2 \quad (2.9)$$

Gradzielski noted the importance of determining the elastic constants in order to attain understanding of the behaviour and properties of microemulsions. As a result, in 1996 Gradzielski et al conducted a study of a simple system which could be varied systematically in order to investigate how parameters such as the chain length of the surfactant influenced the elastic constants<sup>79</sup>. They found that the elastic theory of the surfactant film aided understanding of microemulsion microstructure and macroscopic properties such as interfacial tension by observing that macroscopic interfacial tension, droplet radii and polydispersity index could be related to  $K$  and  $\bar{K}$ . The sum,  $2K + \bar{K}$ , was found to scale approximately with surfactant chain length to the power of three; the oil hydrocarbon chain length was found to have little influence on the elastic constants.

### 2.2.9| Phase Behaviour

A phase can be defined as a region of space filled homogenously with a physically distinctive form of matter. Light, neutron and X-ray scattering techniques can be used to distinguish between phases based on their diffraction properties. More simply, viscosity can be used to distinguish phases; however, this cannot be used as an unambiguous method since viscosity

is dependent on concentration and surfactant. For droplet phases, a distinction between reverse or normal micelles can be made based on composition, as characteristically reverse micelles form in an oil-rich environment and normal micelles form in a water-rich environment<sup>31</sup>.

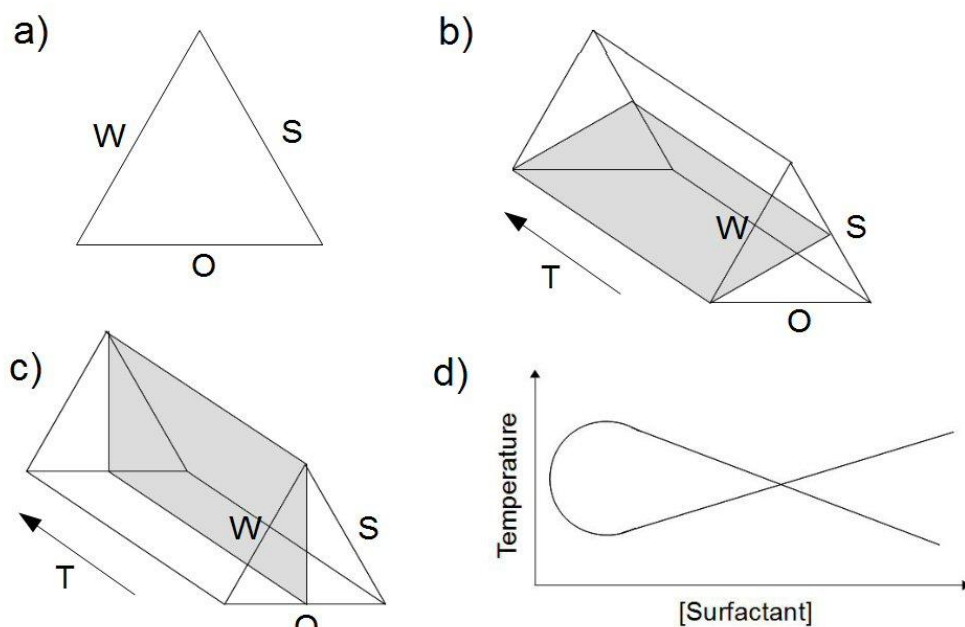
Gibbs introduced the phase rule as defined in Equation 2.10, where  $P$  is the number of phases that coexist,  $C$  is the number of components that constitute the system and  $F$  is the number of degrees of freedom.

$$P + F = C + 2 \quad (2.10)$$

Within a microemulsion, the degrees of freedom include temperature, pressure and composition variables. For the purposes of this discussion pressure will be considered to be constant, thus reducing the number of degrees of freedom by one.

Phase diagrams enable the schematic representation of a microemulsion's phase equilibria, depicting how many phases there are present in a system, what the phases are and detailing the composition of the phase in question. Completing a phase diagram becomes increasingly difficult as the number of components within a system increases. Typically, a three component phase diagram, also known as a ternary phase diagram, is used to describe a microemulsion which includes an aqueous phase, oil phase and surfactant phase. If co-surfactant is required, a pseudo-ternary phase diagram can be used in which one of the three components consists of a mixture of surfactant and co-surfactant at a fixed ratio. It is often useful to consider phase behaviour at a fixed temperature as depicted in Figure 2.10a. Considering the temperature dependence of phase behaviour gives rise to a triangular prism consisting of stacks of isothermal phase diagrams (Figure 2.10b and c). Different cuts through the triangular phase prism can be made in order to understand the effects that different microemulsion components have on phase behaviour. Such cuts include the Lund cut<sup>80</sup>, which gives a fixed ratio between the surfactant and oil phases while varying the water content (Figure 2.10b), and the Kahlweit fish cut<sup>81</sup>, which gives a fixed ratio between the water and oil phases (typically 1:1) while varying surfactant concentration (Figure 2.10c). The Kahlweit Fish phase diagram (Figure 2.10d) enables information regarding the surfactants' effectiveness to be inferred<sup>82</sup>.





**Figure 2.10|** a) Pseudo ternary phase diagram at fixed temperature; b) Lund cut through phase prism; c) Kahlweit fish cut through phase prism; d) Kahlweit fish phase diagram.

Pseudo ternary phase diagrams of the form pictured in Figure 2.10a are the most appropriate phase diagram for the aims of this investigation. These phase diagrams will aid selection of suitable composition ratios that will enable the formation of stable microemulsions for each surfactant system explored (Section 3.2.2.1).

### 2.2.10| Microemulsions: Droplet Polydispersity

There is a slight droplet polydispersity observed in microemulsions which can be measured using electrical birefringence experiments<sup>83</sup>. Such polydispersity is an equilibrium property<sup>78</sup> due to the thermodynamic stability of the microemulsion micellar phase. Polydispersity is partially a result of droplet collisions which result in the formation of transient aggregates, also referred to as transient dimers. The formation of transient aggregates allows transfer of solubilised materials from droplet to droplet. The transient droplets have a short life-time, typically of the order of microseconds. However, if there exists attractive interactions between droplets, the transient dimer's life-time may be slightly extended<sup>84</sup>. For the purpose of the following investigation discussed in this thesis, droplets will be assumed to be relatively monodisperse.

### 2.2.11 | Applications of Microemulsions

The applications of microemulsions across both academic research and industry have been extensively explored and reviewed<sup>74</sup>. Interest in microemulsions accelerated following their use in enhanced oil recovery<sup>74, 85, 86</sup>, in which approximately 20% of otherwise unrecovered underground oil was obtained using a process referred to as surfactant-polymer flooding. In this process, the high interfacial tension between crude oil and reservoir brine, which caused oil to remain trapped in porous material underground, was reduced through the formation of a middle-phase microemulsion in situ between crude oil and excess reservoir brine.

Exploring further, microemulsion fuels have successfully been shown to reduce soot formation and the emission rates of nitrogen oxides and carbon monoxide during combustion of microemulsion fuels<sup>87</sup>. Other applications of microemulsions include their use in cosmetics<sup>88</sup> and as a chemical reaction medium, the first use of which was in 1973, where microemulsions were used to accelerate the hydrolysis of esters<sup>89</sup>. More recently, interest in microemulsions has grown based on their ability to provide thermodynamic control for crystallisation of polymorphic compounds<sup>3</sup>.

## 2.3 | Crystallisation

The development of X-ray crystallography, a valuable tool for structure determination, has called for an in-depth understanding of the process of crystallisation and for the design of suitable methods that will yield single crystals of a high quality appropriate for X-ray diffraction experiments. Preparative methods of compounds of interest often yield the product in a 'crystalline' form but frequently such crystals are of an insufficient quality. Appropriate quality crystals typically have well formed, clear faces and will shine brightly when viewed with polarised light under a microscope. An exception to this observation occurs for crystals of high symmetry and for those that are cubic<sup>90</sup>. Although visually some crystals may appear of a good quality, it is their internal order which determines their diffraction pattern. Only crystals which are internally ordered will produce diffraction patterns. For membrane proteins it is quite common to produce visually pleasing objects; however, they often have very little internal order and this diffract poorly<sup>91</sup>.

Crystallisation comprises of two stages: nucleation and crystal growth<sup>92</sup>. The occurrence of nucleation is a prerequisite for crystal growth to take place. Each

crystallisation method aims to create a supersaturated solution (a solution in which the solubility limit of the crystallisable material is exceeded) as this facilitates the formation of nucleation sites. This section will lay out the fundamental scientific principles that dictate crystallisation and highlight the wealth of crystallisation techniques available for crystallising both proteins and small molecules.

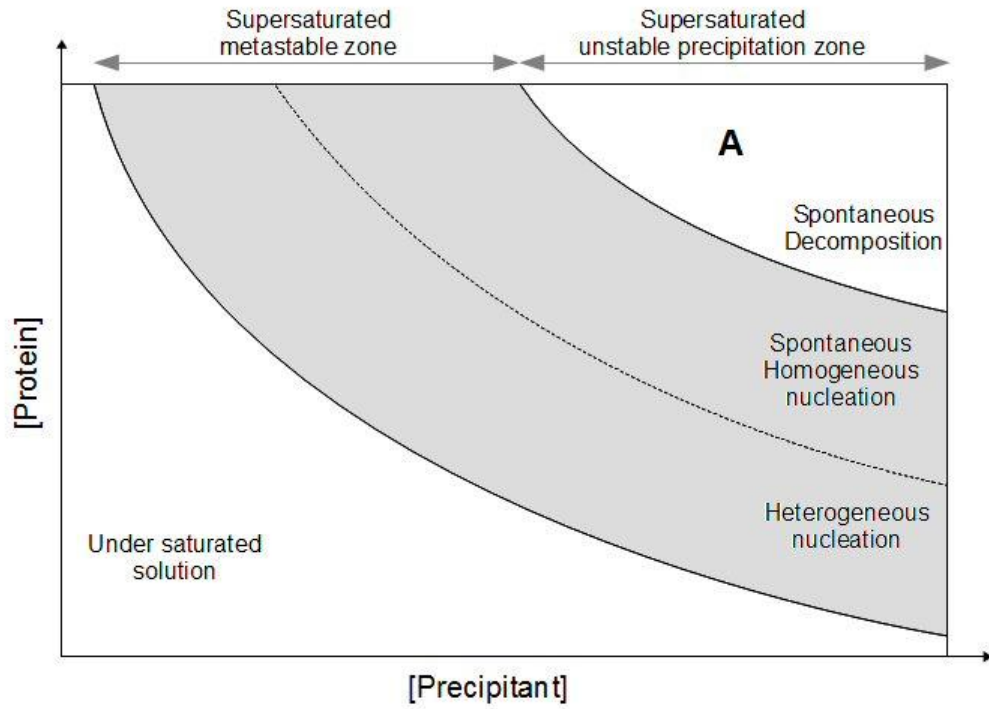
### 2.3.1| Nucleation and Supersaturation

A prerequisite for crystallisation to occur is nucleation. Nucleation is the phase change from solution to solid at a localised point; it results in the formation of small clusters of building units consisting of regularly ordered molecules associated in identical orientations. How many nucleation events take place in a solution is influenced by several variables including temperature, pressure and the concentration of the solution. The continued adsorption of the specimen molecules to the surface of the critical nuclei will result in the growth of a single crystal given that the molecules adsorb in an identical orientation.

Nucleation is strongly influenced by a solution's degree of supersaturation. Supersaturation is a metastable state (Figure 2.11) where the system is not in equilibrium<sup>93</sup>. The solution in the metastable region has more dissolved compound compared to a saturated solution which is in equilibrium. If nucleation overcomes an activation barrier, which enables the metastable system to move towards equilibrium, the dissolved compound will precipitate out of solution (ideally in a crystalline state, but this may not be the case). The newly formed precipitate will then be in equilibrium with the saturated solution which subsequently forms. The stability condition (Equation 2.11) thermodynamically defines the limits of the metastable region of supersaturation where  $\bar{G}$  is the mean molar Gibbs energy of the system and  $x_1$  is the molar fraction of the sample compound.

$$\left(\frac{\partial^2 \bar{G}}{\partial x_1^2}\right) > 0 \quad (2.11)$$

Spontaneous decomposition of a solution results by further increasing the concentration of the sample compound to form an extremely supersaturated solution (Point **A** in Figure 2.11). At this point the second derivative in Equation 2.11 becomes negative.



**Figure 2.11** | Crystallisation phase diagram. The region of supersaturation in which nucleation can occur is highlighted grey. Point **A** marks the area in which the crystallisable material is likely to crash out of solution as a result of the solution being extremely supersaturated.

### 2.3.2| Homogeneous Nucleation

Nucleation that occurs spontaneously in the interior of a pure supersaturated solution is termed homogeneous nucleation. The total Gibbs free energy change associated with homogeneous nucleation, which leads to the formation of a spherical critical nuclei of radius  $r$ , can be described by Equation 2.12<sup>94</sup>, where  $\rho_s$  is the number-density of the newly formed nuclei and  $\gamma$  is the interfacial tension of the newly formed solid-liquid interface.

$$\Delta G = \frac{4}{3}\pi r^3 \rho_s \Delta\mu + 4\pi r^2 \gamma \quad (2.12)$$

The chemical potential,  $\Delta\mu$  ( $\Delta\mu = \mu_s - \mu_l$  ( $\Delta\mu < 0$ )), is the difference between the chemical potential of the solid phase,  $\mu_s$  and the liquid phase,  $\mu_l$ . The change in Gibbs free energy (Equation 2.12) consists of two terms: the 'bulk' term ( $\frac{4}{3}\pi r^3 \rho_s \Delta\mu$ ) and the 'surface' term ( $4\pi r^2 \gamma$ ). The bulk term is negative and proportional to the volume of the nuclei; it conveys the greater stability of the newly formed solid compared to the supersaturated

solution. The loss of free energy due to the formation of a solid-liquid interface is accounted for by the surface term, which is negative and proportional to the surface area of the nuclei<sup>94</sup>.

If a system experiences free energy fluctuations that have insufficient free energy to form nuclei of a critical size, the nuclei are likely to re-dissolve instead of growing into crystals. Nuclei that do not re-dissolve have a radius of  $r^*$  and are termed critical nuclei. The Gibbs free energy for the formation of critical nuclei is a maximum value. The radius  $r^*$  can be determined using the Gibbs-Thomson equation (Equation 2.14) which is found by setting the first derivative of  $\Delta G$  with respect to  $r$  to zero (Equation 2.13).

$$\frac{d\Delta G}{dr} = 4\pi r^2 \rho_s \Delta\mu + 8\pi r \gamma = 0 \quad (2.13)$$

$$r^* = \frac{2\gamma}{\rho_s |\Delta\mu|} \quad (2.14)$$

Substituting Equation 2.14 into Equation 2.12 gives the Gibbs free energy of formation for a critical nucleus,  $\Delta G^*$  (Equation 2.15). The formation of critical nuclei of radius  $\geq r^*$  will result in further crystal growth.

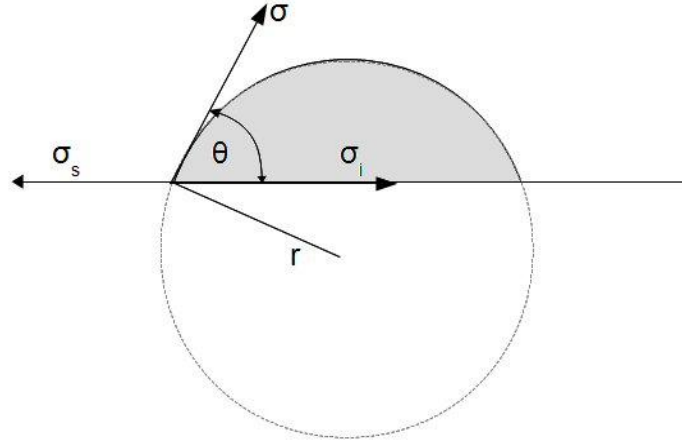
$$\Delta G^* = \frac{16\pi\gamma^3}{3(\rho_s |\Delta\mu|)^2} \quad (2.15)$$

Within the microemulsion systems detailed in this thesis it is hoped that homogeneous nucleation will be facilitated within the microemulsion droplets, resulting in the formation of critical nuclei of radius  $\geq r^*$  and thus supporting the subsequent growth of Lysozyme crystals.

### 2.3.3| Heterogeneous Nucleation

Typically, it is undesirable for nuclei to form on the wall of the reaction vessel. This occurs when nucleation is stimulated by the presence of impurities such as ions, foreign surfaces and particles. Such a process is known as heterogeneous nucleation<sup>95</sup>.

To account for the energetic influence of impurities on the free energy change of heterogeneous nucleation a 'wetting' function,  $\phi(\theta)$ , needs to be taken into consideration . The wetting function is dependent on the wetting angle,  $\theta$ , as shown in Figure 2.12.



**Figure 2.12|** Heterogeneous nucleation of a liquid droplet (with radius of curvature  $r$ , and projected radius  $r \sin \theta$ ) on a smooth structureless substrate, where  $\theta$  is the wetting angle which characterises the influence of the substrate. The Young equation<sup>96</sup> is used to determine the wetting angle using the surface specific energies of the free surfaces of the substrate and droplet, and the interface between the droplet and substrate, denoted by  $\sigma_s$ ,  $\sigma$  and  $\sigma_i$ , respectively. Wetting angle,  $\theta$ , on which The wetting function  $\phi(\theta)$  is dependent on the wetting angle,  $\theta$ . Adapted from Markov<sup>95</sup>.

Taking the wetting function,  $\phi(\theta)$  into consideration the Gibbs free energy change associated with heterogeneous nucleation can be described by Equation 2.16.

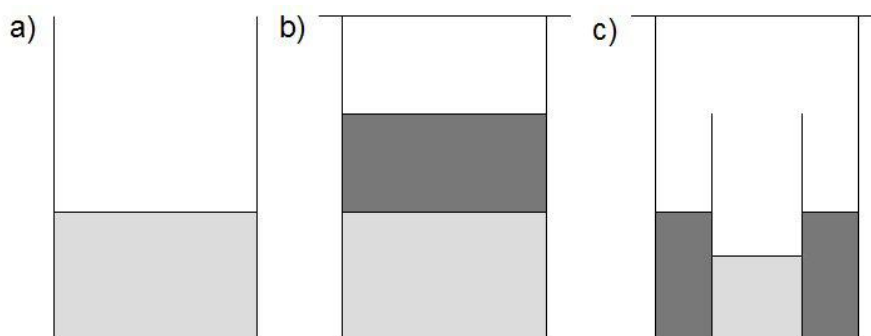
$$\Delta G^*_{het} = \Delta G^*_{homo} \phi(\theta) \quad (2.16)$$

For the case when  $\phi(\theta = 0)$  equals zero, known as complete wetting, the Gibbs free energy change,  $\Delta G^*_{het}$  equals zero indicating that it is thermodynamically unfavourable for heterogeneous nucleation to occur. A polar case to this would be complete non-wetting in which  $\phi(\theta = \pi)$  equals one and  $\Delta G^*_{het}$  equals  $\Delta G^*_{homo}$ . For this case, the critical nuclei formed are spherical and the impurities present in the sample do not have an energetic influence on the Gibbs free energy change for formation<sup>95</sup>.

### 2.3.4 | Chemical Crystallisation

Chemical crystallisation is typically concerned with the crystallisation of relatively small compounds and peptides composed of less than twenty-four amino acids. This branch of crystallography is of significant importance due to the large spectrum of applications to which such molecules may be applied. For example, the structure solution of Cyclolinopeptide A, a nine residue cyclopeptide extracted from linseed oil<sup>97-99</sup>, has encouraged continued research exploring the cyclopeptide's function as a potential immunosuppressor<sup>100</sup>. Successful, published structure solutions are submitted to the Cambridge Structural Database (CSD), the world repository of small molecule crystal structures which performs vital checks to ensure correct structures are published<sup>101</sup>.

Solution methods are versatile and present a vast array of potential solvents, alone or in combination, which can be used to create a supersaturated solution of the given compound. There exist several variants of the solution method, including simple evaporation of the solvent, re-crystallisation by liquid diffusion and crystallisation through vapour diffusion in a closed system<sup>90</sup> (Figure 2.13). The variant which yields the best crystals is entirely dependent on the compound under study. The compound's solubility, thermal stability and chemical properties will all influence the choice of method and choice of solvent.



**Figure 2.13 |** Methods of chemical crystallisation. a) Evaporation of solvent in an open system b) liquid diffusion in a closed system c) Vapour diffusion in a closed system. Dark grey indicates anti-solvent and light grey indicates crystallisable material in solution. Adapted from Jones<sup>90</sup>.

### 2.3.5| Protein Crystallisation

Advances in molecular biology such as recombinant DNA technology had a profound effect on protein crystallisation. The development of various expression systems facilitated the production of large amounts of pure protein, a feat that could rarely be achieved using natural sources<sup>102</sup>. More recently, the biotechnology group within The Structural Genomics Consortium (SGC)<sup>103</sup> have worked on determining which proteins can be expressed in a soluble and stable form which can be used for structural and functional studies. The group have continued the successful development and optimisation of high-throughput protocols for protein production and validation. Such advances have led to what is known as the 'bottleneck of crystallisation', an increasingly acute problem<sup>1</sup>, and has seen the rapid development of protein crystallisation techniques within both industry and the academic community<sup>2</sup>.

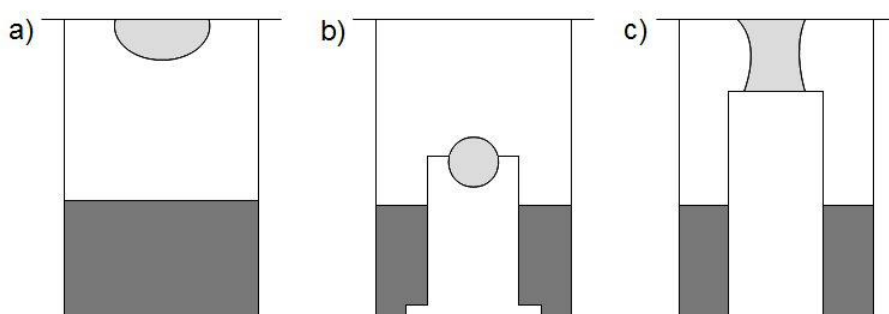
Substantial commitment has been put into developing rapid automation of protein crystallisation techniques to allow extensive screening of crystallisation conditions. Robots have now been successfully implemented and are routinely used within laboratories to great effect and efficiency<sup>104, 105</sup>. The structural information that can be gained from X-ray crystallography is extremely valuable, promoting the need for successful crystallisation techniques. For example, through X-ray crystallography, insight has been gained into the structure and mechanism of the ribosome, a key cellular organelle that enables the synthesis of proteins in all kingdoms of life. The structure of the Eukaryotic ribosome has successfully been solved to 3.0 Å by X-ray crystallography using crystals grown from hanging drop vapour diffusion crystallisation trays<sup>106</sup>, a commonly used technique detailed in Section 2.3.6. The work achieved through X-ray crystallography is vast and is enabled both by advances in X-ray diffraction experiments and the development of successful crystallisation techniques, several of which are detailed in this following section. The success of this extremely valuable technique was celebrated through the Nobel Prize in Chemistry 2012, jointly awarded to Robert J. Lefkowitz and Brian K. Kobilka in<sup>107</sup> *"for studies on G-protein-coupled-receptors"*.

### 2.3.6| Vapour Diffusion Methods

For protein crystallisation, the most frequently and successfully used crystallisation technique is that of vapour diffusion which includes the hanging drop, sitting drop and



sandwich variants (Figure 2.14). While hanging drop and sandwich vapour diffusion are manual methods, sitting drop vapour diffusion has efficiently been automated allowing beneficial rapid screening of crystallisation conditions. All variants consist of a reservoir solution containing precipitants and a crystallisation drop containing the protein and buffer solution. Water diffuses down its concentration gradient from the crystallisation drop to the reservoir solution bringing the crystallisation drop into supersaturation. This facilitates nucleation and subsequent crystal growth. Vapour diffusion set ups allow screening of many crystallisation conditions; an experimental necessity, as in most samples crystallisation will not occur due to incorrect external parameters such as, pH and type of precipitant (anti-solvent).

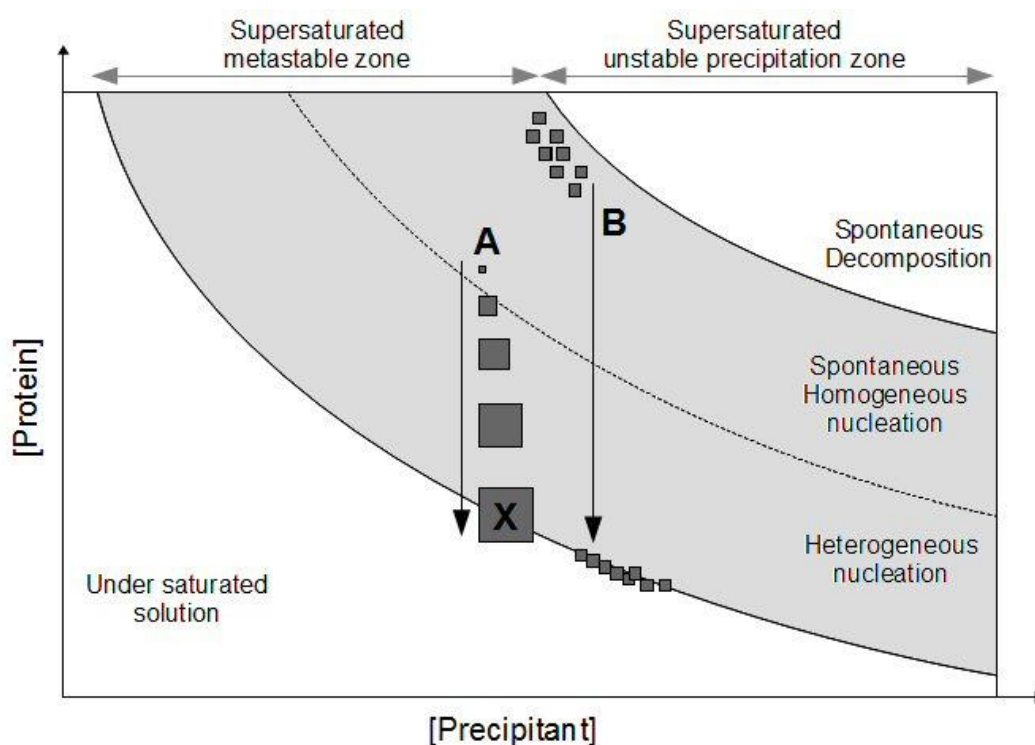


**Figure 2.14** | Three vapour diffusion setups for protein crystallisation. a) Hanging drop b) Sitting drop c) sandwich drop. Light grey indicates the protein solution and dark grey indicates the reservoir solution.

Sandwich vapour diffusion is a rarely used variant of the vapour diffusion technique. However, the method facilitates the ability to reduce the area of a drop that is exposed to air, resulting in a slower rate of diffusion between the reservoir solution and the crystallisation drop compared to the rate observed for hanging and sitting drop setups.

Crystallisation (phase) diagrams (Figure 2.15) can conveniently be used to schematically visualise the events that occur during a vapour diffusion experiment. If nucleation does not occur early on in the metastable supersaturation region where spontaneous nucleation can take place, numerous critical nuclei may form resulting in potential growth of several small crystals (Pathway **A** in Figure 2.15). This is not ideal, and conditions which facilitate nucleation early in the spontaneous nucleation region should be found to allow ideally a single nucleation event resulting in the growth of a large single crystal (Pathway **B** in Figure 2.15) which may be suitable for X-ray diffraction experiments. Upon the formation of critical nuclei, crystal growth may occur until the crystals reach

equilibrium with the saturated solution, at which point (Point **X** in Figure 2.15) crystal growth does not continue.



**Figure 2.15 |** Crystallisation phase diagram. Pathway **A**: An ideal situation in which nucleation occurs early on in the supersaturated metastable region resulting in a singular nucleation event and subsequent growth of a large single crystal. Pathway **B**: nucleation occurs further into the supersaturated metastable region resulting in numerous small crystals. **X** indicates the point at which the growing crystals reach equilibrium with the saturated solution, thus no more crystal growth occurs.

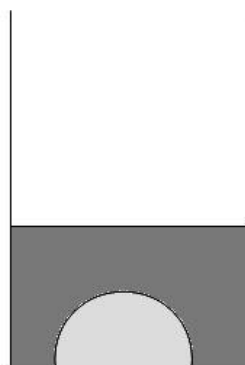
In both hanging drop and sitting drop vapour diffusion, crystals may not form as a result of the closed system not reaching supersaturation, making it thermodynamically impossible for crystals to form. This negative result may be rectified by increasing the precipitant concentration of the reservoir solution<sup>108</sup>. Another plausible problem may be inadequate nucleation events due to a large kinetic barrier; this is potentially solved through seeding, which is the introduction of external nucleation points.

A clear advantage of sitting drop vapour diffusion compared to hanging drop vapour diffusion is the ability to automate the setting up of trays. Trays of 96 wells can rapidly be made with widespread crystallisation conditions; automatic dispensing robots have enabled the drop size to be reduced from typically 1  $\mu$ l in manual setups to 100 nl, facilitating an

order of magnitude more experiments to be made with the same amount of valuable compound available. However, sitting drop trays are sealed with a sheet of adhesive tape which does not allow easy and repeatable access to crystals. Comparatively, for hanging drop trays, each well is covered by a siliconised glass cover slip which allows easy access to crystals, one well at a time, and enables the system to be resealed easily.

### 2.3.7| Batch Methods

In contrast to vapour diffusion, the batch crystallisation set up involves the reservoir solution and the crystallisation solution being in direct contact with one another (Figure 2.16) as opposed to separation through a gaseous phase.



**Figure 2.16|** Experimental setup for protein crystallisation using the batch method; the system is isolated and undisturbed to allow equilibrium to be reached. The drop (pale grey), a mixture of the protein and reservoir solutions is isolated from the environment via oil (dark grey).

Conveniently, the batch method can be readily automated and miniaturised using nanolitre drops and immediate sealing of the system using oil. This microbatch method<sup>109</sup> is efficient for the initial screening of crystallisation conditions and has successfully been implemented<sup>110, 111</sup>.

### 2.3.8| Polymorphism

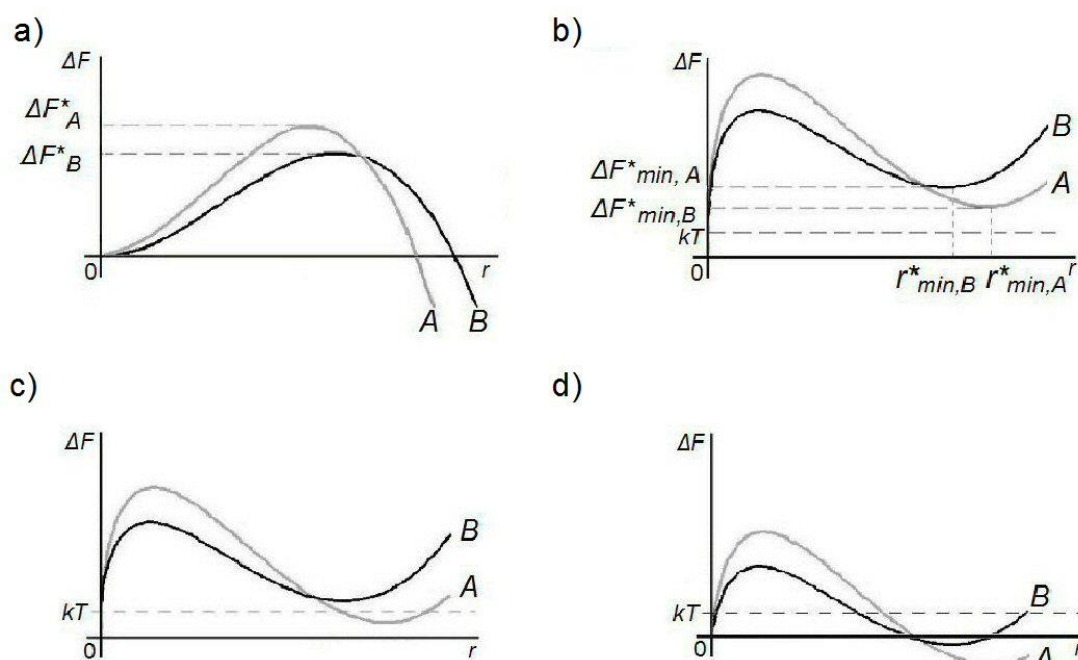
Polymorphism is a phenomenon whereby a particular compound in a solid crystalline state exists in two or more different lattice structures. Different crystal forms may be observed by varying crystallisation conditions and it can be advantageous to optimise these conditions to

obtain good quality crystals of numerous morphologies for a particular compound under study. Advantages include the ability to select a crystal morphology that gives the highest quality X-ray diffraction data. Also, information regarding crystallisation artefacts may be gained by studying several morphologies.

While advantageous in some respects polymorphism can be problematic within the pharmaceutical industry as great efforts are required to control polymorphism of Pharmaceutical active ingredients (APIs). Ostwald's rule of stages<sup>11</sup> states that the least stable (the metastable) polymorph tends to crystallise first, as this involves the crystallisation system moving to a lower energy via the smallest possible free energy change. This is the most likely result due to the typical kinetic control of crystallisation rather than thermodynamic control. Upon crystallisation of the metastable polymorph, it may then transform to a more thermodynamically stable form over a variable time period. APIs can display different crystal forms and morphologies which present varying bioavailability, absorption and release. Consequently, the pharmaceutical industry must ensure that a particular morphology of a particular API is obtained and that there is no question as to whether the polymorph obtained will transform over time. Approval of the API will not be granted if this is not the case.

#### **2.3.9| The Microemulsion Method: Thermodynamic Control of Crystallisation**

The favoured crystallisation of a metastable crystal form compared to a more stable form according to Ostwald's rule of stages can be visualised using a free energy profile (Figure 2.17). As discussed in Section 2.3.1, for crystal growth to occur there has to be sufficient energy to overcome a free energy barrier of nucleation, resulting in the formation of critical nuclei of radius  $r^*$ , thus permitting crystal growth. Figure 2.17a displays a Helmholtz free energy profile for conventional, unconfined crystallisation conditions. Under such conditions, the nucleation barrier for the metastable polymorph, B, is smaller than that for the more stable polymorph, A, and consequently the metastable polymorph will crystallise first, displaying kinetic control of crystallisation.



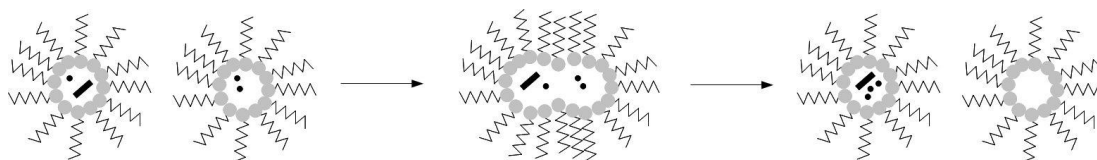
**Figure 2.17** | Example graphs of Helmholtz free energy changes,  $\Delta F$  vs nucleus radius,  $r$ , for systems crystallising from a) bulk solution and b), c), d), a 3D nano-confined microemulsion solution. Polymorph A is the more thermodynamically stable, and polymorph B is metastable. (a) Ostwald's rule of stages is observed. (b) Crystallisation is disfavoured and a minimum in free energy is formed due to 3D nano-confinement. (c) Thermodynamic control of crystallisation is achieved. (d) Thermodynamic control is lost and both polymorphs will typically crystallise out. Adapted from Cooper et al<sup>3</sup>.

Microemulsions give the ability to 'leap-frog' Ostwald's rule of stages and provide an elegant method of thermodynamically controlling crystallisation through three dimensional (3D) nano-confinement to directly crystallise the most stable polymorph. When a solution is three dimensionally nano-confined, a minimum in free energy is observed as a result of the substantial decrease in supersaturation as the crystal nuclei/phase forms and increases in size. This minimum in free energy is denoted  $\Delta F^*_{\min,x}$ , and the corresponding nuclei has a radius of  $r^*_{\min,x}$ . Typically the minimum in free energy for the more stable polymorph, A, is less than that of the metastable polymorph, B, ( $\Delta F^*_{\min,A} < \Delta F^*_{\min,B}$ ). This difference in free energy is depicted in Figure 2.17b and can be expected as a result of polymorph A's greater stability in solution. Before supersaturation is depleted polymorph A is able to grow to a larger size, with a greater radius ( $r^*_{\min,A}$ ), compared to the metastable polymorph, B. This is because the stable polymorph has a lower solubility in solution.

The Boltzmann Factor,  $\exp(-\Delta F^*_{\min,x}/kT)$ , determines the population of nuclei of radius  $r^*_{\min,x}$  when the system is at equilibrium and stipulates that a significant population of stable nuclei results when  $\Delta F^*_{\min,x} \leq kT$ . Subsequently, as schematically illustrated in Figure 2.17c, thermodynamic control can be established in 3D nano-confined microemulsions when  $\Delta F^*_{\min,x} \leq kT$  for the most stable polymorph, A, only. This condition would result in a significant population of post-critical nuclei for polymorph A given that the nucleation barrier for formation could be overcome. With smaller droplets within a microemulsion, higher initial supersaturations are reached ensuring that nucleation barriers can be overcome.

The continued increase of supersaturation within a confined droplet has two possible outcomes: the retention of thermodynamic control or the system converting to kinetic control with the loss of advantageous thermodynamic control. The outcome is dependent on the relative proportions of  $r^*_{\min,A}$  and  $r^*_{\min,B}$  which results in favouring crystallisation of one polymorph over another. The equilibrium concentration of  $r^*_{\min,x}$  can be maintained if the reverse process of  $r^*_{\min,x}$  dissolution is of a sufficient rate. This would result in thermodynamic control being retained and is dependent on the magnitude of  $\Delta F^*_x - \Delta F^*_{\min,x}$ . The rate of dissolution of  $r^*_{\min,x}$  nuclei will be slow if  $\Delta F^*_x - \Delta F^*_{\min,x} \gg kT$  and the nucleation barrier,  $\Delta F^*_x$ , can be overcome. This is shown in Figure 2.17d where  $r^*_{\min,x} < 0$ . In this case the relative proportion of  $r^*_{\min,A}$  and  $r^*_{\min,B}$  then becomes dependent on their rates of formation only, and the system reverts to kinetic control as would be found in a non-confined bulk system.

Upon establishing thermodynamic control within the 3D nano-confined microemulsion and the subsequent formation of a significant population of stable nuclei of the most stable polymorph, crystal growth follows. Brownian motion describes the movement of microemulsion droplets and the potential for collisions to occur between droplets. If sufficient in energy, droplet collisions can result in the formation of transient dimers (Figure 2.18) which allow the exchange of material between droplets. The solute confined within the droplets will move according to its concentration gradient; a droplet containing one or several nuclei will have a lower local concentration surrounding the mentioned nuclei compared to a droplet in which no nuclei were established. Once crystal growth exceeds the limited size of the droplet the microemulsion will break and the crystal will precipitate out of the system and often settle at the bottom of the reaction vessel.



**Figure 2.18|** Formation of transient dimers and subsequent exchange of material between droplets upon collision of microemulsion droplets.

Microemulsions have successfully been used to implement thermodynamic control over the crystallisation of Glycine<sup>4</sup>. Glycine was an ideal small molecule to use as it can crystallise in three different polymorphic forms, with the most thermodynamically stable  $\gamma$  polymorph being just  $0.2 \text{ kJmol}^{-1}$  more stable at ambient temperatures than the metastable  $\alpha$  polymorph<sup>112</sup>. Using microemulsion crystals of the most thermodynamic,  $\gamma$  polymorph were directly grown in ambient conditions.

### 2.3.10| Lysozyme: A Model Protein for Crystallisation Studies

Lysozyme was the first enzyme structure to be solved by X-ray crystallography. It was first found in nasal mucus and named by Fleming in 1922<sup>113</sup> when he observed the protein's antibacterial properties. Known as a glycoside hydrolase enzyme, Lysozyme presents antibacterial properties through catalysing the hydrolysis of 1,4-beta-glycosidic bonds between N-acetylmuramic acid and N-acetyl-D-glucosamine residues of peptidoglycan, a protective layer found on the cell walls of gram positive bacteria<sup>114-116</sup>. The main source of Lysozyme for research purposes is from hen egg-white (HEWL) but Lysozyme can also be found in animal tissues and fluids<sup>117</sup>.

Since its discovery, Lysozyme has undergone extensive investigations<sup>118</sup> and has been used to establish models for protein crystal growth and investigate some general crystalline properties of proteins<sup>119-121</sup>. Lysozyme is commonly used as a model system due to its stability, solubility and ability to crystallise under different conditions<sup>122</sup> yielding different polymorphic crystals. Variation of additives, ions, pH and temperature have lead to the formation of six different symmetries of Lysozyme crystals<sup>123</sup> tetragonal, monoclinic, triclinic, orthorhombic, hexagonal and trigonal. Appendix A1 summarises the varying crystallisation conditions that have been successfully used to grow different crystal forms of Lysozyme to yield structural information for the protein.

The first crystal structure of Lysozyme to be solved was a tetragonal crystal of Hen-egg-white-Lysozyme (HEWL)<sup>124</sup>. Crystal structures of different crystal polymorphic forms rapidly followed including triclinic<sup>118, 122</sup>, monoclinic<sup>122, 125-127</sup>, orthorhombic<sup>118, 128</sup> and hexagonal<sup>13, 128</sup>. Crystal structures for turkey egg-white Lysozyme (TEWL)<sup>129, 130</sup> and guinea fowl egg-white Lysozyme (GEWL)<sup>131</sup> have also been solved from hexagonal crystal forms.

### **2.3.11 | Membrane proteins: A Crystallisation Challenge**

Crystallisation of aqueous soluble proteins is a time consuming process involving extensive trial and error in order to obtain well ordered three-dimensional crystals, a prerequisite to high resolution X-ray structural determination. However, membrane proteins, which traverse hydrophobic cellular membranes, present a further crystallisation challenge and typically prove to be more problematic due to the difficulty associated with their isolation and purification, a consequence of their hydrophobic nature.

Domains of membrane proteins that display on the cell surface provide a large target for pharmaceuticals facilitating the potential therapeutic control of cell signal pathways. Aided by the three dimensional structure of membrane proteins, the structural based design of small molecules becomes an attainable goal. Industry values the potential held within membrane protein structure determination and requires a series of protein structures rather than a single result, in order to screen their pharmaceuticals as potential therapeutics. For this to be a reality, there is need for a reliable way of producing crystals of membrane proteins that diffract at a high resolution<sup>132</sup>.

Membrane proteins are abundant in nature. Genome-wide analysis has predicted that 20-30% of the open reading frames from eubacterial, archaean and eukaryotic organisms encode for the production of integral membrane proteins<sup>133</sup>. In humans, 15-39% of the 23000 or so human proteins are thought to be integral membrane proteins. However, despite their abundance, there is a disproportionately low number of membrane protein structures submitted to the Protein Data Bank (PDB)<sup>134</sup>; of approximately 300 integral membrane proteins, about twenty or so are human. This clearly reflects the difficulty in obtaining and crystallising membrane proteins.

This difficulty in crystallising membrane proteins results from the hydrophobic nature of the integral membrane domains which, when embedded in the cell membrane, are in contact with the hydrophobic acyl chains of the phospholipids. In comparison, soluble domains of membrane proteins are in contact with the surrounding aqueous phase



and the polar head groups of the phospholipids. When removed from the hydrophobic membrane environment into an aqueous solution, integral domains of membrane proteins become unstable and typically aggregate and precipitate out of solution. Amphiphilic detergents are therefore often required to solubilise membrane proteins in aqueous solutions. When the detergent is used above its CMC, a detergent micelle is established covering the hydrophobic surface of the membrane and providing stability for the membrane protein in an aqueous environment<sup>135-137</sup>.

Currently, detergent based techniques remain the method of choice giving rise to the most success in the crystallisation of membrane proteins<sup>138</sup>. The protocol resembles that used to crystallise aqueous soluble proteins, in which detergent solubilised and purified membrane proteins are crystallised using standard vapour diffusion protocols. However, despite numerous examples of success, the quality of crystals gained from detergent based methods can be difficult to maintain, and in some cases require frustrating and time consuming crystal treatment in order to obtain a crystal of appropriate quality for structural determination<sup>139</sup>. It is therefore with good reason that time and resources have to be committed to explore alternative methods for the crystallisation of membrane proteins. Progress has been made through the use of protein specific antibodies which enable the enlargement of soluble domains to provide larger surface contacts for crystal formation<sup>140</sup>. This methodology has enabled crystallisation<sup>141</sup> and structure solution<sup>142</sup> of membrane proteins as complexes with anti-body fragments, but presents specialised protocols that may restrict access to the technique in many laboratories. An alternative to using protein specific antibodies to increase the soluble domains of membrane proteins is provided by protein engineering<sup>143</sup>.

Lipidic phases offer an increasingly popular and promising methodology for membrane protein crystallisation. First demonstrated by Landau and Rosenbusch<sup>144</sup>, it was thought that by reintroducing purified membrane proteins into a lipid bilayer environment there would be an enhancement in the protein's stability, which would support the crystallisation process. Three mesophases, lipid cubic phases (LCP), lipid sponge phases (LSP) and lipid bicelles, are method variants that branch from this central hypothesis. The characteristics of both LCP<sup>145</sup> and LSP<sup>146</sup> have been clearly established and, with the aid of small-angle X-ray scattering and cross-polarised microscopy, different lipid phases can easily be distinguished. Lipid bicelles can be thought as solubilised lipid bilayer disks<sup>147, 148</sup> that successfully maintain the functionality of reconstituted membrane proteins<sup>149</sup>. A

hypothesis has been proposed regarding how *in meso* crystallisation takes place at the molecule level<sup>150-152</sup>.

Lipid phases were first successfully used in 1997, permitting the structure determination of bacteriorhodopsin to 2.5 Å<sup>153</sup>; however, the crystals used were later found to be twinned<sup>154</sup>. A twinned crystal contains two or more single crystals of the same crystal lattice type but they lie in different directions resulting in some overlap between the respective crystal lattice points. Continuing from this initial success, the *in meso* method has enabled the crystallisation of both eukaryotic and prokaryotic membrane proteins, including chromophore-containing and chromophore-free proteins, multimeric proteins and α-helical and β-barrel proteins<sup>155</sup>. This highlights the method's potential as a general protocol for the crystallisation of membrane proteins. The understanding of how membrane proteins function at a molecular level has been furthered by the use of lipid phases to crystallise membrane proteins for structural determination. For example, the structure of a sensory rhodopsin II-transducer complex revealed critical details into the modes of signal communication that takes place in phototaxis and chemotaxis<sup>156</sup>. Similarly, in 2007, the first high resolution structures of two non-rhodopsin G-protein coupled receptors (GPCR) were achieved using crystals grown from lipid phases<sup>157, 158</sup>.

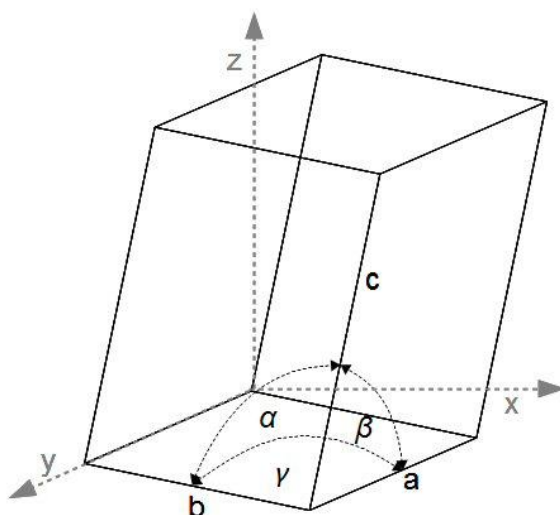
The importance of further developing techniques for the crystallisation of membrane proteins is emphasised by the financial support given to the pursuit of membrane protein structure determination. In 2011, the Structural Genomics Consortium (SGC) received nearly £32 million from funding bodies, including the Wellcome Trust, to sustain four years of operations following their success in solving the structure of a human mitochondrial ABC transporter<sup>159, 160</sup>.

## 2.4| X-ray Crystallography

X-ray crystallography is the most powerful tool for accurately determining the three dimensional structure of a compound. The diffraction pattern which forms as a result of a crystal being exposed to X-ray radiation enables the structure of a compound to be determined. This valuable technique can be used on a wide range of compounds, from small molecules to macromolecular proteins.

### 2.4.1 | Crystal Structure

In 1611, Johannes Kepler was the first to explore the relationship between the regular external morphology of a crystal and the crystal's internal order<sup>161</sup>. This led to the development of a central concept in crystallography describing the composition of a crystal in terms of building blocks termed unit cells. A crystal can be generally described as a self-assembled, periodic array of identical unit cells which are displaced repeatedly in three dimensions with translational and orientational long-range order. A unit cell (Figure 2.19) is described by three axial lengths,  $a, b, c$  and three angles,  $\alpha, \beta, \gamma$  where  $\alpha$  lies between axes  $b$  and  $c$ . Axial lengths are expressed in terms of Ångströms (Å), and the inter-axial angles are expressed in terms of degrees (°) in most published papers.



**Figure 2.19 |** A schematic depiction of a unit cell showing the three angles ( $\alpha, \beta, \gamma$ ) and three axes ( $a, b$  and  $c$ ).

The contents of a unit cell vary depending on the internal symmetry of the crystal ranging from a fraction of a molecule to one or more molecules. Some unit cells may even encompass a whole protein or large multi-component complexes. Unit cell geometries can be described using the seven crystal systems which result from restrictions in both rotational and reflectional symmetry. For structures which display more than purely translational symmetry, it is conventional to include more than one point in the unit cell so that the unit cell can better describe its symmetry. As a result, there exists what are known as the 14 Bravais lattices which each belong to one of the 7 crystal systems. It is the unit cells of the Bravais lattices which can be regarded as the “building blocks” of crystals. The

internal symmetry of a crystal is restricted as it must obey the translational symmetry of the crystal; consequently, 32 point groups and 230 crystallographic space groups are generated that can be used to describe the symmetry of a crystal.

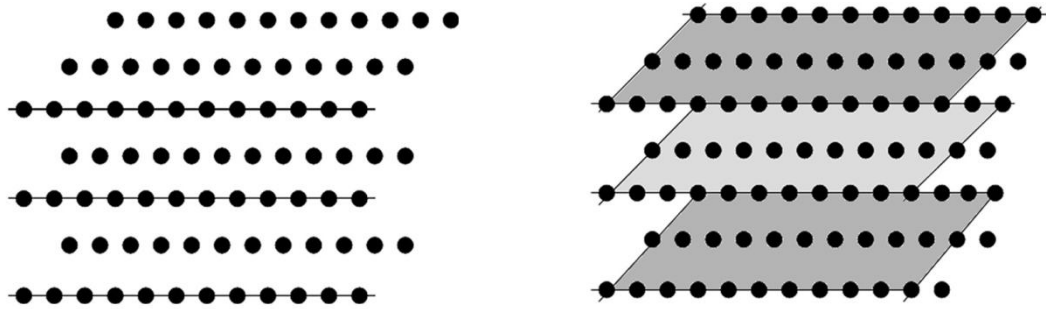
Protein molecules lack symmetry due being built from L- $\alpha$ -amino acids, resulting in their chiral nature. This limits the possible combinations of symmetry operations; all mirror symmetry operations are eliminated, generating only 65 discrete chiral space groups from which a protein crystal can be described.

#### **2.4.2| The Reciprocal Lattice**

Mathematical constructs are required to aid the description of a crystal in relation to the diffraction events that emanate from it when exposed to X-rays. Developed by P. Ewald in 1921<sup>162</sup>, the reciprocal lattice is one such mathematical construct which also enables the determination of the conditions necessary for diffraction to occur. To construct the reciprocal lattice, the crystal lattice in real 3D-space first has to be considered. The crystal lattice is dependent on the crystal's unit cells geometry, as it is generated by representing each unit cell with an isolated point, with each lattice point being in exactly the same environment. Consequently, if the unit cell is large, a widely spaced crystal lattice would be generated. The reciprocal lattice is seen in the pattern of the diffracted spots and has a reciprocal relationship with the real 3D-space crystal lattice generated from the unit cell of the crystal.

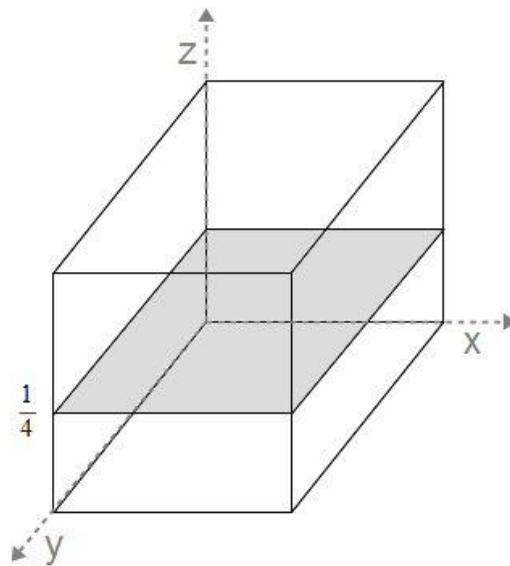
#### **2.4.3| Miller Indices**

Lattice planes, both in 2D (Figure 2.20a) and 3D (Figure 2.20b), can be drawn using lines through the points of the real 3D-space crystal lattice. There are multiple ways of classifying lattice planes. However, some are not ideally suited to aid the description of X-ray diffraction experiments. For example, the generation of Weiss indices for each set of lattice planes using a direct indexing scheme proves problematic, as planes that are parallel to a lattice vector intersect the corresponding lattice vector an infinite number of times which is mathematically unhelpful. Consequently, it is most beneficial to use reciprocal Miller indices to uniquely classify sets of lattice planes within the crystal.



**Figure 2.20** | Regularly arranged crystal lattice points of a) 2D lattice planes b) 3D lattice planes.

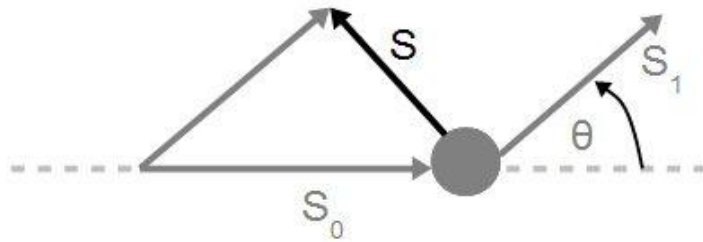
Miller indices  $(h, k, l)$  are always integers and are generated by selecting axes that facilitate the alignment of the axes  $x$ ,  $y$ , and  $z$  with the unit cell axes  $a$ ,  $b$ , and  $c$  respectively. Using the Miller Indices, planes can be defined by  $1/ha$ ,  $1/kb$  and  $1/lc$  as shown in Figure 2.21.



**Figure 2.21** | Miller Indices; here the Miller plane intersects the  $x$  axis at zero, the  $y$  axis at zero and the  $z$  axis at  $1/4$ . The plane is therefore defined as 004.

#### 2.4.4| X-ray Scattering

X-rays are a form of electromagnetic radiation that interacts with matter mainly through their oscillating electric field vectors. A fundamental tool to understand X-ray diffraction experiments is the ability to geometrically describe the scattering events that take place when X-rays are scattered by electrons in the regularly arranged and orientated atoms present in the crystal. This can efficiently be achieved using scattering diagrams (Figure 2.22), which describe scattering using wave vectors. The difference between the initial incoming wave vector,  $\mathbf{S}_0$ , and the wave vector of the scattered wave,  $\mathbf{S}_1$ , gives the scattering vector,  $\mathbf{S}$ . Only coherent scattering (also known as elastic scattering) is relevant to the diffraction of X-rays. This is when a scattering event takes place without a transfer of energy between the electron and the photon. As a result of coherent scattering, all excited electrons emit photons which are in-phase. The diffraction pattern results from the sum of all independent, in-phase scattered photons.



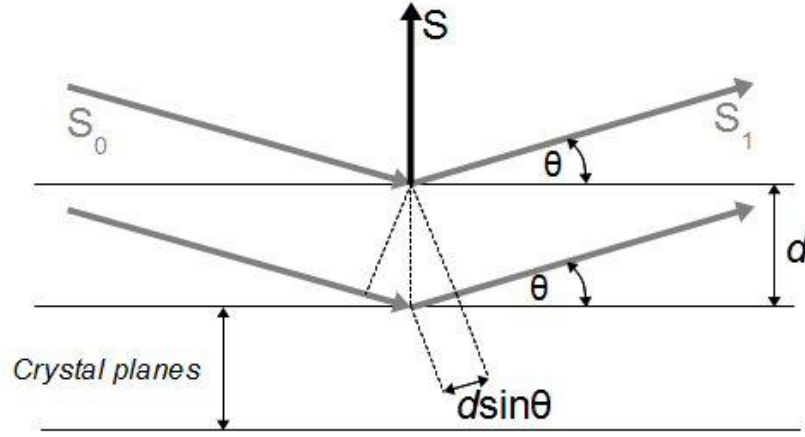
**Figure 2.22|** Scattering diagram used to geometrically describe the scattering events that take place when X-rays are scattered by electrons in the regularly arranged and orientated atoms present in the crystal.

To simplify the interpretation of X-ray diffraction, Bragg's Law can be applied. This central concept to X-ray crystallography, developed by Sir William Laurence Bragg, views the scattering vector,  $\mathbf{S}$ , as a normal to the reflection of X-rays from a set of equidistant lattice planes  $a$ .

$$n\lambda = 2d_{hkl} \sin \theta \quad (2.17)$$

This allowed the formulation of Bragg's equation (Equation 2.17), which forms a quantitative relationship between the spacing between lattice planes,  $d_{hkl}$ , and the diffraction angle,  $\theta$ , of separate reflections. Consequently, it can be seen that for maximum

constructive interference, the path difference between two diffracted waves,  $2d \sin \theta$ , has to be a multiple of  $n\lambda$ .



**Figure 2.23** | Bragg's law viewing X-ray diffraction as reflections from equivalent crystal lattice planes.

#### 2.4.5 | The Phase Problem

Information regarding the phase of the waves emanating from excited electrons is required in order to determine the electron density, and hence crystal structure, from the diffraction pattern. However, the attainment of such information is the central problems presented by X-ray crystallography as only the intensity, equal to the square magnitude of the diffracted wave amplitude, is recorded and all phase information is systematically lost. The extraction of phase information is termed the *phase problem*. Herbert A. Hauptman and Jerome Karle were awarded the 1985 Nobel Prize in Chemistry for their work on direct methods used to help solve the phase problem; this clearly indicates the importance and significance of the phase problem in the determination of crystal structures.

The structure factor  $F_{(h,k,l)}$  for a reflection  $(h, k, l)$  is a complex number defined by Equation 2.18 and is calculated by summing over all atoms,  $j$ .

$$F_{(h,k,l)} = \sum_{j=1}^{atoms} f_{(j)} \exp[2\pi i(hx_{(j)} + ky_{(j)} + lz_{(j)})] \quad (2.18)$$

The type of atom and the diffraction angle of the associated reflection  $(h, k, l)$  influences the scattering factor of an atom,  $f_{(j)}$ . From the positions of each reflection collected in a diffraction experiment, the indices  $(h, k, l)$  can be determined, and an appropriate intensity can be assigned to each reflection. The square of the structure factor amplitude can be determined experimentally, as it is proportional to the scalar intensity value. Subsequently, a Fourier Transform (FT) can be applied to the structure factor, which is a periodic function, to enable electron density to be evaluated and thus the structure determined. Equation 2.19 describes the electron density resulting from the FT which enables an image in reciprocal space, the diffraction pattern, to be transformed into an image in real or direct space, the electron density.

$$\rho_{(x,y,z)} = \frac{1}{V} \sum_h \sum_k \sum_l F_{(h,k,l)} \exp \left[ -2\pi i (hx_{(j)} + ky_{(j)} + lz_{(j)}) \right] \quad (2.19)$$

The phase problem prevents the immediate calculation of electron density as the structure factor is only known in part; phase information, which is not recorded, is still required. Several techniques have been developed with the aim of solving the phase problem. The first crystal structures were solved by trial and error<sup>163</sup>; however, this method had a very low efficiency, particularly for crystals of low symmetry. Alternative phase techniques include the Patterson method<sup>164</sup>, which was later developed and relies on additional experimental information gained through the use of heavy atoms within the structure. Today the more widely used direct methods approach<sup>165</sup> is applied to solving the phase problem which was developed by Woolfson and Sheldrick into widely used programs. The methods above were developed for the structure solution of small molecules; other methods have been developed for solving the phase problem for protein crystals.

#### 2.4.6| Small Angle X-ray Scattering (SAXS)

Colloidal dimensions are comparatively large with respect to the wavelength of X-rays. This makes the angular range of observable X-ray scattering experiments comparatively small. Therefore, for solids and fluids of colloidal size (in the nanometre range), small angle X-ray scattering (SAXS) can be utilised to explore their structural characterisation through probing inhomogeneities in their electron densities on a length scale of typically 1-100 nm. SAXS enables the determination of size, shape and internal structure of colloidal particles,



measuring at angles less than  $1^\circ$ . This analytical technique typically only considers coherent scattering since incoherent scattering is weak at very small angles.

$$q = \frac{4\pi}{\lambda} \sin \theta \quad (2.20)$$

The data gained from SAXS experiments is commonly presented in scattering vectors of  $q$  (Equation 2.20), instead of  $2\theta$  which is quoted in X-ray crystallography. This proves beneficial for obtaining results which are independent of the wavelength used.

# Chapter Three

---

## *Experimental Methods*

### **3.1 | Chemical Crystallisation**

All chemical compounds for crystallisation were provided by members of Dr Steven Cobb's research group in the Department of Chemistry, Durham University. The compounds ASH89, ASH81/87, ASH93, ASH91, ASH82, ASH90 and ASH59 compounds were stored in the fridge at 4°C and GDL02, GDL38 and GDL39 compounds were stored at room temperature. None of the compounds were air sensitive; however, as a precaution compounds were stored in tape sealed glass vials. Appendix A2 details the preparation of each of the above mentioned compounds.

#### **3.1.1 | Initial Solubility Screens**

Prior to solubility screens, initial observations of the sample were made under an optical microscope and the nature of the sample was noted including the sample's crystallinity (as shown through birefringence using a polarised light filter), colour and habit as well as the presence of any crystals from which a crystal shape could be predicted. A small amount of compound for study was spread in a central thin line over the length of a standard glass microscope slide and up to 6 µl of solvent was used. A range of solvents were used with a broad range of boiling points.

A clean needle was used to add a small amount of powdered compound to each solvent drop which was deposited onto the glass slide using a 2-20 µl Gilson pipette. The relative extent of the compound's solubility in each solvent was visualised under the optical microscope and noted. Further observations were also made regarding the occurrence of any crystallisation upon evaporation of the solvent and the manner in which the powdered compound separated upon being added to the solvent. This could potentially indicate the shape of the crystalline material in the sample and may also suggest the habit that would result upon crystallisation of the compound.

### **3.1.2| Crystallisation by Evaporation**

For solvent evaporation experiments it is preferable to use a watch glass, a nine-well glass plate or a glass vial. All glass must be free from dust and clean and have a means of easily removing small crystals. For example, the aperture of the glass vial must be of a large enough size for efficient crystal removal. When using solvents of a comparatively higher boiling point, such as Polyethylene Glycol (PEG), it may be suitable to carry out the evaporation experiment on the initial glass slide used for solubility screening.

It is often preferable to use a glass vial as these can be stored at a slight angle to promote crystal growth on the side of the vial rather than at the bottom of the vial, thus aiding collection of the crystals. Also, the rate of evaporation for volatile solvents can be more readily controlled through the use of a perforated cap. For slow evaporating solvents the vial can be left uncapped. Altering the temperature or the rate of evaporation may allow a stable and sustainable growth phase to occur. To explore this, in some cases, evaporation experiments were repeated in the refrigerator at 4°C. Lowering the temperature of evaporation experiments may prevent crystallisation failure by allowing molecules of the compound to orientate in identical conformations for a period adequate for sustaining crystal growth.

Supersaturation of the system is achieved through the evaporation of the solvent. This allows nucleation to occur with the system relaxing into the metastable region and facilitating crystal growth. However, evaporation experiments are difficult to reproduce due to the many varying conditions that can influence an open system. Upon evaporation of the solvent no crystallisation may occur due to the system not reaching the point of supersaturation. This undesirable result can potentially be solved by varying the ratio of solvent and sample. However, with a limited amount of material (less than 5 mg) this methodology may waste material if the solvent is unsuitable. If this is the case, it is desirable to seek an alternative solvent in which the compound displays a lower solubility.

### **3.1.3| Crystallisation by Liquid Diffusion**

The open system of evaporation experiments may not result in crystallisation. Alternatively, a closed system may be more successful by enabling a higher degree of control over the conditions for crystallisation experiments. Crystallisation from evaporation experiments may fail as a result of the compound's solubility being too high in the chosen solvent,

preventing supersaturation from being reached. Anti-solvents offer a solution to this problem and can be implemented using liquid diffusion experiments.

Solvents in which the sample is insoluble (or barely soluble) are by definition anti-solvents. The anti-solvents for each sample can easily be identified using the initial solubility screen. By using solvents in combination with anti-solvents the sample's solubility can be modified and supersaturation can be established within a closed system, making nucleation and crystal growth attainable.

Ideally the solvent used should provide moderate solubility for the sample. However, if this is not available, a solvent in which the sample has a high degree of solubility has to be used and consequently a stronger anti-solvent is required. The solvent and anti-solvent should be miscible but have distinct densities. This requirement facilitates the formation of a diffusion region, an area in which the solvent and anti-solvent are in contact but to a limited degree. An undesirable extent of mixing will occur if the two solvents have too similar densities. It is most helpful if the solvent with the dissolved sample has a higher density and volatility than the anti-solvent, allowing the anti-solvent to form the top layer within the glass vial. The system can be reversed but at the disadvantage of not being able to add more anti-solvent upon requirement.

If liquid diffusion experiments do not yield any crystals, they can readily be altered in an attempt to improve the crystallisation conditions. More anti-solvent can be added to ensure supersaturation is attained and temperature can easily be varied. However, care must be taken to ensure as little disturbance to the system as possible in order to avoid over-mixing of the two solvents.

#### **3.1.4| Crystallisation by Vapour Diffusion**

Vapour diffusion is a flexible technique suitable for small amounts of sample. Compared to liquid diffusion, vapour diffusion is a slower crystallisation technique which will aid the growth of more ordered, single crystals. If no crystallisation results, the glass vials containing the solvent/sample solution can easily be moved to a different anti-solvent, thus preventing sample from being wasted. As with liquid diffusion, it is preferable for the sample/solvent solution to be less volatile than the anti-solvent; however, it is less problematic in vapour diffusion if this is not the case.

### **3.1.5| Selecting and Harvesting a Crystal**

As briefly discussed in Section 2.3 there exist key indicators to aid selection of a suitable crystal for X-ray diffraction experiments. The shape of a crystal is the most immediate indicator of quality. Crystals with well defined edges and no 'satellite' crystals are preferred. 'Satellite' crystals cannot be removed from the surface of crystals, and therefore present no potential use in single crystal X-ray diffraction experiments. Except for a few cases (cubic crystals and tetragonal and hexagonal crystals if viewed along the c axis), crystals are birefringent. A crystal which displays even birefringence across the whole crystal when rotated under polarised light is likely to be highly ordered and therefore of appropriate quality. Often the equipment being used for X-ray diffraction experiments may influence the size of crystal required to produce a good data set. It is only through screening potential crystals (Section 3.5.2) that the required size of a particular crystal can be inferred.

To harvest a selected crystal a paper taper is used to transfer the crystal from the crystal growth medium (mother liquor) to a small amount of inert oil placed on a glass slide. Care should be taken to ensure the crystal remains intact. It is advantageous to transfer a crystal to a drop of inert oil (Fomblin), as often this provides a more viscous medium which aids the manipulation of crystals and helps secure the crystal once it is mounted and frozen in the Cryo stream. In some cases crystals grow as clusters from which a fragment may be broken off to produce a single crystal which may potentially be suitable for X-ray diffraction experiment. Clusters can be teased apart or fragmented using a needle or a paper taper which is less likely to cause destructive damage.

To mount the crystal onto the X-ray diffractometer for screening (Section 3.5.2), a glass fibre attached to a pin is used. The pin is then attached to the goniometer head ready for screening the crystal. Before the crystal was collected onto the glass pin the pin was approximately centred on the diffractometer. Care was taken to ensure a minimal amount of fomblin oil was collected with the crystal.

### **3.2| Protein Crystallisation**

Surfactants and solvents were of a laboratory reagent grade (unless stated otherwise) and were used as supplied: Span80 (Sigma), Brij30 (Sigma-Aldrich), Tween80 (Sigma-Aldrich), Aerosol-OT (AOT) (Fisher - general purpose grade), TritonX-100 (Fisher - Electrophoresis grade), TritonX-114 (Sigma-Aldrich), n-heptane (Fisher), cyclohexane (Fisher), 1-hexanol

(Sigma-Aldrich), sodium chloride (sigma  $\leq 99.5\%$ ). Lysozyme from chicken egg white, provided by Sigma-Aldrich (Fluka), was used for crystallisation experiments. Water was obtained from a *USF Elga Purelab* water purifier and purified to a resistivity of 18 M $\Omega$ cm.

### 3.2.1| Preparation of Hanging Drop Vapour Diffusion Trays

Hanging drop vapour diffusion trays for Lysozyme crystallisation were set up as shown in Table 3.1. A protein solution of 50 mgml<sup>-1</sup> Lysozyme in 0.1M NaAc pH 4.8 buffer was prepared and centrifuged using a desk-top centrifuge for three minutes to sediment any dust and/or non-dissolved Lysozyme. Stock reservoir solutions were prepared consisting of 10% (w/V) NaCl, 0.1M NaAc buffer of varying pH (pH 4.4, 4.8, 5.2, 5.6) and 25% (V/V) ethylene glycol. A volume of 1  $\mu$ l was used per drop and the wells were filled with 0.5 ml of reservoir solution. Each well was sealed using vacuum grease and a siliconised cover slip. Crystallisation trays were stored at room temperature.

	Ratio for Protein solution( $\mu$ l):Reservoir solution( $\mu$ l)	3:1	2:1	3:2	2:2	1:2	1:3
pH of Buffer solution	Well reference	1	2	3	4	5	6
4.4	A						
4.8	B						
5.2	C						
5.6	D						

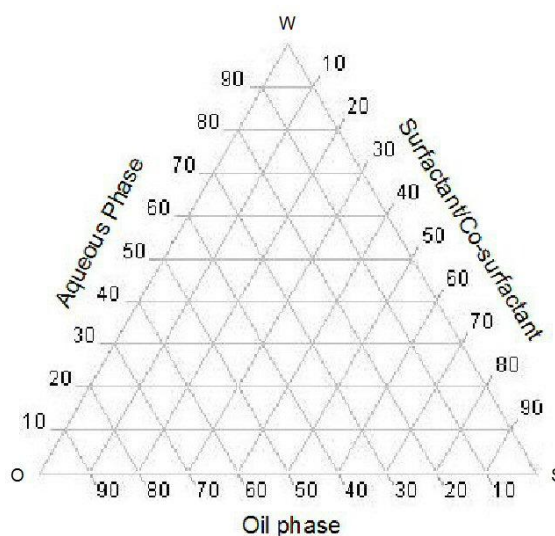
**Table 3.1|** Set up for 4x6 hanging drop vapour diffusion crystallisation tray.

### 3.2.2| Microemulsion Preparation

To date, the crystallisation of proteins using microemulsions to produce single crystals of an appropriate quality for X-ray diffraction experiments has not been explored. Previous work involving proteins and microemulsions includes the use of w/o AOT microemulsions as a medium to control aggregation of Ferritin<sup>166</sup>, a water soluble, iron storage protein, in order to produce discrete protein nanocrystals. Also, microemulsions have successfully been used as a reaction medium for the immobilisation of proteins to hydrophilised surfaces<sup>167</sup> and a means of separating protein mixtures<sup>168, 169</sup>.

### 3.2.2.1| Phase Diagrams

Conducted at room temperature, ternary phase diagrams (Figure 3.1) for different surfactant systems were made, varying the ratio (percentage by mass) of aqueous, oil and surfactant phases.



**Figure 3.1|** Ternary phase diagram used to select appropriate ratios of aqueous, oil and surfactant phases to give stable, transparent microemulsions.

For systems in which a co-surfactant was used the ratio of the two surfactant components remained fixed. Assessment was conducted visually noting a colourless, transparent, non-gel like solution to be a microemulsion. Table 3.2 gives the components used in each ternary phase diagram.

Aqueous Phase	Oil Phase	Surfactant/co-surfactant
H <sub>2</sub> O	Cyclohexane	TX-114
H <sub>2</sub> O	Cyclohexane	TX-100:1-hexanol (1:1 w/w)
5% (wt) NaCl by mass in H <sub>2</sub> O	Cyclohexane	TX-114
5% (wt) NaCl by mass in H <sub>2</sub> O	Cyclohexane	TX-100:1-hexanol (1:1)
0.1M NaAc pH 4.8	Heptane	Span80:Tween80 (1:1)
5% (wt) NaCl by mass is H <sub>2</sub> O	Heptane	AOT
H <sub>2</sub> O	Heptane	AOT

**Table 3.2|** Components of ternary phase diagrams.

### 3.2.2.2| Ionic Surfactant Systems

Test protein Lysozyme is an aqueous soluble, globular protein. Subsequently, to explore thermodynamic control of Lysozyme crystallisation via 3D nanoconfinement in microemulsions, water-in-oil microemulsions (Winsor II) are required. Following the successful application of microemulsions for Ferritin aggregation<sup>166</sup>, the use of AOT as a surfactant system provides a starting point for the application of microemulsions for Lysozyme crystallisation.

Stock solutions of 10% (wt) and 5% (wt) of AOT in heptane were prepared and sonicated for one hour to ensure all AOT was dissolved and a homogenous solution was formed. To explore the amount of aqueous phase that could be confined within the surfactant/continuous phase and to serve as a control experiment, varying amounts of pure water (10-100  $\mu$ l) was added to varying volumes of surfactant/continuous phase solution (0.5-5 ml). A ternary phase diagram was generated at room temperature to aid the determination of a suitable ratio of surfactant/continuous to aqueous phase. Upon addition of the aqueous phase to the surfactant/continuous phase the sample was shaken by hand or vortexed to facilitate the complete dispersion of the aqueous phase. In some cases where shaking and vortexing appeared insufficient, the sample was placed in a sonicator bath set at room temperature to form, in successful cases, a transparent, single phase microemulsion.

Moving forward, stock solutions of varying Lysozyme concentrations (5-50 mgml<sup>-1</sup>) were made using solvents of pure water and four different buffer solutions of 0.1 M NaAc with varying pH (4.6, 4.8, 5.2 and 5.6). Lysozyme solutions were stored in the fridge at 4°C and were not sonicated in order to prevent denaturing the protein by the potential localised increase in temperature<sup>170</sup>. Aliquots of Lysozyme solution were added to the surfactant/continuous phase, vortexed or sonicated, and then stored at room temperature. A series of experiments were conducted to explore the effects of varying the ratio of dispersed (aqueous) phase to surfactant/continuous phase, the concentration of Lysozyme and the aqueous buffer used. The same microemulsion preparation method was used for each surfactant system used as detailed in below sections.



### **3.2.2.3| Non-ionic Surfactant Systems**

As previously mentioned, thermodynamic control of crystallisation has been successfully demonstrated with the crystallisation of glycine polymorphs<sup>4</sup>. This was achieved using a surfactant system of Span80:Brij30 in a 1:1 ratio dissolved in heptane to make a 40% (wt) surfactant solution. Subsequently both Span80:Brij30 and Span80:Tween80 surfactant systems were applied to Lysozyme crystallisation experiments. This would also enable a comparison to be drawn between non-ionic surfactant systems and ionic (AOT) surfactant systems in the use for Lysozyme crystallisation.

Batch solutions of Span80:Brij30 in a 1:1 ratio 40% (wt) in heptane and Span80:Tween80 in a 1:1 ratio 20% (wt) in heptane were prepared and sonicated for two hours and left to settle for 24 hours to allow the homogeneous surfactant solution to return to room temperature. As with the AOT surfactant system, a phase diagram and a series of experiments were conducted to explore the affects of several variables including the ratio of dispersed (aqueous phase) to surfactant/continuous phase, the concentration of Lysozyme and the aqueous buffer.

Further exploring the use of non-ionic surfactant systems, both TritonX-100 (TX-100) and TritonX-114 (TX-114) were used. The TX-100 surfactant required the use of a co-surfactant, 1-hexanol, in order to form stable w/o microemulsions. A 1:1 ratio of surfactant to co-surfactant was used for TX-100, and for both TX-100 and TX-114, cyclohexane was used as the continuous phase. Appropriate ratios of water:surfactant/co-surfactant:oil were noted from the phase diagrams and samples of these ratios were made in which the water was replaced by a solution of Lysozyme in water of varying concentrations for both TX-100 and TX-114 .

### **3.2.2.4| Methods for Further Facilitating Crystallisation in Microemulsions**

As with other crystallisation methods, it is sometimes found that addition of an anti-solvent, also known as a precipitant, is required to bring the solution into supersaturation to enable nucleation and subsequent crystal growth. To apply this to the microemulsion method, several approaches were employed using solutions of sodium chloride (NaCl) as the anti-solvent.

The direct addition of bulk solutions was used to first establish an approximate ratio of protein to anti-solvent solutions that would bring the protein concentration into

supersaturation and facilitate crystal growth as detailed in Table 3.3. The ratio was then applied to microemulsions by directly adding an aliquot of anti-solvent solution directly to the microemulsion and mixing the two together via vortexing.

	[NaCl] (% wt)	500 $\mu$ l Lysozyme 50 mgml <sup>-1</sup> in water	500 $\mu$ l Lysozyme 50 mgml <sup>-1</sup> in water	500 $\mu$ l Lysozyme 50 mgml <sup>-1</sup> in 0.1M NaAc pH 4.8	500 $\mu$ l Lysozyme 50 mgml <sup>-1</sup> in 0.1M NaAc pH 4.8
Volume of NaCl solution ( $\mu$ l)	5	500	1000	500	1000
	10	500	1000	500	1000
	15	500	1000	500	1000
	20	500	1000	500	1000

**Table 3.3** | Direct addition of anti-solvent solution (NaCl solution) to bulk Lysozyme solution of concentration 50 mgml<sup>-1</sup>.

An alternative, mixed microemulsion method was also used in an attempt to introduce anti-solvent into the system. Mixed microemulsions have previously been used in the crystallisation of glycine in which methanol was used as the anti-solvent<sup>4</sup>. Phase diagrams incorporating different concentrations of an anti-solvent solution as the dispersed aqueous phase were established for each surfactant system. Both Lysozyme microemulsions and anti-solvent microemulsions were separately made then directly mixed together and vortexed. Again, the ratio of Lysozyme solution to anti-solvent solution was applied to the mixed microemulsion method where possible. In some cases, ratios of the three microemulsions components for the anti-solvent system that lay just outside the region in which a microemulsion was formed were also used. This explored the possibility that the mixing of a Lysozyme microemulsion with an anti-solvent emulsion or nano-emulsion may form a microemulsion overall.

In the absence of anti-solvent, a method in which the continuous phase was evaporated was used. The mass of the microemulsion was taken before and after the evaporation of continuous phase and the volume of the microemulsion was allowed to reduce by approximately two thirds, as judged by eye. Evaporation experiments were conducted in a fume hood 48 hours after the microemulsions had been made.

### 3.3| Microemulsion Droplet Size Determination

SAXS and subsequent GIFT analysis were used to confirm the formation of microemulsions in samples of each surfactant system by determining the droplet size. Sample that diffract and have droplet sizes within 1-100 nm are considered to be microemulsions.

#### 3.3.1| Geometric Calculations

An estimate of the microemulsion droplet radius can be made using geometrical calculations. When the composition of the microemulsions is known, Equation 3.1 can be used to predict the droplet radius, where  $\phi$  is the dispersed volume fraction,  $c_s$  is the number of surfactant molecules per unit volume and  $\Sigma$  is the area per surfactant molecule<sup>78</sup>.

$$R = \frac{3\phi}{c_s \Sigma} \quad (3.1)$$

Geometric calculations of microemulsion droplet radius assume that all the surfactant/co-surfactant molecules sit at the oil-water interface and that each of them occupies a well-defined area, independent of the microemulsion's composition.

#### 3.3.2| X-ray Scattering Experiments for Microemulsions: SAXS

Small Angle X-ray Scattering (SAXS) can be used to determine the size of droplets within microemulsion samples experimentally, and confirm whether 3D nanoconfinement has been achieved. SAXS data was collected using a Brucker Nanostar SAXS machine operated at 40 kV and 35 mA to produce Cu K $\alpha$  radiation with a wavelength of 1.54 Å. The machine was fitted with a Hi-star 2D detector at a distance of 65 cm and had cross coupled Gobel mirrors and pinhole collimation for point focus geometry.

Microemulsion samples were inserted into the sample chamber via a sealed 2mm, vacuum tight quartz capillary and the chamber evacuated to a pressure of 10<sup>-1</sup> mbar. It is important for the capillary to be positioned correctly at a point where minimal transmission occurs. The ideal positioning of the capillary can be ensured using the Gadds program Radiography/nanography run with the attenuator in the dropped position. A data collection can be made once the sample stage has been set to the ideal position and the attenuator returned to the lifted position. The time taken to collect sufficient SAXS data can easily be

changed and depends on the nature of the sample. The duration of the SAXS experiment should be modified in order to gain a good signal to noise ratio. For each surfactant system, SAXS data was collected for 2 hours.

### 3.3.3| Generalised Indirect Fourier Transform (GIFT)

SAXS data collected from a dilute solution can be directly related to the scattering particles using an indirect Fourier transformation. However, for more concentrated solutions, evaluation of SAXS data diverges away from a solution to a linear weighted least-squares problem. This is due to the resultant scattering intensity including both intra- and inter-particle scattering contributions. Unlike dilute solutions, particle interactions have to be taken into consideration and it can no longer be assumed that the average distance between particles is much greater than the dimensions of the particles themselves<sup>171</sup>.

Scattering from isolated particles, as found in dilute solutions, can be expressed by the form factor,  $P(q)$ , where  $q$  is the length of the scattering vector, which describes intra-particle scattering. The structure factor,  $S(q)$ , corresponds to the inter-particle scattering. Under certain conditions, the product of the form factor and the structure factor can be used to approximate the total scattering intensity,  $I(q)$  (Equation 3.2). In these cases evaluation of the scattering data becomes a non-linear problem<sup>171</sup>.

$$I(q) = P(q)S(q) \quad (3.2)$$

For concentrated solutions, it is important not to neglect inter-particle interactions as the influence of the corresponding structure factor can readily be seen in the experimental data through the deviation of the scattering curve from the ideal particle scattering curve at low  $q$  values. Also, scattering intensity decreases at low  $q$  values due to repulsive interactions between particles. Oscillations in the pair distance distribution function may result from these deviations at low  $q$  values, leading to incorrect evaluation of the experimental scattering data.

The structure of aggregates in solution is dependent on the concentration of amphiphilic molecules. It is therefore not possible to eliminate the influence of inter-particle interactions by conducting SAXS experiments at several concentrations and then extrapolating the scattering data to a concentration of zero. Consequently, a global technique for the evaluation of SAXS data was developed that allows the simultaneous determination of the form factor and the structure factor through the use of an algorithm to

solve the non-linear least squares problem. The technique developed, known as generalised indirect Fourier transformation (GIFT)<sup>171</sup>, is possible due to the different analytical behaviour of the two functions for the form and structure factors. GIFT does not use models or analytical restrictions for the determination of the form factor. However, the determination of the structure factor is parameterised. For a particular particle interaction model, up to four parameters (including volume fraction, polydispersity, radius and effective charge) can be utilised.

The pair distance distribution function,  $p(r)$ , which can be obtained by the Fourier transform of the scattering curve, measures the probability, weighted by the electron density contrast, of finding a distance  $r$ , within the scattering particle. Hence  $p(r)$  falls to zero at the largest dimension of the scattering particle. The scattering data will fit one of several models; the model can be inferred from the shape of the  $p(r)$  function. For a core shell model, the  $p(r)$  function will have minima corresponding to regions of electron density of alternating sign, often relating to differences in the electron densities of the inner phase, the surfactant and the continuous phase. The  $p(r)$  function for the hard sphere model has no minima and results due to there being negligible difference in the electron densities of the surfactant tail groups and the continuous phase. If there is only a very slight difference between the electron densities of the surfactant tails and the continuous phase, the surfactant tails may not be effectively seen by SAXS due this difference being negligible and there may be partitioning of the oil continuous phase among the surfactant tails.

GIFT analysis has been successfully applied to many cases including an investigation into various intrinsic parameters that influence structural variation of reverse micelles in non-ionic surfactant/oil systems<sup>172</sup>. Within the investigation detailed in this thesis, GIFT analysis is applied to determine the droplet size of reverse micelles to confirm the formation of microemulsions in systems used to attempt crystallisation of Lysozyme.

### **3.4| Optical Microscopy**

Optical microscopes enable the magnification of small objects using visible light and a lens system. Typically, this is an appropriate means of clearly viewing crystals which is aided by the use of filters to polarise light, highlighting the birefringent nature of crystals. Materials that appear birefringent which have a refractive index dependent on the polarisation and propagation direction of light. Optical microscopes were used to monitor crystal growth, aid initial solubility screens for small molecule crystallisation, harvest crystals for X-ray

diffraction experiments and to capture images of crystals. Both a Leica MZ16 and Leica M165C were used to do this.

### **3.5| X-ray Diffraction Experiments for Single Crystals: X-ray Crystallography**

Upon selection of a high quality single crystal, X-ray diffraction experiments were conducted as a means of further differentiating the quality of crystals grown using microemulsions. The quality of data obtained from crystals grown using microemulsions was compared to the quality of data sets collected from crystals grown using standard vapour diffusion methods.

#### **3.5.1| Harvesting a Crystal**

Upon selection of potential crystal(s) (Section 3.1.5), taking into consideration the quality of crystal, a method for extracting the crystals from their growth environment has to be established. The method of extraction used depends on the type of experimental setup. Individual wells from hanging drop vapour diffusion trays can be independently selected; the cover slip can then be turned over and placed on a suitable stage (typically the lid of the hanging drop tray). The crystal(s) can then be directly harvested from the crystallisation drop. If more than one crystal is present in a drop, the cover slip can be returned to the hanging drop tray and the system resealed, ready for harvesting a crystal for a later experiment. Harvesting crystals grown via microemulsions required a less direct approach. Due to the depth of the glass vials which contained the microemulsions, crystals could not be independently and directly selected from the bottom of the glass vial. Aliquots of the microemulsion/crystal mixture were taken by gently drawing up a sample from the bottom of the glass vial using a Pasteur pipette to which the opening had been increased by breaking off the bottom glass part (care was taken to prevent contamination with glass shards/dust). The aliquots were then deposited on a glass slide from which crystals could be selected and directly harvested.

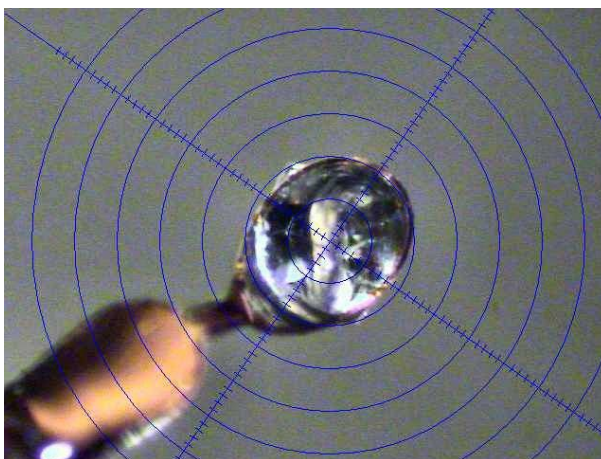
Crystals selected were then screened on a diffractometer. This required crystals grown from both hanging drop vapour diffusion trays and microemulsions to be harvested using a CryoLoop<sup>173</sup>. The size of the CryoLoop was selected to accommodate the size of the crystal. Typically a 0.4-0.5 mm CryoLoop was required. Care was taken to include a minimal amount of solution that surrounded the crystal when picking up the crystal in the CryoLoop.

Some liquid is required to secure the crystal once it has been frozen in the Cryo stream, however an excess should not be used to avoid interference with diffraction.

### 3.5.2| Screening a crystal

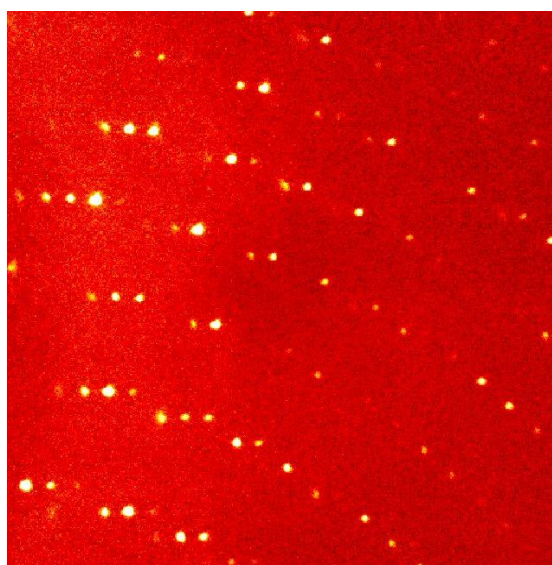
Screening on the diffractometer<sup>174</sup> can be used to indicate the diffraction quality of the crystals. This is required as, although in some cases a crystal appears of a good quality under the microscope it may diffract poorly and vice versa, a crystal which visually appears to be a poor quality crystal may in fact diffract well.

Before picking up the selected crystal, the head of the CryoLoop was roughly centred on the diffractometer using the attached camera. This ensured that once mounted onto the goniometer the crystal was likely to be directly in the Cryo stream and be in a good starting position for the crystal to be centred. Centring (Figure 3.2) the crystal required finding the crystal's centre of gravity. This ensures the crystal remains in the path of the X-ray beam at all times by preventing the crystal from slipping or becoming dislodged when rotated. To centre the crystal, small pins on the goniometer head were used to alter the position of the CryoLoop while rotating through  $\varphi$  at an  $\Omega$  angle of  $60^\circ$ .



**Figure 3.2|** Centring a crystal, approximately 0.5 mm x 0.4 mm x 0.3 mm in size, is aided through use of the attached camera which gave rise to this image.

To screen the crystals for diffraction quality single frames of widths  $1^\circ$  and  $0.5^\circ$  were taken at angles  $\varphi$  of  $0^\circ$  and  $90^\circ$ . An exposure time of 10 seconds was adequate for the testing of Lysozyme crystals grown from both hanging drop vapour diffusion trays and from microemulsions. Exposure times can be varied to give reflections of an appropriate intensity that do not exceed the limits of the detector. An idea of diffraction quality can be obtained from the diffraction image (Figure 3.3); ideally reflections are bright, have well defined edges and are not doubled as this would indicate that the crystal is not a single crystal. Data should not be collected from crystals that diffract poorly.



**Figure 3.3 |** A diffraction image can give an initial idea of the quality of diffraction from a single crystal by considering the brightness and shape of the diffraction spots.

An orientation matrix was determined for the first crystals grown from a hanging drop vapour diffusion tray and from microemulsions that diffracted well enough to warrant collecting a data set from. This process enabled the unit cell of the crystals to be determined by determining the matrix function. The matrix function relates the real-space unit cell of the crystal to the reciprocal lattice.

The determination of the crystal unit cell is an important piece of information to initially obtain. Through collecting sufficient data in order to determine the unit cell it is possible to infer the ability of the crystal to diffract well at a variety of  $\varphi$  and  $\Omega$  angles and also the crystal's ability to retain sharp and intense reflections as initially observed through the screening of the crystal. For collection of data in the aim of solving the crystal structure, knowledge of the unit cell aids the design of the data collection in order to gain a data set which is complete. If there is doubt to the correct unit cell, data collection should be



designed assuming that the correct unit cell is the one with the lowest symmetry. This will reduce the possibility of collecting an incomplete data set which would have limited benefits.

### **3.5.3| Data collection and Processing**

A Bruker MicroStar diffractometer was used for the screening of crystals and for data collection of crystals grown from both hanging drop vapour diffusion and microemulsions. X-ray radiation was sourced from a copper rotating anode and the diffractometer was set up with a Helios mirror monochromator system and a Platinum 135 CCD area detector. The diffractometer was operated at 40 kV and 60 mA.

The same data collection strategy was used for all Lysozyme crystals consisting of a range of  $\varphi$  and  $\Omega$  scans. An exposure time of 30 seconds was used. A manual design of the data collection strategy was sufficient to achieve a complete data set. However, if required, there is data collection strategy software which can be utilised to design a complete diffraction experiment with an appropriate redundancy. Redundancy is the term used to describe repeated collection of equivalent reflections. The software also gives an estimated time of completion taking into consideration the exposure time for each frame.

Upon completion of a data collection the data is merged, integrated and scaled using SAINT and automatic absorption corrections are made using SADABS. Following this initial processing, XPREP<sup>175</sup> is used to examine the systematic absences in the reflection data and determine the space group of the crystal. For the Lysozyme crystals, data processing was not taken any further and statistical values were compiled for each data set.

# Chapter Four

---

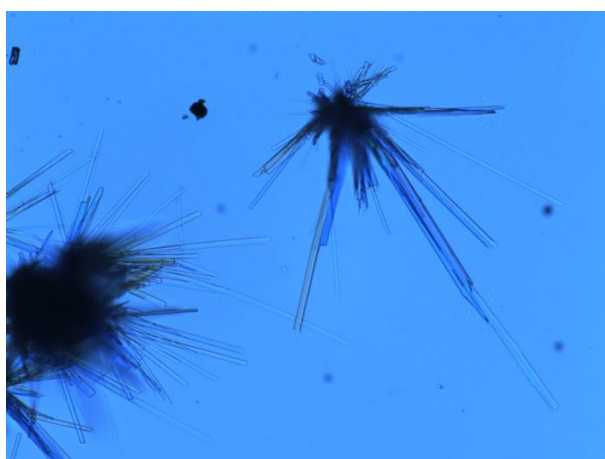
## *Results*

### **4.1 | Chemical Crystallisation**

The following sections (Section 4.1.1 – 4.1.8) details the crystallisation results for compounds described in Appendix A2. The methods for the crystallisation of these compounds are discussed in Sections 3.1.1 – 3.1.4.

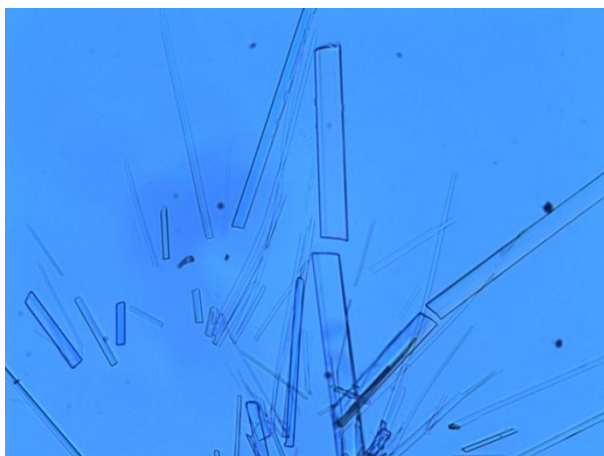
#### **4.1.1 | Crystallisation of ASH89**

The sample of ASH89 provided appeared birefringent under polarised light, was off-white in colour and no prediction of crystal habit could be made from the bulk sample. An initial solubility screen showed ASH89 to be soluble in methanol, acetonitrile, ethanol, DMSO, ethyl acetate and chloroform and partially soluble in ethylene glycol, cyclohexane, 1-pentanol, heptane, 1-hexanol and decane. Although the sample was soluble in several solvents, not all were suitable for crystal growth. For example, when dissolved in both methanol and acetonitrile, oil was produced upon evaporation of the solvents.



**Figure 4.1 |** Clusters of ASH89 crystals grown via evaporation of solvent, ethylene glycol. Needles were thin, approximately a width of <10  $\mu\text{m}$ .

After three days at room temperature crystal growth was observed on the initial solubility screen slide for the sample dissolved in ethylene glycol and in DMSO. In DMSO a network of fine, wispy needles were formed from which no single crystal could be isolated. The formation of disordered crystals may be due to too rapid crystal growth upon a high rate of solvent evaporation. When dissolved in ethylene glycol, crystals of the tri-peptide grew in clusters of needles (Figure 4.1). The clusters were small, with needles approximately 10  $\mu\text{m}$  in width and 50  $\mu\text{m}$  in length. Clusters of crystals are not suitable for X-ray diffraction experiments; therefore a paper taper was used to separate the clusters to try and isolate a single crystal needle (Figure 4.2). Upon dispersion of the needle cluster, fragments of needles, which may potentially be suitable for X-ray diffraction experiments, were selected and carefully transferred to a drop of inert oil, Fomblin.



**Figure 4.2|** Cluster of ASH89 crystals that has been separated using a paper taper in an attempt to isolate single crystal needle for X-ray diffraction experiments.

Needles were thin, approximately a width of <10  $\mu\text{m}$ .

Screening of the crystals found them to diffract weakly. Two crystal needles were tested but both were probably not of sufficient size. Testing the crystals on intense synchrotron beamlines available at resources such as Diamond Light Source LTS may have given better results for structure determination.

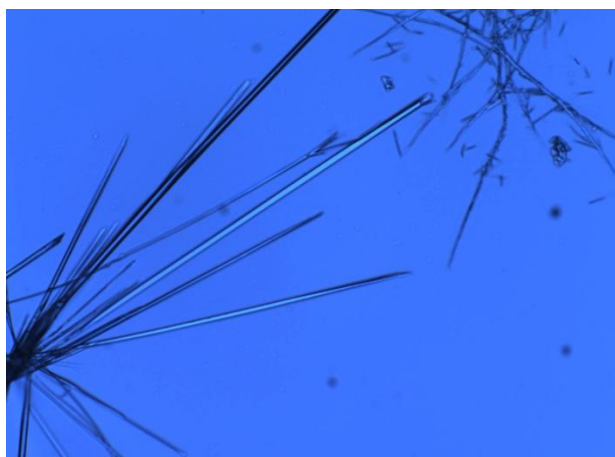
Attempts were made to grow larger crystals which may be suitable for X-ray diffraction experiments. Firstly, attempts were made to form a larger volume of ASH89 saturated ethylene glycol solution by using a glass well plate in which larger volumes of solvent could be used. A supersaturated solution was achieved in 6  $\mu\text{l}$  of ethylene glycol and again clusters of needle crystals were observed at the edge of the drop with the tip of the

needles protruding towards the centre of the drop. The needles present in the clusters grew length ways to a greater extent than those observed in the initial solvent screen; however, the width of the crystals was still too limiting for good quality diffraction. Another saturated drop of ethylene glycol was prepared and seeded with a needle originally grown for the initial solvent screen; a crystal which appeared to have the largest width was selected. This however did not lead to single crystal growth but clusters.

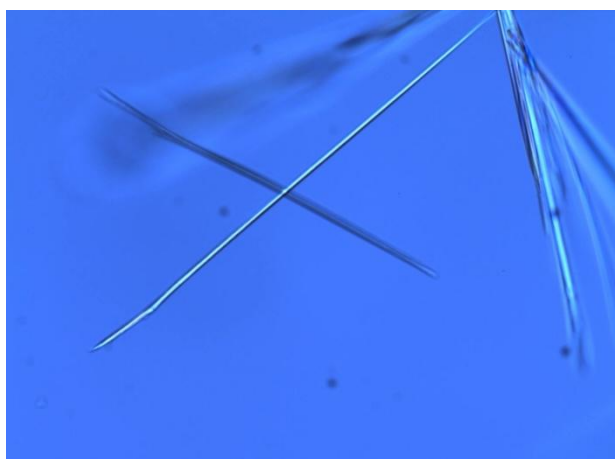
#### **4.1.2| Crystallisation of ASH81/87**

The sample of ASH81/87, a white crystalline material, was observed to be soluble in methanol, acetonitrile, ethanol, DMSO, 1-pentanol, ethyl acetate and insoluble in water, cyclohexane, decane, hexane and toluene. Partial solubility was observed in ethylene glycol and 1-hexanol. As expected not all solvents lead to re-crystallisation of the compound upon evaporation of the solvent. Oil was formed upon evaporation of 1-pentanol, heptane and ethyl acetate. Two of solvents, ethanol and DMSO, gave a crystalline material from the evaporation of solvent leaving a ring of crystalline material on the initial solvent screen glass slide. Although crystalline, no single crystals were observed and crystal habit could not be predicted from the material gained from DMSO. However, the ring of crystalline material left upon evaporation of ethanol appeared to be in clusters of very small, thin needles, giving an indication of the compound's potential crystal habit.

Needles were grown from the drop of ethylene glycol on the initial solubility screen glass slide stored at room temperature. The crystals grew in clusters of thin needles, less than 10  $\mu\text{m}$  in width, after 36 hours. At this point the clusters of needles were extremely small; the slide was therefore left for a further two days at room temperature. This led to further lengthwise growth of the crystal needles in the clusters but no change in the width of the crystals was observed (Figure 4.3). The larger crystal clusters were carefully teased apart using acupuncture needles resulting in the isolation of single needles approximately 70  $\mu\text{m}$  in length (Figure 4.4). Several attempts to isolate single crystals were required, rapidly depleting the number of potential crystals for experiment as the needles were extremely brittle and fractured effortlessly.



**Figure 4.3 |** Cluster of ASH81/87 needle crystals grown via evaporation of ethylene glycol at room temperature for three and a half days. Needles were very thin, approximately 5  $\mu\text{m}$ .



**Figure 4.4 |** An isolated needle of ASH81/87 grown via evaporation of ethylene glycol at room temperature for three and a half days. Needles were very thin, approximately 5  $\mu\text{m}$ .

Larger volumes of saturated ASH81/87 solutions in ethylene glycol were prepared in a glass well plate. Crystal growth was observed as seen on the initial solvent screen slide; clusters of needles grew over five days. There was little difference in the size of the clusters of needles, however more clusters were grown. Clusters were transferred to inert oil and attempts were made to isolate single needles for screening. Using single needles grown in the glass well plate from ethylene glycol, two saturated solutions were seeded. In ethylene glycol no single crystal growth occurred and the expected clusters of needles resulted. Seeding a saturated solution of ASH81/87 in DMSO resulted in the growth of numerous clusters of insignificant size for experimental use.

#### **4.1.3 | Crystallisation of ASH82**

The initial solvent screen for ASH82, a birefringent compound, showed the compound to be soluble in a limited number of solvents including acetonitrile and ethyl acetate. Partial solubility in toluene, 1-pentanol and 1-hexanol was observed and the compound was insoluble in water, methanol, ethanol and decane. On the glass slide used for the initial screen, evaporation of acetonitrile led to the formation of a mesh of long, thin, fibre-like crystals. ASH82 displayed a low solubility in toluene; however addition of the bulk sample to toluene lead to a separation of the material into what appeared to be single needles. These needles were far too small and fragile for analysis by X-ray diffraction.

Evaporation of 100% acetonitrile in a glass well plate lead to the same result as observed in the initial solvent screen. The mesh of fibre-like needles was transferred to another drop of acetonitrile and re-dissolved. Re-crystallisation did not occur. Similarly, crystal growth was not facilitated by evaporation of 100% toluene. Evaporation experiments were set up using a mixture of acetonitrile and toluene in ratios 1:1, 1:2 and 1:3. No single crystal growth resulted; therefore attempts were made to slow the rapid and abundant nucleation using liquid diffusion experiments. Water and decane were used as anti-solvents for ASH82 dissolved in acetonitrile. A 2:5 ratio of solvent to anti-solvent was used. After three weeks, no crystal growth had occurred for each of the liquid diffusion experiments; the solutions were allowed to evaporate, but still no crystal growth occurred.

#### **4.1.4 | Crystallisation of ASH90**

No crystal habit of ASH90, a birefringent solid, could be inferred upon initial observations under an optical microscope. The initial solvent screen found ASH90 to be soluble in acetonitrile, DMSO, and ethyl acetate, and partially soluble in 1-pentanol. Potential anti-solvents may be selected from water, methanol, ethanol, ethylene glycol, cyclohexane, heptane, 1-hexanol, decane and hexane, in all of which ASH90 was observed to be insoluble. No crystal growth was observed for solvents in which ASH90 was readily soluble. Upon evaporation of 1-pentanol a ring of birefringent material was left deposited on the glass slide. No crystal habit could be predicted.

The liquid diffusion method was applied using a 2:5 ratio of ethyl acetate to hexane. However, very small clusters of needles were formed in a gel like manner which grew on the

side of the glass wall. This indicated that the compound was likely to crystallise in a bad habit unsuitable for structure determining X-ray diffraction experiments.

#### **4.1.5 | Crystallisation of ASH93**

A 3 mg sample of ASH 93, a white crystalline compound, was provided for crystallisation and subsequent structure determination. Potential anti-solvents were found to be water, methanol, ethanol, cyclohexane, 1-pentanol, hexane, heptane and decane. The compound was found to be soluble in a limited number of solvents including acetonitrile, DMSO, and ethyl acetate. Solutions of ASH93 in these three solvents were prepared in small glass vials with the lid partially open in attempt to slow evaporation rate. No crystal growth was observed for experiments conducted at room temperature and at 4 °C.

Vapour diffusion experiments were tested for each solvent using methanol, 1-pentanol, cyclohexane and decane as an anti-solvent. This was an advantageous method for the small amount of material provided, requiring only three solutions of ASH93 which could easily be transferred to each of the anti-solvents. The vapour diffusion systems were closed and left for three days with each anti-solvent; however, no crystal growth resulted.

#### **4.1.6 | Crystallisation of ASH91**

The sample of ASH91 provided (2 mg) displayed a limited solubility in the solvents used in the initial solvent screen. Partial solubility was observed in acetonitrile, ethylene glycol (when gently heated), DMSO and ethyl acetate. DMSO was found not to be a promising solvent for crystal growth as evaporation of the solvent left an oily residue behind on the glass slide. Evaporation of both acetonitrile and ethyl acetate left a small ring of a birefringent material, from which no deduction of the crystal habit could be made. The ethylene glycol drop did not yield any crystals.

A similar approach was taken to that used in attempts to crystallise ASH93. Vapour diffusion experiments were set up for the two solvents and these were screened against each of the anti-solvents. Initially a 2:5 ratio of solvent to anti-solvent was used, but this did not yield any crystal growth, leading to the trial of a 2:9 ratio. Crystal growth did not occur through vapour diffusion experiments.

#### **4.1.7 | Crystallisation of ASH59**

ASH59 was observed to be soluble in mainly polar solvents including methanol, acetonitrile, ethanol, DMSO, 1-pentanol, and ethyl acetate. ASH59 also showed partial solubility in larger alcohol solvents such as 1-hexanol. Potential anti-solvents were observed to be water, cyclohexane, heptane, decane and toluene. No crystal growth was observed from the initial solvent screen, and evaporation of methanol, acetonitrile, and 1-pentanol left a deposit of oil.

Evaporation experiments were conducted in a glass well plate with 20  $\mu$ l of 100% DMSO which lead to the growth of clusters of needles that aggregated together as more solvent evaporated. This experiment was repeated and a cluster of needles removed and transferred to a drop of inert oil before aggregation of clusters prevented their isolation. Unfortunately, no single needle crystal of sufficient quality and size could be separated from the clusters for analysis by X-ray diffraction. No evaporation experiments were conducted for methanol or ethanol as at room temperature these solvents evaporate too quickly.

Vapour diffusion experiments were set up for ASH59 dissolved in both methanol and acetonitrile, exploring several anti-solvents including water, cyclohexane and heptane. After two weeks no crystal growth was observed. Unfortunately, despite considerable effort, no crystals for ASH59 have yet been obtained for X-ray diffraction experiments.

#### **4.1.8 | Crystallisation of GDL02, GDL38 and GDL39**

Three birefringent compounds, GDL02, GDL38 and GDL39, yellow orange, yellow and orange in colour respectively, were provided for crystallisation and subsequent structural studies. All three compounds displayed similar results in the initial solubility screens, typically soluble in methanol, acetonitrile, ethanol, ethylene glycol, DMSO and toluene. Partial solubility was observed in water, ethyl acetate, 1-pentanol and 1-hexanol while typically the compounds were insoluble in cyclohexane, hexane, heptane and decane. Some variations in the solubility profiles of each compound were observed; GDL02 was insoluble in water, ethylene glycol and DMSO; GDL38 was partially soluble in toluene and GDL39 was soluble in ethylene glycol and 1-pentanol.

No crystallisation was observed on the initial solvent screen glass slides for each of the three molecules. However, when GDL02 was added to a drop of 1-hexanol, although only slightly soluble, small platelets with ill defined edges that had an oily appearance



appeared to grow out from the material that had not been dissolved. Evaporation of 25  $\mu$ l 1-hexanol in a glass well plate resulted in the formation of an oil upon evaporation of the solvent.

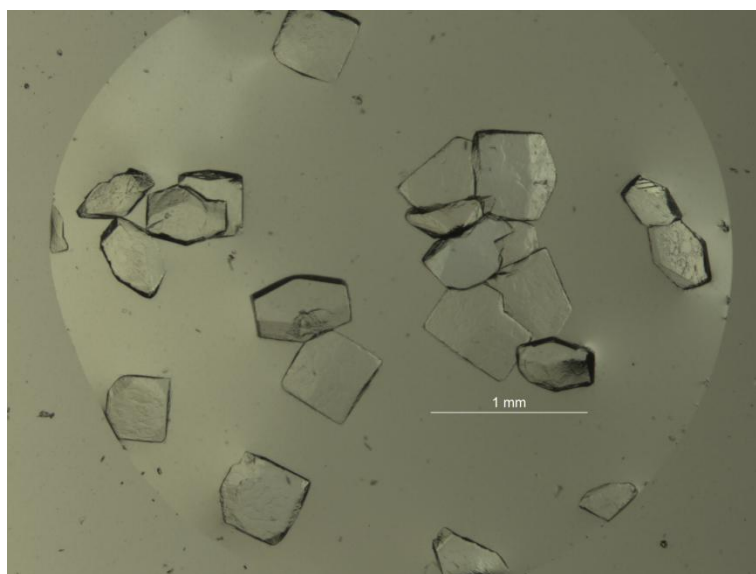
#### 4.2. | Protein Crystallisation from Hanging Drop Vapour Diffusion Trays

Crystals were observed in several drops of the crystallisation tray twelve hours after set-up. The differing conditions (pH of the reservoir solution and ratio of protein solution to reservoir solution in the hanging drop) resulted in different crystallisation outcomes including variation in the size and quality of crystals grown and the number of crystals grown per drop. After initial observation of crystal growth, the trays were stored at room temperature for a further 48 hours to allow the crystals present to grow larger. Crystallisation results from hanging drop vapour diffusion trays are summarised in Table 4.1.

pH of Buffer solution	Ratio for Protein solution( $\mu$ l):Reservoir solution( $\mu$ l)					
	3:1	2:1	3:2	2:2	1:2	1:3
4.4	Two, medium, single crystals.	Two, medium, single crystals.	Two, large, single crystals.	Some crystalline material.	No crystals	No crystals
4.8	Some crystalline material.	No crystals	No crystals	Large, single crystal.	No crystals	No crystals
5.2	Large, single crystal. Figure 4.6	No crystals	No crystals	No crystals	No crystals	No crystals
5.6	Multiple, small, single crystals. Figure 4.5	Multiple, small, single crystals.	No crystals	Some crystalline material.	No crystals	No crystals

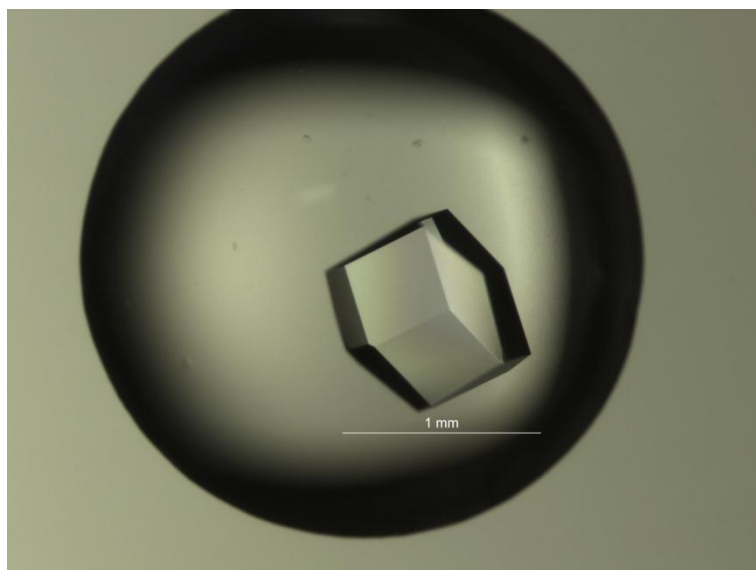
**Table 4.1 |** Crystallisation outcome of hanging drop vapour diffusion crystallisation tray stored at room temperature for 48 hours. The pH of the buffer solution and the protein to buffer solution ratio in the hanging drops were varied.

Several of the drops were unsuccessful and no crystallisation resulted from vapour diffusion. Also, despite the occurrence of crystallisation in some of the drops, the crystalline material that resulted was not suitable for single crystal X-ray diffraction experiments. Drops with a pH of 5.6 and a 3:1 drop ratio of protein solution to reservoir solution resulted in the crystallisation of numerous small crystals which lacked the defined shape and edges required for the collection of a good X-ray diffraction data set (Figure 4.5).



**Figure 4.5 |** Crystallisation outcome from hanging drop vapour diffusion tray in a well with reservoir solution of pH 5.6 and a hanging drop ratio of 3:1 of protein solution to reservoir solution.

Single crystals were grown to a large size, approximately 500  $\mu\text{m}$  x 750  $\mu\text{m}$ , from several drops in the crystallisation tray. These crystals had well defined edges and displayed birefringence under polarised light (Figure 4.6).



**Figure 4.6|** Crystallisation outcome from hanging drop vapour diffusion tray in a well with reservoir solution of pH 5.2 and a hanging drop ratio of 3:1 of protein solution to reservoir solution.

Three repeats of the hanging drop vapour diffusion crystallisation tray were made and large, single crystals were harvested from wells of pH4.8 (drop ratio, 2:2) and wells of pH4.4 (drop ratio, 3:2) for X-ray diffraction experiments (the results of which are discussed in Section 4.6).

### 4.3| Bulk Anti-solvent Experiments

Varying concentrations of NaCl solution (% by mass) were added to bulk 50 mgml<sup>-1</sup> Lysozyme solutions in 1:1 and 1:2 ratios of Lysozyme solution to NaCl solution. The crystallisation results of these bulk experiments are summarised in Table 4.2.

[NaCl] (% by mass)	50 mgml <sup>-1</sup> Lysozyme in water: NaCl solution		50 mgml <sup>-1</sup> Lysozyme in 0.1M NaAc, pH 4.8: NaCl solution	
	1:1	1:2	1:1	1:2
1%	No crystal growth	No crystal growth	No crystal growth	No crystal growth
5%	Crystal growth	Crystal growth	Crystal growth	Crystal growth
10%	Amorphous solid	Amorphous solid	Crystal growth	Amorphous solid
20%	Amorphous solid	Amorphous solid	Amorphous solid	Amorphous solid

**Table 4.2|** Crystallisation results from bulk anti-solvent experiments.

A 10-20% NaCl solution led to the rapid formation of a white amorphous solid when added to the Lysozyme solutions in both 1:1 and 1:2 ratios. However, crystal growth was observed when 10% NaCl was added in a 1:1 ratio to the Lysozyme in 0.1M NaAc, pH 4.8 solution. The crystalline material grew quickly and was therefore disordered and irregular in shape. The addition of 1% NaCl solution did not facilitate crystal growth suggesting that supersaturation of the Lysozyme solution was not reached with this low NaCl concentration.

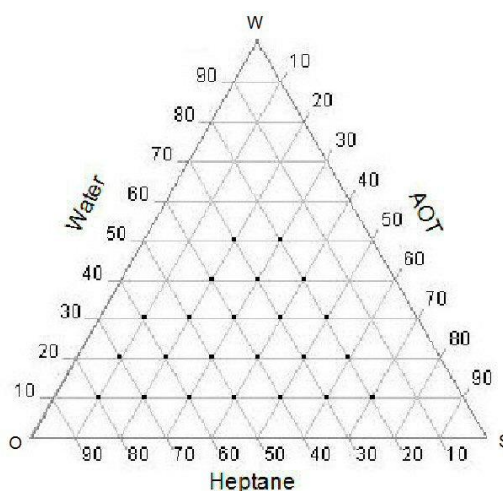
A ratio of 1:1 and 1:2 with a 5% (wt) NaCl solution was found to be suitable for promoting growth of single Lysozyme crystals. Crystal formation was quicker with a ratio of 1:2. However, little differentiation could be made between the quality of crystals obtained from both 1:1 and 1:2 ratios. Consequently, for direct addition of anti-solvent to microemulsion samples and for mixed microemulsion experiments, a 5% (wt) NaCl solution was typically used.

#### **4.4| Protein Crystallisation from Microemulsions**

The below sections (Section 4.4.1 – 4.4.8) detail the crystallisation results for AOT, Span80/Brij30, Span80/Tween80, TX-114 and TX-100/1-hexanol surfactant systems. Results of varying the microemulsion method, including direct addition of anti-solvent, evaporation of the continuous phase and mixed microemulsion methods, are also discussed.

##### **4.4.1| AOT Surfactant System**

Phase diagrams were constructed for AOT, an anionic surfactant, and comparisons were drawn between a dispersed phase of pure water and a 5% by mass NaCl solution. A NaCl solution of 5% by mass was chosen as this concentration was found to promote crystal growth of Lysozyme in bulk experiments with a ratio of both 1:1 and 1:2 for protein solution to salt solution.



**Figure 4.7|** Ternary phase diagram constructed at room temperature for AOT, pure water and heptane. Markers indicate composition ratios which formed microemulsions.

As depicted in Figure 4.7, a large region of stable microemulsions was possible for a dispersed phase of pure water. This usable region incorporated a large range of surfactant concentrations ranging from 10-50% by mass. The flexibility in composition of the three microemulsion components presented by an AOT surfactant system may therefore enable expansive variations in the microemulsions environment in order to find the niche composition that might enable Lysozyme crystallisation.

In comparison, no stable microemulsions were formed for the tested compositions within a phase diagram when a solution of 5% (wt) NaCl was used as the dispersed aqueous phase. This restricted the flexibility for the design of mixed microemulsion experiments for the AOT surfactant system.

A series of experiments were set up for the AOT surfactant system in which the Lysozyme concentration was varied. It was initially thought that it would be advantageous to prepare microemulsions on a small scale so that the methodology maintained the potential to be applied to the crystallisation of other proteins for which only small amounts of material were available.

Consequently, microemulsions samples were prepared in 500  $\mu$ l of both a 10% (wt) and 5% (wt) AOT/heptane solution. It was possible to incorporate a large range of Lysozyme concentrations into the 10% (wt) AOT surfactant system. However, Lysozyme solutions in a buffer of 0.1M NaAc of varying pH could not be dispersed in the surfactant system to form stable microemulsions. Table 4.3 summaries the samples which formed stable microemulsions with the 10% (wt) and 5% (wt) AOT in heptane surfactant systems and a dispersed aqueous phase of Lysozyme in water.

500 $\mu$ l AOT 10% (wt) in heptane		500 $\mu$ l AOT 5% (wt) in heptane	
Lysozyme concentration (mgml <sup>-1</sup> )	Volume of aqueous phase ( $\mu$ l)	Lysozyme concentration (mgml <sup>-1</sup> )	Volume of aqueous phase ( $\mu$ l)
50	10-40	50	10-20
40	10-50	40	10-50
30	10-50	30	10-50
20	10-70	20	10-60
10	10-100	10	10-60

**Table 4.3** | Samples which formed stable microemulsions prepared from the AOT surfactant system.

No crystallisation was observed for single Lysozyme microemulsions. Therefore, experiments involving direct addition of the anti-solvent were set up in an attempt to facilitate crystal growth. Direct addition of 5% (wt) NaCl in 1:1, 1:2 and 1:0.5 ratios of microemulsion aqueous phase to anti-solvent solution to each of the microemulsions samples listed in Table 4.3 lead to phase separation. Subsequently, a methodology which did not involve an anti-solvent solution was applied.

Evaporation of the continuous phase was conducted on microemulsions that were prepared on a larger scale. The move to make microemulsions on a 2 ml scale as opposed to the previously used 500  $\mu$ l scale was made because viewing the microemulsion samples via optical microscopy proved difficult for samples contained within such a small glass vial. Also, in anticipation of crystallisation, it was thought that a larger sample volume, and thus larger glass vial, would aid the crystal harvesting process and potentially produce larger crystals if more of the crystallisable material was contained within the microemulsions.

Table 4.4 lists the samples which formed stable microemulsions prepared from 2 ml of 10% (wt) AOT in heptane. Two repeats of the samples were made; for the first repeat no further experimental procedure was carried out and the samples were observed using an optical microscope to monitor crystallisation. The second repeat was used for experiments involving the evaporation of the continuous, heptane phase. Over a period of 16 hours the mass of each sample was reduced by approximately 15%. A third repeat of the samples was made; upon evaporation of the continuous phase the samples became cloudy and viscous when the mass of the samples was reduced by over 25%. No crystallisation of Lysozyme resulted from evaporation of the continuous phase.

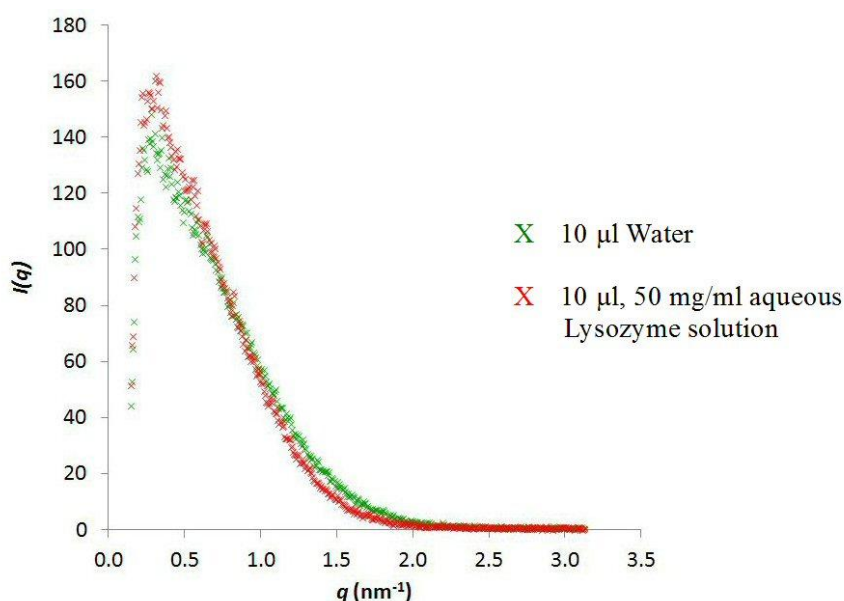
Lysozyme concentration (mgml <sup>-1</sup> )	Volume of aqueous phase (μl)
30	20-200
32	20-200
34	20-200
36	20-200
38	20-200
40	20-200
42	20-200
44	20-200
46	20-180
48	20-160
50	20-160

**Table 4.4|** Samples which formed stable microemulsions in 2 ml of AOT 10% (wt) in heptane. Three repeats of these samples were made two of which were used for evaporation of the continuous phase experiments.

Two methodologies, direct addition of an anti-solvent solution and evaporation of the continuous phase, failed to facilitate crystal growth from microemulsions using the AOT surfactant system. Mixed microemulsion experiments provide an alternative method; however, for the AOT surfactant system it was not possible to disperse NaCl solutions, 5-10% by mass, to form stable microemulsions. In 1 ml of 10% (wt) AOT in heptane 10-40 μl of both a 1% and 0.5% (wt) NaCl solution was successfully dispersed. However, these NaCl concentrations, considering the initial bulk experiments, are not known to facilitate crystallisation of Lysozyme. Despite this, single Lysozyme microemulsions listed in Table 4.4 were systematically combined with the NaCl microemulsions. No stable microemulsions were formed from the prepared mixed microemulsion samples.

#### 4.4.2| AOT Surfactant System: SAXS/GIFT Analysis

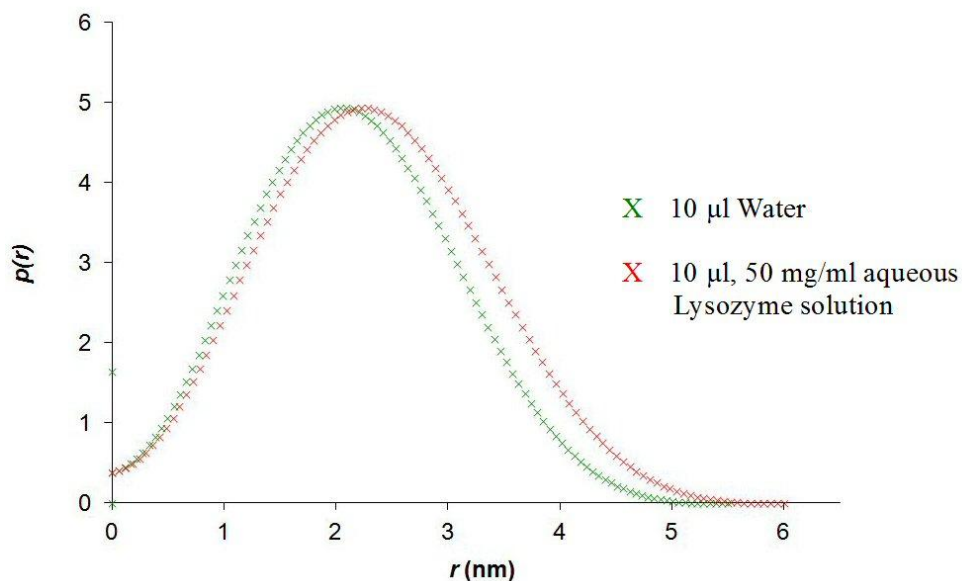
A white precipitate was observed which formed immediately upon the addition of the aqueous Lysozyme solution to the surfactant system. However, once the sample was vortexed the precipitate was no longer observed and a transparent, colourless microemulsion was formed. To confirm that that precipitate was not being dispersed but was re-dissolving into the system, SAXS and subsequent GIFT analysis were applied to confirm the formation of microemulsion droplets.



**Figure 4.8|** Plot of  $I(q)$  against  $q$  for single Lysozyme microemulsions consisting of 500  $\mu\text{l}$  AOT 10% (wt) in heptane and a dispersed phase of either 10  $\mu\text{l}$  of pure water or 10  $\mu\text{l}$  of an aqueous Lysozyme solution of concentration  $50 \text{ mgml}^{-1}$ .

The formation of microemulsion droplets was confirmed by SAXS experiments (Figure 4.8) and by subsequent GIFT analysis which found the droplet for each sample to be within the expected size range for microemulsions. From Figure 4.9 it can be seen that the droplet radius increases when an aqueous Lysozyme solution is incorporated into the microemulsion system compared to when a dispersed phase of pure water is used. GIFT analysis found the radius to be 2.1 nm and 2.5 nm for a dispersed phase of pure water and of a  $50 \text{ mgml}^{-1}$  Lysozyme solution respectively. The confirmed presence of microemulsions droplets suggests that the white precipitate observed upon addition of the aqueous Lysozyme phase to the surfactant system is re-dissolved into the system upon vortexing of the sample.





**Figure 4.9|** Pair distance distribution plot,  $p(r)$ , for single Lysozyme microemulsions consisting of 500  $\mu\text{l}$  AOT 10% (wt) in heptane and a dispersed phase of either 10  $\mu\text{l}$  of pure water or 10  $\mu\text{l}$  of an aqueous Lysozyme solution of concentration 50  $\text{mgml}^{-1}$ .

#### 4.4.3| Span80/Brij30 Surfactant System

Following the success of glycine crystallisation from microemulsions<sup>4</sup>, samples of a similar nature were adapted for the application to Lysozyme crystallisation experiments. For the glycine experiments, 0.25g of aqueous phase in 7g of 40% Span80/Brij30 by mass in a 1:1 ratio dissolved in heptane, formed stable microemulsions<sup>4</sup>. Applying this as a starting point for Lysozyme crystallisation experiments, it was found that 0.1-0.3g of 2.6  $\text{mgml}^{-1}$  Lysozyme in water could be dispersed within 7g of the surfactant system to form stable microemulsions. No crystallisation occurred from the prepared samples. Lysozyme concentrations above 2.6  $\text{mgml}^{-1}$  formed emulsions when the same microemulsion compositions were applied.

Samples were prepared for varying concentrations of Lysozyme solution in the four buffers of differing pH. Only samples which incorporated an aqueous phase of Lysozyme solution in water formed stable microemulsions. No stable microemulsions were formed for the four buffer solutions of different pH.

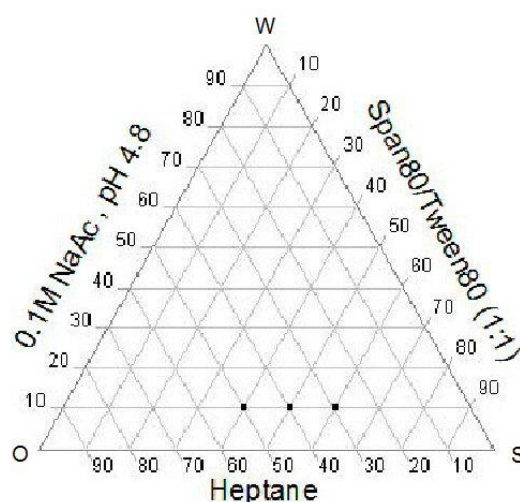
It was possible to incorporate 0.1-0.3g of 1% (wt) NaCl solution into 7g of 40% by mass Span80/Brij30 in a 1:1 ratio dissolved in heptane. Mixed microemulsion samples were prepared, combining the single Lysozyme microemulsions and single NaCl microemulsions. All mixed samples formed emulsions and over time phase separated. If it was possible to

form stable mixed microemulsions from the single microemulsions mentioned, crystallisation may not have been expected based on the bulk anti-solvent experiments discussed in Section 4.3. The addition of a 1% (wt) NaCl solution to a 50 mgml<sup>-1</sup> Lysozyme solution in both a 1:1 and 1:2 ratios did not lead to crystal growth. Thus formation of mixed microemulsions which incorporated a 1% (wt) NaCl in similar ratios and a Lysozyme solution much lower in concentration is not likely to achieve supersaturation within the microemulsions droplets and therefore subsequent crystallisation will not result.

It is also worth noting that at such a low Lysozyme concentration there will be approximately  $1 \times 10^{16}$  to  $3 \times 10^{16}$  Lysozyme molecules within each single microemulsion sample. Consequently, based on geometrical droplet size calculations, this would result in a Lysozyme molecule being present in 1 of approximately 3000 droplets. The probability of collisions between droplets containing Lysozyme molecules to form transient dimers for exchange of material and therefore support crystal growth is therefore significantly reduced. This may explain why no crystal growth occurred from the single Lysozyme microemulsions. However, this is of course assuming that the microemulsion droplets were supersaturated and nucleation had occurred.

#### **4.4.4| Span80/Tween80 Surfactant System**

For the surfactant system Span80/Brij30 it was not possible to form stable microemulsions when Lysozyme was dissolved in a 0.1M NaAc buffer of varying pH. Consequently, in an attempt to explore an alternative surfactant system that would disperse the four buffer solutions, a Span80/Tween80 in heptane surfactant system was explored. A pseudo ternary phase diagram incorporating an aqueous phase of 0.1M NaAc buffer with a pH of 4.8 was established.



**Figure 4.10|** Pseudo ternary phase diagram constructed at room temperature for Span80/Tween80 (1:1), 0.1M NaAc buffer solution of pH 4.8 and heptane. Markers indicate composition ratios which formed microemulsions.

Only a small region of stable microemulsions (Figure 4.10) was formed. Stable microemulsions only formed with a low percentage by mass of aqueous phase, approximately 10%, and a surfactant concentration of approximately 40-60% by mass. Despite a small region of stable microemulsions, the surfactant system Span80/Tween80 does allow dispersion of the buffer solution which will aid examination of the affect of pH on Lysozyme crystallisation from microemulsions. Consequently, a series of samples were setup for the Span80/Tween80 surfactant system in which pH of the buffer solution and the Lysozyme concentration was varied.

It was found that for a solution of Lysozyme to be dispersed within the surfactant system to form stable microemulsions, a lower amount of surfactant was required compared to the amount thought to be required according to the pseudo ternary phase diagram (Figure 4.10). In 1 g of 20% by mass Span80/Teen80 in a 1:1 ratio dissolved in heptane, a maximum Lysozyme concentration of  $2 \text{ mgml}^{-1}$  could be dispersed to form stable microemulsions with each of the four buffer solutions. Prepared samples within this series of experiments which formed stable microemulsions are summarised in Table 4.5. No crystallisation resulted from the single Lysozyme microemulsions of varying buffer pH and Lysozyme concentration.

Lysozyme concentration (mgml <sup>-1</sup> )	pH of buffer solution	Volume of aqueous phase dispersed in 1 g of 20% (wt) Span80/Tween80 (1:1) in heptane (μl)
1	4.4	40-100
	4.8	20-120
	5.2	40-100
	5.6	40-100
2	4.4	50-90
	4.8	70-110
	5.2	60-100
	5.6	60-100

**Table 4.5|** Samples which formed stable microemulsions incorporating an aqueous phase of Lysozyme solutions in 0.1M NaAc buffer of varying pH within a surfactant system of 1 g Span80/Tween80 (1:1) 20% (wt) in heptane.

Consequently, in an attempt to increase the supersaturation of the microemulsion droplets, an experimental method was explored in which an anti-solvent solution of 5% (wt) NaCl was directly added to the single Lysozyme microemulsions listed in Table 4.5. The anti-solvent solution was added 24 hours after initial formation of the single Lysozyme microemulsions. For each Lysozyme microemulsion, 5% (wt) NaCl solution was added in a 1:1 and 1:2 ratio of microemulsion aqueous phase to anti-solvent solution. Direct addition of the anti-solvent solution in both 1:1 and 1:2 ratios led to the phase separation of the Lysozyme microemulsions. A ratio of 1:0.5 was thus conducted but this also led to phase separation.

Following this, mixed microemulsions were explored providing an alternative method for the facilitation of Lysozyme crystallisation by ensuring supersaturation within the microemulsion droplets was reached. A volume of 40-80 μl of 5% (wt) NaCl solution was successfully dispersed to form microemulsions in 1 g of 20% (wt) Span80/Tween80 in a 1:1 ratio dissolved in heptane. Table 4.6 summarises the mixed microemulsion samples which formed stable microemulsions upon combining single Lysozyme and single anti-solvent microemulsions.

Aqueous phase volume ratio of single Lysozyme microemulsions to single anti-solvent microemulsions	Lysozyme concentration (mgml <sup>-1</sup> ) in single microemulsions	pH of Lysozyme buffer solution	Aqueous phase in single Lysozyme microemulsions (μl)
1:1	1	4.4	40-80
		4.8	30-100
		5.2	40-90
		5.6	40-90
	2	4.4	50-100
		4.8	40-90
		5.2	70-90
1:2	1	4.4	40-50
		4.8	40-50
		5.2	40-50
		5.6	40-50
	2	4.4	40-50
		4.8	40-50

**Table 4.6|** Summary of mixed microemulsion samples which formed stable microemulsions upon combining single Lysozyme and anti-solvent microemulsions. All single Lysozyme and anti-solvent microemulsions were made from 1 g of Span80/Tween80 in a 1:1 ratio, 20% (wt) dissolved in heptane, to which the stated volume of aqueous phase was added.

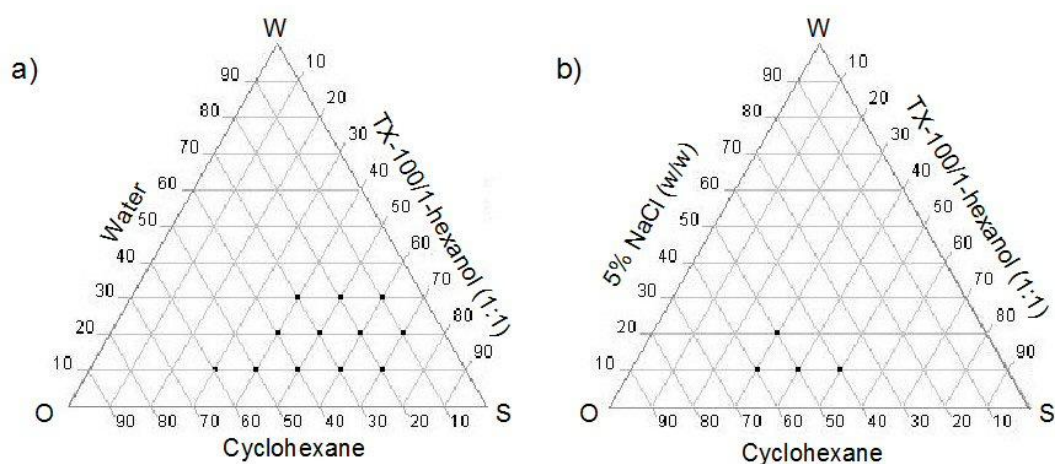
For the Span80/Tween80 surfactant system no crystallisation resulted from the mixed microemulsions. As thought with the Span80/Brij30 surfactant system this may be a consequence of the low Lysozyme concentration used. Such a low concentration of Lysozyme may mean that supersaturation within the microemulsions droplets is not reached even when an anti-solvent is introduced through mixed microemulsions. Also, assuming nucleation has occurred, few droplets within the microemulsions systems will contain Lysozyme molecules and therefore collisions between droplets to form transient dimers in support of crystal growth may be rare events.

#### 4.4.5| TX100/1-hexanol and TX-114 Surfactant Systems: Phase Diagrams

It has previously been reported that inclusion of electrolytes and additives such as acid, can affect the phase behaviour of microemulsions depending of the nature of the surfactant used<sup>176, 177</sup>. In some cases the affect of salt has been significant; phase separation has been reported<sup>178</sup>. Within this study previous surfactant systems (AOT, span80/Brij30 and span80/Tween80) have demonstrated such difficulties; their phase diagrams incorporating

a solution of electrolytes (NaCl solution of varying concentrations, % by mass) found either a very small or no area of stable microemulsion to be possible for varying compositions of the oil, aqueous and surfactant phases. An alternative surfactant system was sought that would enable a solution of NaCl to be utilised as the dispersed phase within a stable microemulsion. This was desirable in order to explore the application of the mixed microemulsion method to introduce an anti-solvent into the protein microemulsion in an attempt to increase supersaturation and mediate crystal growth.

Surfactant systems Triton X-100/1-hexanol and Triton X-114 offered a system that, compared with the other systems explored, enabled the largest region of stable microemulsion to be formed when a 5% (wt) NaCl solution was used as the dispersed phase. This was indicated through the preparation of their phase diagrams. Visualisation of the effect caused by the use of a NaCl solution was addressed by comparing the phase diagram incorporating 5% (wt) NaCl solution with an equivalent phase diagram in which pure water was used.

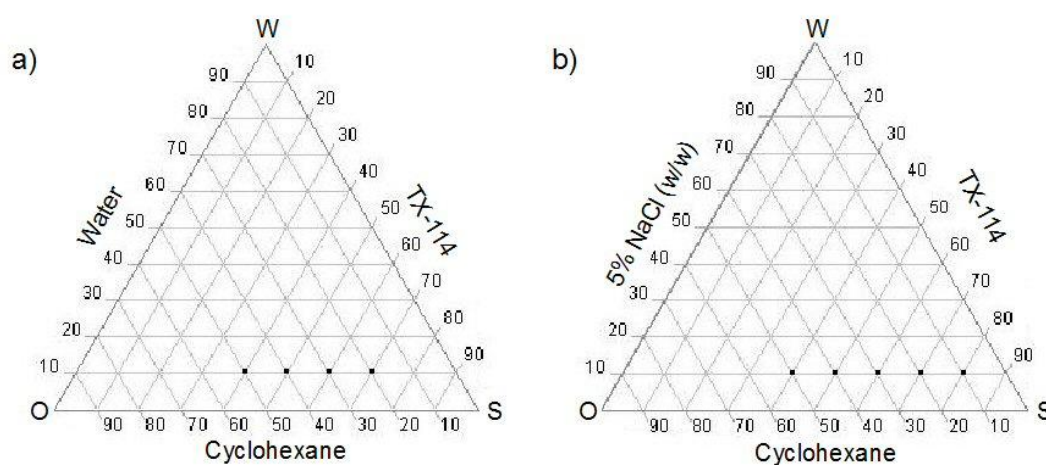


**Figure 4.11 |** Pseudo ternary phase diagrams for TX-100/1-hexanol surfactant system with a continuous phase of cyclohexane and an aqueous phase of a) pure water b) 5% (wt) NaCl solution. Markers indicate composition ratios which formed microemulsions.

First examining the phase diagrams for the Triton X-100/1-hexanol system (Figure 4.11) it can be clearly seen that replacement of pure water with 5% (wt) NaCl solution restricts the region in which stable microemulsions can be formed. The number of suitable compositions for the three microemulsion components is reduced by approximately two thirds. Typically, for microemulsions containing a pure water dispersed phase, stable

microemulsions are formed with a low percentage by mass of aqueous phase, approximately 10-30%, and a high surfactant concentration, approximately 40-60% by mass. Use of 5% (wt) NaCl solution as the dispersed phase reduces the amount of aqueous phase that can be incorporated in a stable microemulsion to approximately 10% mass. To facilitate the formation of these stable microemulsions approximately 30-50% of surfactant is required.

A similar result was observed for the Triton X-114 surfactant system (Figure 4.12). Using 5% (wt) NaCl solution as the dispersed phase led to a reduction in the compositional area in which stable microemulsions were formed. Stable microemulsions with a dispersed phase of pure water only formed when the aqueous phase contributed approximately 10% by mass of the whole microemulsion; however, a broad range of surfactant concentrations could be used, ranging from approximately 30-70% by mass. A dispersed phase of 5% (wt) NaCl solution achieved stable microemulsion with a percentage mass of approximately 10%. The required surfactant concentration was shifted slightly higher to 40-80% compared to the phase diagram incorporating pure water. Unusually, the composition area for stable microemulsions was expanded when 5% (wt) NaCl solution was used instead of pure water.



**Figure 4.12|** Ternary phase diagrams for TX-114 surfactant system with a continuous phase of cyclohexane and an aqueous phase of a) pure water b) 5% (wt) NaCl solution. Markers indicate composition ratios which formed microemulsions.

#### 4.4.6| TritonX-114 Surfactant System

Based on the initial results from the pseudo ternary phase diagram (Figure 4.12), samples were made in which Lysozyme solutions of varying concentrations were used for the aqueous, dispersed phase, replacing pure water. The phases of these samples are summarised in Table 4.7. Composition ratios found to form stable microemulsions in the pseudo ternary phase diagram typically also formed stable microemulsions when different Lysozyme concentrations were used in the aqueous phase. There were a few exceptions for the composition ratio 1:7:2 for which emulsions were formed with Lysozyme concentrations of 50 mgml<sup>-1</sup> and 40 mgml<sup>-1</sup>. The microemulsions formed were monitored regularly using an optical microscope for a period of two months during which no crystallisation was observed.

Lysozyme solution: TX-114: Cyclohexane	Lysozyme concentration (mgml <sup>-1</sup> )					
	50	40	30	20	10	5
1:4:5	✓	✓	✓	✓	✓	✓
1:5:4	✓	✓	✓	✓	✓	✓
1:6:3	✓	✓	✓	✓	✓	✓
1:7:2	e	e	✓	✓	✓	✓

**Table 4.7|** Phase results for samples prepared for the TX-114 surfactant system incorporating a Lysozyme solution of varying concentrations (50-5 mgml<sup>-1</sup>) as the dispersed phase. An emulsion is indicated by 'e' and a microemulsion is indicated by '✓'.

Subsequently mixed microemulsions were made in an attempt to facilitate crystal growth. The mixed microemulsions consisted of combining each of the samples listed in Table 4.7 with each of the composition ratios that formed stable microemulsions when a dispersed phase of 5% (wt) NaCl solution was used. All mixed systems formed stable microemulsions and did not degrade into emulsions or phase separate over time. No crystal growth resulted from mixed microemulsions made for the TX-114 surfactant system.

#### 4.4.7| TritonX-100/1-hexanol Surfactant System

Composition ratios of the three microemulsion components that gave stable, transparent microemulsions were selected from the pseudo ternary phase diagram in which the



dispersed phase used was pure water. The aqueous solution was replaced by a solution of Lysozyme in water with varying protein concentrations for each of the selected composition ratios. The phases of the resultant samples are summarised in Table 4.8. Although able to form microemulsions with a dispersed phase of pure water, some compositions did not permit microemulsions regardless of Lysozyme concentration. A dependence on Lysozyme concentration was observed for some compositions, typically forming emulsions at higher Lysozyme concentrations. Only two composition ratios, 2:4:4 and 2:5:3, formed microemulsions with each concentration of Lysozyme used.

Lysozyme solution: TX-100/1-hexanol (1:1): Cyclohexane	Lysozyme concentration (mgml <sup>-1</sup> )					
	50	40	30	20	10	5
1:3:6	✓	✓	✓	✓	✓	✓
1:4:5	e	✓	✓	✓	✓	✓
1:5:4	e	e	e	e	e	✓
1:6:3	e	e	e	e	e	e
1:7:2	e	e	e	e	e	e
2:4:4	✓	✓	✓	✓	✓	✓
2:5:3	✓	✓	✓	✓	✓	✓
2:6:2	e	✓	✓	✓	✓	✓
2:7:1	e	e	e	e	e	e
3:4:3	e	e	✓	✓	✓	✓
3:5:2	e	e	e	e	e	e
3:6:1	e	e	e	e	e	e

**Table 4.8|** Phase results for samples prepared for the TX-100/1-hexanol surfactant system incorporating a Lysozyme solution of varying concentrations (50-5 mgml<sup>-1</sup>) as the dispersed phase. An emulsion is indicated by 'e' and a microemulsion is indicated by '✓'.

All samples were stored at room temperature; microemulsions listed in Table 4.8 displayed no degradation towards forming emulsions over time. Examination, by eye and optical microscope, of all Lysozyme microemulsions showed no crystal growth after four weeks. The lack of crystal growth led to the application of the mixed microemulsion method and evaporation of continuous phase in an attempt to facilitate crystal growth from these samples.

#### 4.4.8| TritonX-100/1-hexanol Surfactant System: Mixed Microemulsions

Given the phase results displayed in Table 4.8 a 2:5:3 ratio was selected for use in the mixed microemulsion method, as this composition formed stable microemulsions with all Lysozyme concentrations used.

The mixture formed from combining protein and anti-solvent microemulsions has to be a stable microemulsion in order for thermodynamic control of crystallisation through 3D nanoconfinement to be achieved. However, this is not to say that the two components of the mixture have to be microemulsions themselves. It may be possible to combine one stable microemulsion with a nano- or macro-emulsion and still form a stable microemulsion for the final mixture. This has been demonstrated through the use of the mixed microemulsion method in the crystallisation of glycine polymorphs<sup>4</sup>.

Mixed microemulsions were prepared for the TX-100 surfactant system, combining stable Lysozyme microemulsions of varying Lysozyme concentrations and a composition ratio of 2:5:3 with different compositions of a 5% (wt) NaCl, anti-solvent microemulsion. Table 4.9 summarises the phases that were formed upon mixing. Generally, a stable microemulsion was made from combining two stable microemulsions. Macro-emulsions (white and cloudy in appearance) were initially formed upon mixing the 1:4:5 and 1:5:4 compositions of the 5% (wt) NaCl microemulsions with higher Lysozyme concentration microemulsions.

Protein Microemulsion (2:5:3)	5% (wt) NaCl microemulsion (aqueous: surfactant/co-surfactant: oil)			
Lysozyme concentration (mgml <sup>-1</sup> )	1:3:6	1:4:5	1:5:4	2:3:5
50	✓	e	e	✓
40	✓	e	e	✓
30	✓	e	e	✓
20	✓	✓	e	✓
10	✓	✓	✓	✓
5	✓	✓	✓	✓

**Table 4.9|** Phase results for the mixed microemulsion method using a TX-100/1-hexanol surfactant system. An emulsion is indicated by 'e' and a microemulsion is indicated by '✓'.

Crystal growth was observed in the mixed microemulsions three days after mixing. Examination under an optical microscope found that after approximately two weeks no further crystal growth occurred. The crystallisation result varied according to the concentration of Lysozyme used and the composition ratio of the anti-solvent microemulsion. Three repeats of the mixed microemulsions were made; for each repeat the same crystallisation outcome was observed as summarised in Table 4.10 with related Figure 4.15a-p.

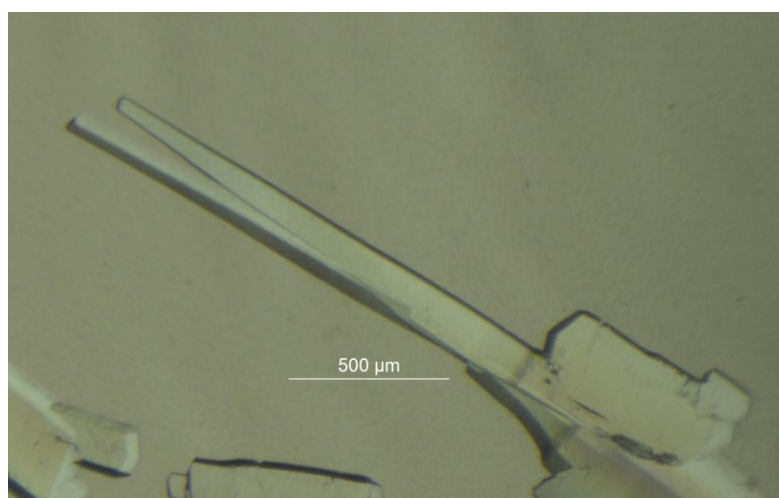
<b>Protein Microemulsion (2:5:3)</b>	<b>5% (wt) NaCl microemulsion (aqueous: surfactant/co-surfactant: oil)</b>			
<b>Lysozyme concentration (mgml<sup>-1</sup>)</b>	<b>1:3:6</b>	<b>1:4:5</b>	<b>1:5:4</b>	<b>2:3:5</b>
<b>5</b>	No crystal growth	No crystal growth	No crystal growth	No crystal growth
<b>10</b>	No crystal growth	No crystal growth	No crystal growth	No crystal growth
<b>20</b>	Figure 4.15a	Figure 4.15e	Figure 4.15i	Figure 4.15m
<b>30</b>	Figure 4.15b	Figure 4.15f	Figure 4.15j	Figure 4.15n
<b>40</b>	Figure 4.15c	Figure 4.15g	Figure 4.15k	Figure 4.15o
<b>50</b>	Figure 4.15d	Figure 4.15h	Figure 4.15l	Figure 4.15p

**Table 4.10|** Crystallisation results for mixed microemulsions prepared with the TX-100/1-hexanol surfactant system.

For each anti-solvent composition ratio, no crystal growth was seen for Lysozyme concentrations of 10 mgml<sup>-1</sup> and 5 mgml<sup>-1</sup>. For these concentrations of Lysozyme it is possible that the droplets are not supersaturated; therefore nucleation cannot take place and no crystal growth will occur. The amount of crystalline material increased as the concentration of Lysozyme used in the microemulsions was also increased. No single crystals with well defined edges were observed for the anti-solvent composition ratios 1:3:6, 1:4:5 and 1:5:4.

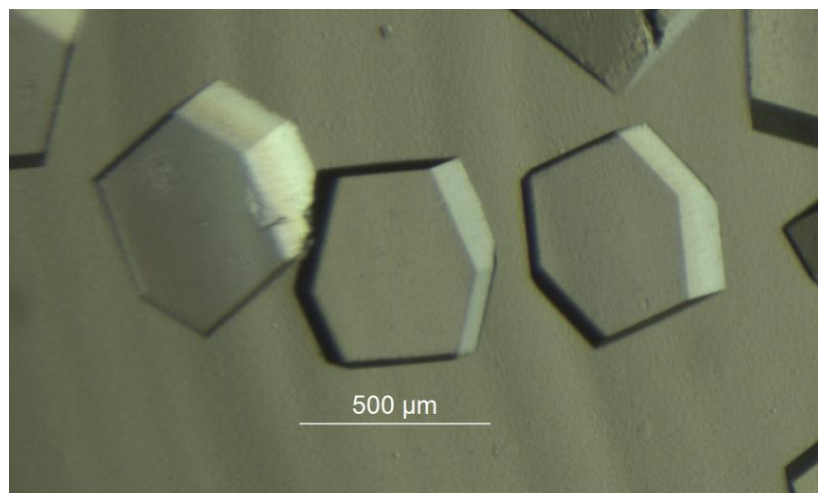
A sheet of crystalline material was formed over the bottom of the glass vial from samples which formed emulsions upon mixing. For low Lysozyme concentrations only small areas of crystalline material were observed surrounded by an amorphous material which appeared dark and dull under the microscope. As Lysozyme concentration was increased the sheet of crystalline material began to present some shape with rough, non-uniform edges. However, the connected nature of the sheet prohibited isolation.

For an anti-solvent composition ratio of 1:3:6, aggregates of crystalline material were formed when a Lysozyme concentration of 30-50 mgml<sup>-1</sup> was used. As Lysozyme concentration was increased, the crystals began to grow into a shape similar to that observed in successful wells in the hanging drop vapour diffusion trays. For Lysozyme concentrations of 40 and 50 mgml<sup>-1</sup>, single needles seemed to grow outwardly from the aggregates of crystalline material (Figure 4.13). With great care these needles may be able to be separated from the crystalline aggregates and used for structural analysis. However, these needles are not of the crystal quality that would be typically selected for analysis.



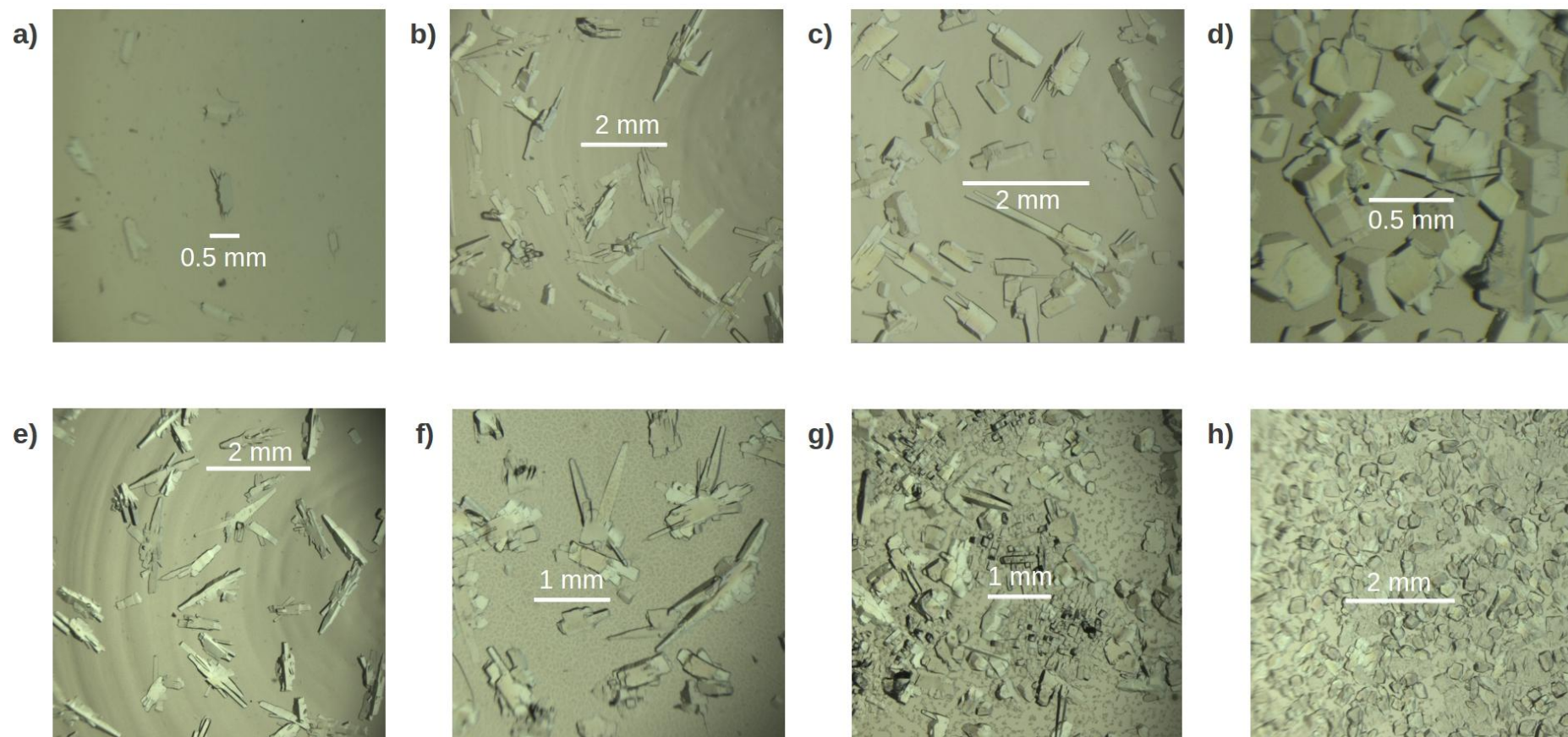
**Figure 4.13** | Crystal grown from a mixed microemulsion composed from a single Lysozyme microemulsion with concentration 40 mgml<sup>-1</sup> and a single NaCl, anti-solvent microemulsion with a composition ratio of 1:3:6.

Single crystals were only observed for mixed microemulsions formed from a NaCl microemulsion with a composition ratio of 2:3:5. However, the nature of these single crystals varied depending on the concentration of Lysozyme used. For each Lysozyme concentration more single crystals were formed compared to the number of crystals which can be grown from one drop in the hanging drop vapour diffusion tray. The quality of single crystals formed improved as Lysozyme concentration was increased. The better quality crystals, approximately 500μm x 500μm x 300μm in size, with a well defined shape and edges, were obtained from a Lysozyme concentration of 50 mgml<sup>-1</sup> (Figure 4.14). Crystals from this mixed microemulsion were used for subsequent X-ray diffraction experiments.



**Figure 4.14** | Single crystals grown from a mixed microemulsion composed from a single Lysozyme microemulsion with concentration  $50 \text{ mg ml}^{-1}$  and a single NaCl, anti-solvent microemulsion of composition ratio 2:3:5.

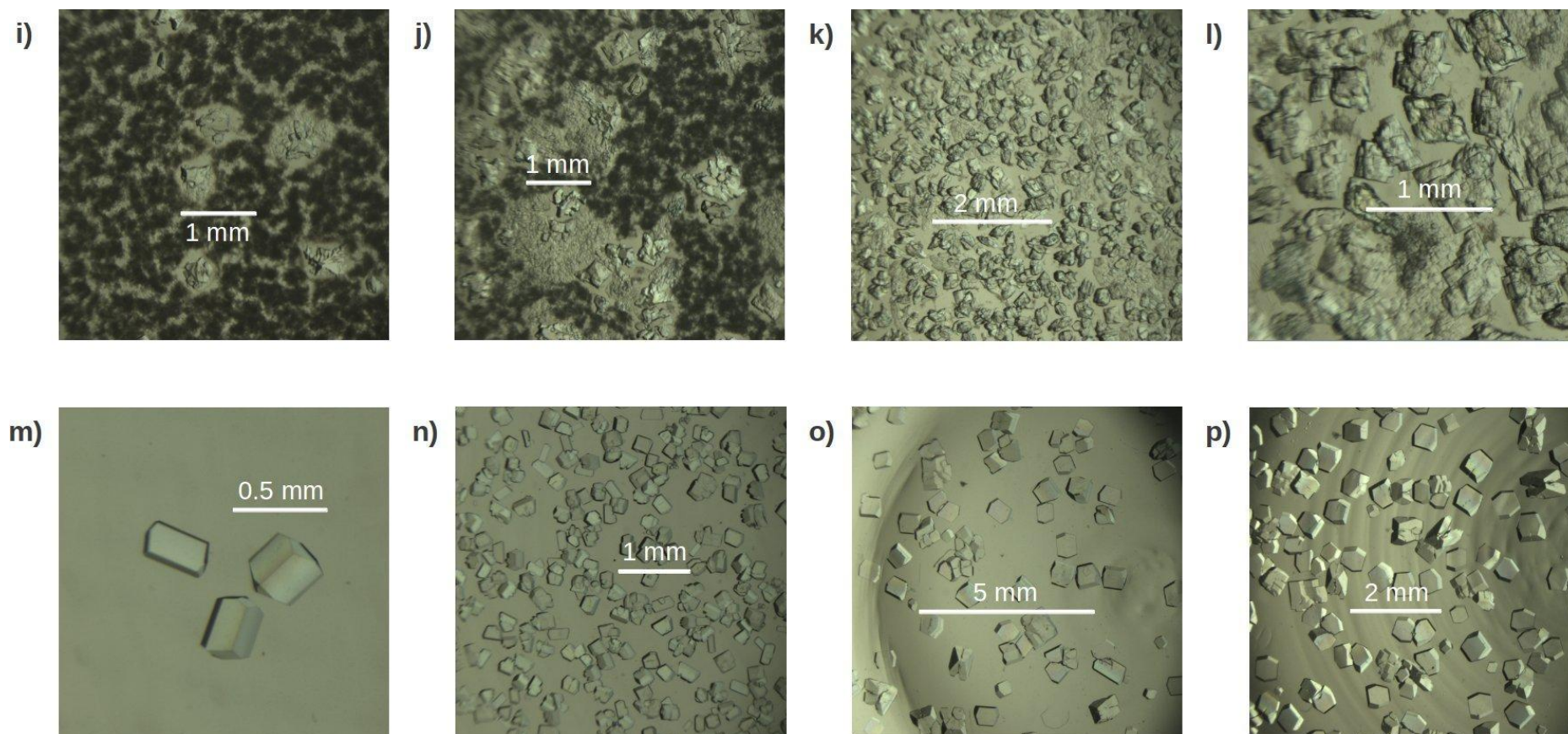
A series of control experiments were conducted for the TX-100 surfactant system. Repeats of the mixed microemulsions were made in which for the first repeat the Lysozyme solution was replaced with pure water and the anti-solvent microemulsion kept the same. This would indicate there was salt, NaCl, crystallising out of the mixed microemulsions. A second repeat was made in which the 5% (wt) NaCl solution was replaced with pure water to see if Lysozyme would crystallise out from the mixed microemulsions in the absence of an anti-solvent. This would aid discussion as to whether the crystallisation of Lysozyme from mixed microemulsions was a result of an increased supersaturation or a function of droplet size. For all of the control experiments conducted, no crystallisation was observed and the phase behaviour observed was identical to that of the original mixed microemulsions.



**Figure 4.15** | Optical microscope images of crystalline material grown from mixed microemulsions formed from an anti-solvent microemulsion with composition ratio X:X:X and a single Lysozyme microemulsion (composition ratio 2:5:3) of concentrations as follows:

a) 1:3:6, 20  $\text{mgml}^{-1}$  b) 1:3:6, 30  $\text{mgml}^{-1}$  c) 1:3:6, 40  $\text{mgml}^{-1}$  d) 1:3:6, 50  $\text{mgml}^{-1}$  e) 1:4:5, 20  $\text{mgml}^{-1}$  f) 1:4:5, 30  $\text{mgml}^{-1}$  g) 1:4:5, 40  $\text{mgml}^{-1}$  h) 1:4:5, 50  $\text{mgml}^{-1}$





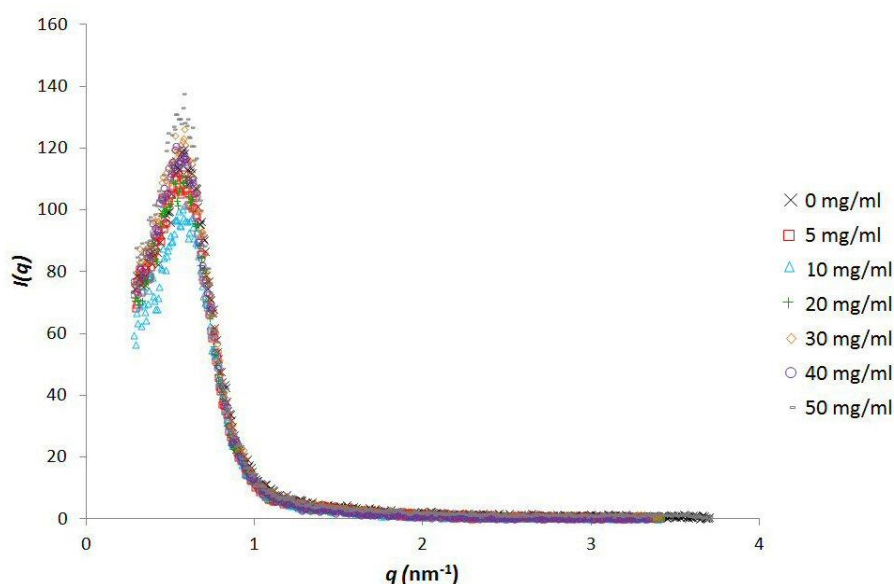
**Figure 4.15** | Optical microscope images of crystalline material grown from mixed microemulsions formed from an anti-solvent microemulsion with composition ratio X:X:X and a single Lysozyme microemulsion (composition ratio 2:5:3) of concentrations as follows:  
i) 1:5:4, 20  $\text{mgml}^{-1}$  j) 1:5:4, 30  $\text{mgml}^{-1}$ , k) 1:5:4, 40  $\text{mgml}^{-1}$  l) 1:5:4, 50  $\text{mgml}^{-1}$  m) 2:3:5, 20  $\text{mgml}^{-1}$  n) 2:3:5, 30  $\text{mgml}^{-1}$ , o) 2:3:5, 40  $\text{mgml}^{-1}$  p) 2:3:5, 50  $\text{mgml}^{-1}$ .

#### 4.5| TritonX-100/1-hexanol Surfactant System: Droplet Size Analysis

The crystallisation results from mixed microemulsions varied depending on the concentration of Lysozyme used and the composition ratio of the NaCl, anti-solvent microemulsions. Variation in both the form and amount of the crystalline material was observed. SAXS experiments and subsequent GIFT analysis of the X-ray scattering data were used to aid discussion as to how such differences in crystallisation results correlate to the environment from which the crystalline material was grown. SAXS data was collected for mixed microemulsions composed of anti-solvent microemulsions with composition ratios 1:3:6 and 2:3:5 and with Lysozyme microemulsions of concentration 50-0 mgml<sup>-1</sup>.

##### 4.5.1| Varying Lysozyme Concentration in Single Microemulsions

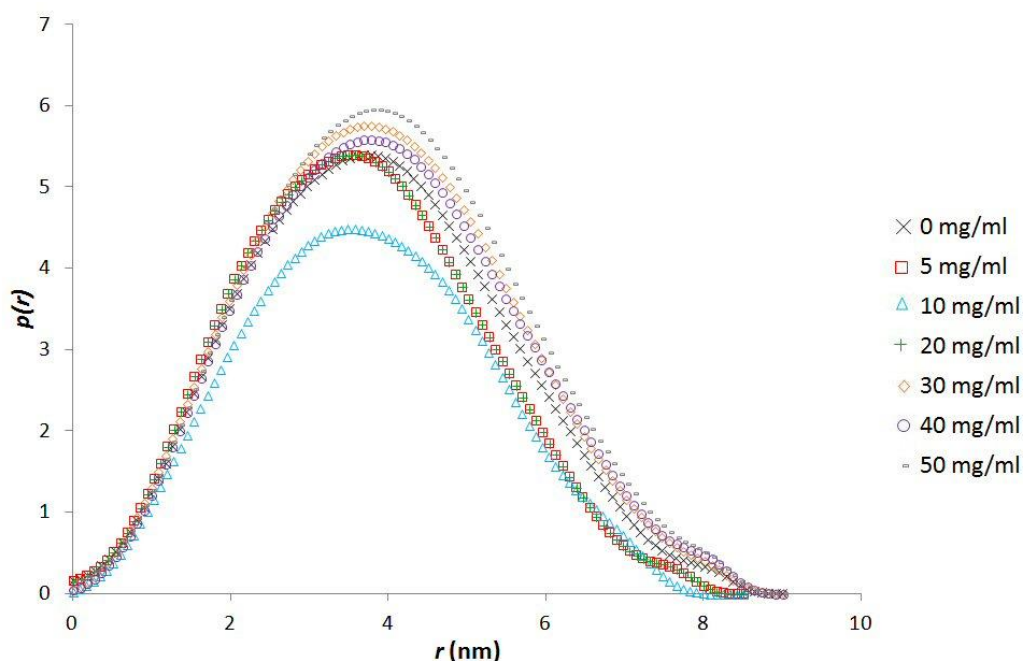
For comparison, the droplet sizes of the single microemulsions that were used to form the mixed microemulsions were also determined. Figures 4.16 and 4.17 show the scattering plots and pair distance distribution plots respectively, for microemulsions formed from a composition ratio of 2:5:3 of the TX-100/1-hexanol surfactant system with varying Lysozyme concentrations of 0-50 mgml<sup>-1</sup>. The samples diffracted well, showing that the aqueous phase had been successfully dispersed and confined, forming microemulsion droplets.



**Figure 4.16|** Plot of  $I(q)$  against  $q$ , obtained from SAXS experiments for single microemulsions of the TX-100/1-hexanol surfactant system with composition ratio 2:5:3 and varying Lysozyme concentrations.



The formation of microemulsions was confirmed using GIFT analysis, which found droplets to be within the expected size range. The data collected fit a hard sphere model. As can be seen in Figure 4.17 and summarised in Table 4.11, there is little variation in the radius of microemulsion droplets as the Lysozyme concentration is varied. The slight differences in radius values calculated using GIFT analysis all occur within the expected error of  $\pm 0.3$  nm for SAXS experiments. This suggests that the radius of microemulsion droplets is not affected by the concentration of Lysozyme.



**Figure 4.17** | Pair distance distribution plot for single microemulsions of the TX-100/1-hexanol surfactant system with composition ratio 2:5:3 and varying Lysozyme concentrations.

	Lysozyme concentration ( $\text{mgml}^{-1}$ ) in single microemulsions with composition ratio 2:5:3						
	50	40	30	20	10	5	0
Mean droplet radius (GIFT) (nm)	3.9	3.9	3.8	3.7	3.6	3.8	3.8
No. of droplets in microemulsion ( $\times 10^{18}$ )	1.43	1.45	1.51	1.64	1.75	1.54	1.56
Normal mean No. Lysozyme molecules per droplet	0.58	0.46	0.33	0.20	0.09	0.05	0

**Table 4.11** | GIFT analysis results for single microemulsions of the TX-100/1-hexanol surfactant system with composition ratio 2:5:3 and varying Lysozyme concentrations.

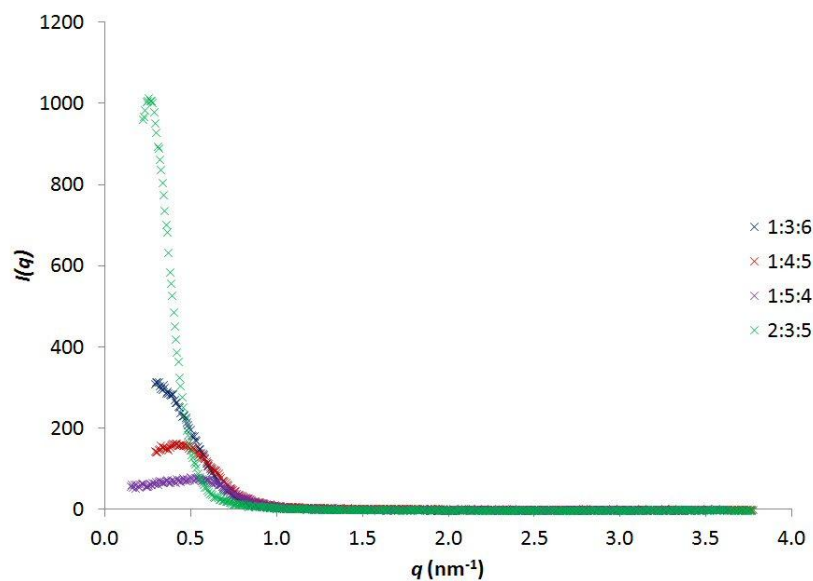
Calculation of the geometric droplet size does not correlate with the droplet size as determined by GIFT analysis. However, for geometric calculations, lowering the mass of the co-surfactant, 1-hexanol, residing at the interface and subsequently increasing the mass of the continuous phase, leads to a calculated geometric droplet radius that is similar to the radius calculated by GIFT analysis. Table 4.12 summarises the radii of droplets predicted using geometric droplet size calculations depending on the amount of 1-hexanol taken to reside at the interface between the water and oil phases. Any 1-hexanol not thought be residing at the interface is taken to partition into the cyclohexane, oil phase. Reducing the mass of 1-hexanol that resided at the interface from 0.5g to approximately 0.25-0.27g, results in a closer agreement between the droplet radii calculated by geometric calculations and by GIFT analysis.

	1-hexanol (g) residing at the interface				
	0.5	0.3	0.27	0.25	0.23
Geometric radius (nm)	2.7	3.6	3.8	3.9	4.1

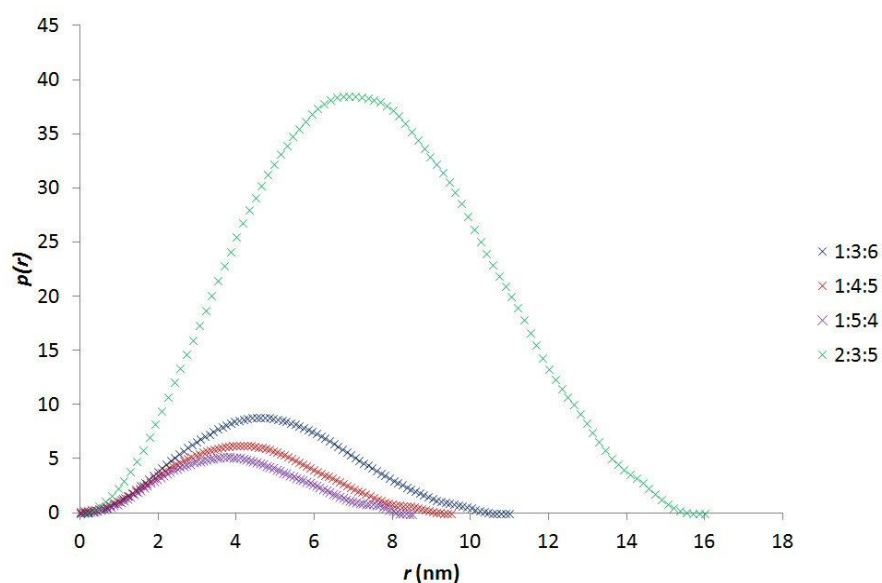
**Table 4.12 |** Variation of geometrically calculated droplet size when the amount of 1-hexanol thought to reside at the interface between the aqueous and oil phases is varied. Calculations made for single microemulsions of the TX-100/1-hexanol surfactant system with composition ratio 2:5:3.

#### 4.5.2| Varying Composition Ratio of Single Anti-solvent Microemulsions

SAXS experiments confirmed that the aqueous phase (5% (wt) NaCl solution) was successfully confined within microemulsion droplets. Changes in droplet size are observed for the single anti-solvent microemulsions as the composition ratio (aqueous phase: surfactant/co-surfactant: oil phase) is varied. Figures 4.18 and 4.19 respectively show the scattering plots and pair distance distribution plots for single NaCl anti-solvent microemulsions with differing composition ratios. The scattering intensity increases significantly as the mass of the aqueous phase is doubled from 0.2 g to 0.4g. The slight dissymmetry observed in the  $p(r)$  plots is thought to be caused by the polydispersity present among microemulsion droplets. The polydispersity observed may be a result of many factors including a slightly non-spherical shape which does not quite fit the hard sphere model, the formation of transient dimers and an inhomogeneous distribution of droplet sizes within the microemulsions sample<sup>78</sup>.



**Figure 4.18** | Plot of  $I(q)$  against  $q$  for single NaCl, anti-solvent microemulsions of different composition ratios, made using a TX-100/1-hexanol surfactant system.



**Figure 4.19** | Pair distance distribution plots for single NaCl, anti-solvent microemulsions of different composition ratios, made using a TX-100/1-hexanol surfactant system.

For these four anti-solvent microemulsions, the largest droplet size is seen for a composition ratio of 2:3:5 and the smallest droplet size with a composition of 1:5:4 (Table 4.13). The droplet radius is found to be larger for composition ratios that have a smaller surfactant/co-surfactant content. Larger droplets are also observed for microemulsions

with a larger amount of aqueous phase. As expected, the number of droplets present in the microemulsions increases as the radius of microemulsion droplets decreases.

	Composition ratio of 5% (wt) NaCl anti-solvent microemulsion			
	1:3:6	1:4:5	1:5:4	2:3:5
Mean droplet radius (GIFT) (nm)	4.8	4.2	3.9	6.8
No. of droplets in microemulsion ( $\times 10^{18}$ )	0.85	1.51	2.20	0.45

**Table 4.13** | Radii of single anti-solvent microemulsions of different composition ratios, made using a TX-100/1-hexanol surfactant system. The radii were determined by SAXS experiments and subsequent GIFT analysis.

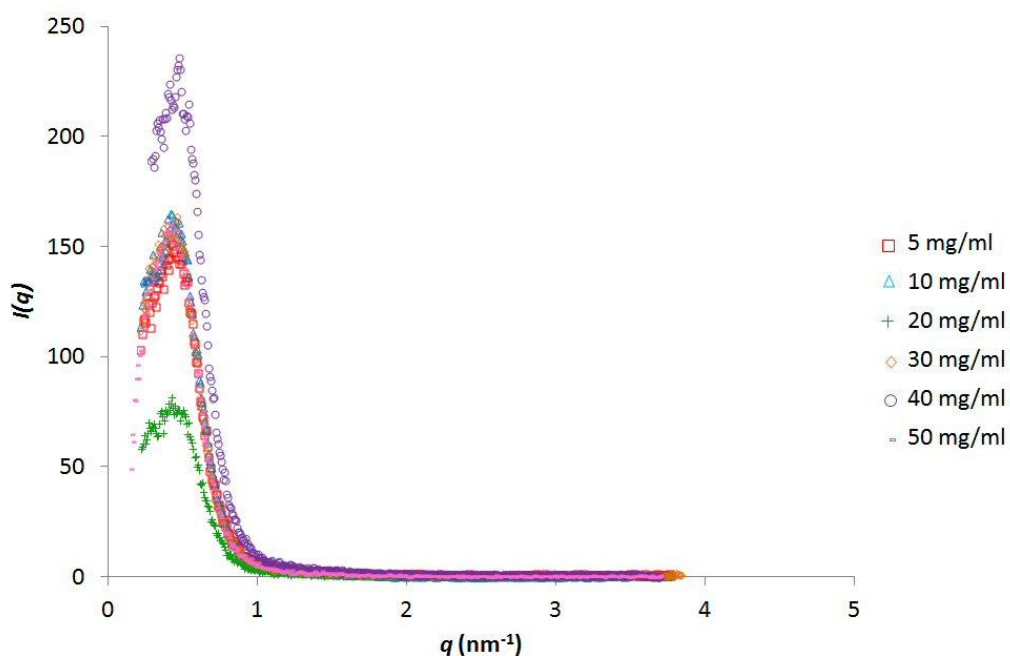
As seen with the single Lysozyme microemulsions, the estimated droplet sizes from geometrical droplet calculations do not correlate closely to the radii values calculated using GIFT analysis. Varying the amount of co-surfactant, 1-hexanol, which resides at the interface leads to a closer correlation between the two calculations of droplet size. However, there is variation in the percentage reduction of 1-hexanol at the interface (and thus subsequent increase in the mass of continuous phase) for each composition ratio of the NaCl microemulsions (Table 4.14)

	Composition ratio of 5% (wt) NaCl anti-solvent microemulsion			
	1:3:6	1:4:5	1:5:4	2:3:5
Mean droplet radius (GIFT) (nm)	4.9	4.2	3.9	6.8
Total 1-hexanol in microemulsion (g)	0.3	0.4	0.5	0.3
Estimate of 1-hexanol at the interface (g)	0.07	0.09	0.105	0.08
% reduction of 1-hexanol at the interface	76.7	77.5	79.0	73.3
Geometric radius (nm)	4.8	4.2	4.0	6.9

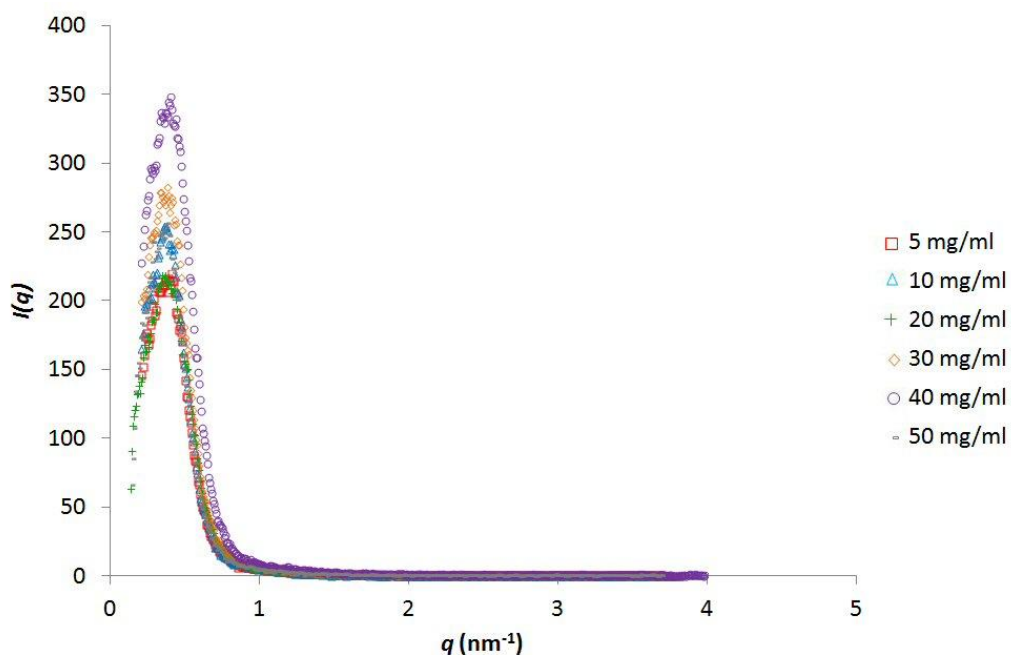
**Table 4.14** | The percentage reduction of 1-hexanol required to bring the estimated droplet size, as determined using geometric droplet size calculations, into closer correlation with the experimentally determined droplets size using SAXS experiments and subsequent GIFT analysis for single NaCl, anti-solvent microemulsions of different composition ratios, made using a TX-100/1-hexanol surfactant system.

#### 4.5.3| Droplet Sizes of Mixed Microemulsions

SAXS experiments were conducted for mixed microemulsions composed of single Lysozyme microemulsions of concentration 50-5 mgml<sup>-1</sup> and single anti-solvent microemulsions with composition ratios 1:3:6 and 2:3:5. SAXS data could not be collected for mixed microemulsions which incorporated single anti-solvent microemulsions with composition ratios 1:4:5 and 2:3:5 as the majority of these samples formed emulsions which have a droplet size larger than the detectable particle size for SAXS experiments. Confinement of the aqueous phase within the mixed microemulsions was confirmed through the scattering of X-rays by the samples as shown in Figure 4.20 and 4.21. Droplet sizes for all the mixed microemulsion samples were found to be within the expected 1-100nm range.



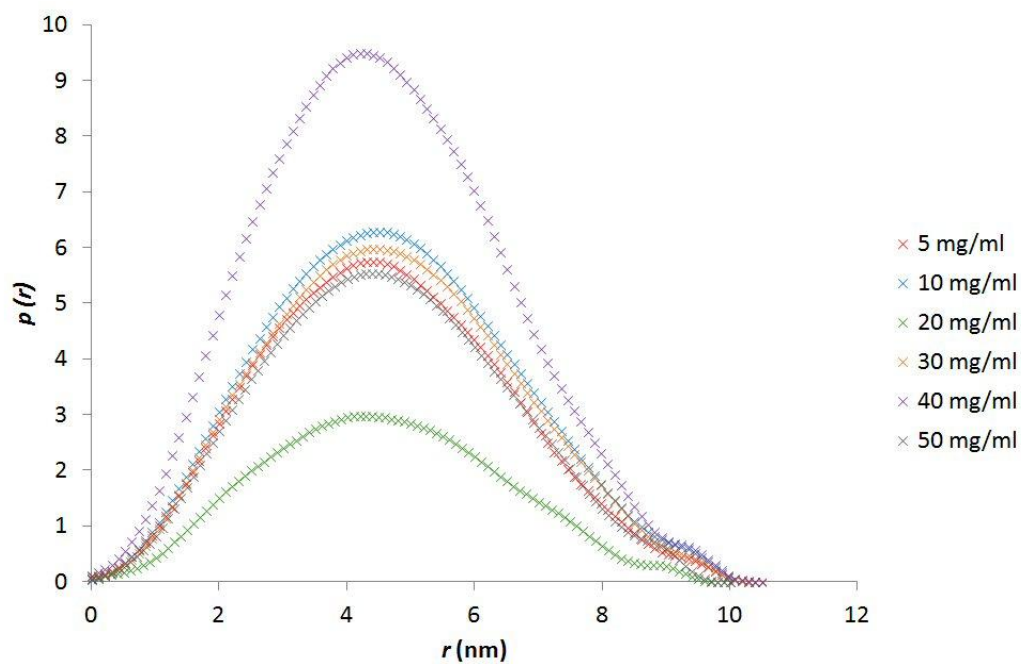
**Figure 4.20|** Plot of  $I(q)$  against  $q$  for mixed microemulsions of the TX-100/1-hexanol surfactant system, composed of single Lysozyme microemulsions with composition ratio 2:5:3 and varying Lysozyme concentration and of single anti-solvent microemulsions with composition ratio 1:3:6.



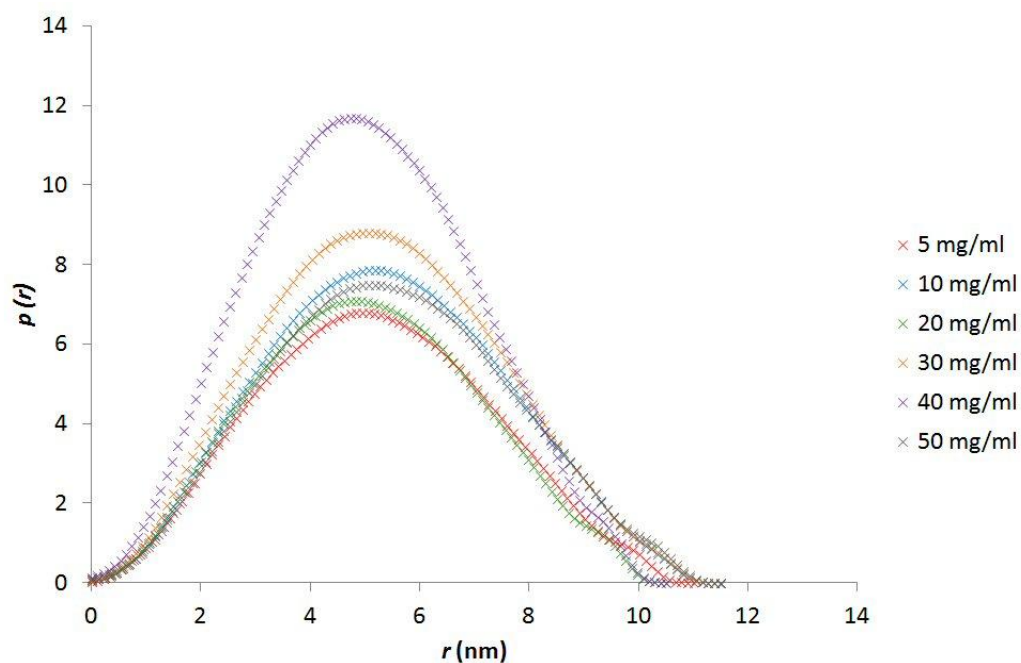
**Figure 4.21** |  $I(q)$  against  $q$  plot for mixed microemulsions of the TX-100/1-hexanol surfactant system, composed of a single Lysozyme microemulsion with composition ratio 2:5:3 with varying Lysozyme concentration and a single anti-solvent microemulsion with composition ratio 2:3:5.

From GIFT analysis, Figures 4.22 and 4.23 and Table 4.15, it can be seen that the variation in Lysozyme concentration in the mixed microemulsions does not have a significant effect on the microemulsion droplet size. The slight variation in droplet size as the concentration of Lysozyme is varied falls within the error of  $\pm 0.3$  associated with SAXS experiments for both the 1:3:6 and 2:3:5 composition ratios. However, a reasonable difference in mixed microemulsion droplet size is observed when anti-solvent microemulsions of different composition ratios are used. Larger microemulsions droplets are observed for mixed microemulsions composed of an anti-solvent microemulsion with a composition ratio 2:3:5. This trend is observed independent of Lysozyme concentration.

Using small angle X-ray diffraction measurements, Krigbaum found the radius of gyration,  $R_g$ , of Lysozyme to be  $14.3 \text{ \AA}$  in solution<sup>179</sup>. This can be approximated to a radius of  $0.9 \text{ nm}$ . Therefore, incorporation of Lysozyme into the aqueous dispersed phase will not perturb the mean droplet size, as determined by GIFT, as droplets sizes of the mixed microemulsions of the TX-100/1-hexanol surfactant system were found to be considerably larger than the approximate radius of Lysozyme.



**Figure 4.22** | Pair distance distribution plots for mixed microemulsions of the TX-100/1-hexanol surfactant system, composed of single Lysozyme microemulsions with composition ratio 2:5:3 with varying Lysozyme concentration and of single anti-solvent microemulsions with composition ratio 1:3:6.



**Figure 4.23** | Pair distance distribution plots for mixed microemulsions of the TX-100/1-hexanol surfactant system, composed of a single Lysozyme microemulsion with composition ratio 2:5:3 with varying Lysozyme concentration and a single anti-solvent microemulsion with composition ratio 2:3:5.

	Lysozyme concentration (mgml <sup>-1</sup> ) in single microemulsions with composition ratio 1:3:6					
	50	40	30	20	10	5
<b>Mena droplet radius (GIFT) (nm)</b>	4.6	4.5	4.6	4.5	4.6	4.5
<b>No. of droplets in microemulsion (x 10<sup>18</sup>)</b>	2.94	3.02	2.80	3.05	2.78	2.95
<b>Normal mean No. Lysozyme molecules per droplet</b>	0.28	0.22	0.18	0.12	0.06	0.03

**Table 4.15** | GIFT analysis results for mixed microemulsions of the TX-100/1-hexanol surfactant system, composed a single anti-solvent microemulsions with a composition ratio of 1:3:6 and single Lysozyme microemulsions of varying concentration.

	Lysozyme concentration (mgml <sup>-1</sup> ) in single microemulsions with composition ratio 2:5:3					
	50	40	30	20	10	5
<b>Mean droplet radius (GIFT) (nm)</b>	5.4	4.9	5.2	5.0	5.3	5.2
<b>No. of droplets in microemulsion (x 10<sup>18</sup>)</b>	2.10	2.75	2.25	2.62	2.17	2.27
<b>Normal mean No. Lysozyme molecules per droplet</b>	0.39	0.24	0.22	0.13	0.08	0.04

**Table 4.16** | GIFT analysis results for mixed microemulsions of the TX-100/1-hexanol surfactant system, composed a single anti-solvent microemulsions with a composition ratio of 2:3:5 and single Lysozyme microemulsions of varying concentration.

As seen with the single microemulsions of the TX-100/1-hexanol surfactant system, the mixed microemulsions also require a reduction in the amount of 1-hexanol thought to reside at the interface between the oil and aqueous phases in order for a correlation to be seen between predicted radii values using geometric calculations and radii values determined experimentally. Table 4.17 details the estimated mass of 1-hexanol through to reside at the interface with the corresponding droplet radii values for mixed microemulsions incorporating anti-solvent microemulsions with composition ratios 1:3:6 and 2:3:5. A percentage reduction of approximately 60-65% in the mass of 1-hexanol is required for mixed microemulsions incorporating anti-solvent microemulsions with composition ratio 1:3:6 and approximately 55-63% for microemulsions incorporating anti-solvent microemulsions with composition ratio 2:3:5.

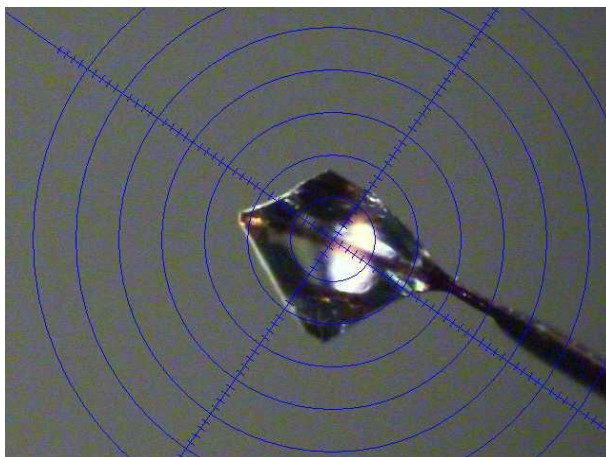


Composition ratio of anti-solvent microemulsion	Total 1-hexanol in mixed microemulsion (g)					
1:3:6	0.8	Estimate of 1-hexanol at the interface (g)	0.28	0.29	0.30	0.31
		Geometric radius (nm)	4.7	4.6	4.5	4.5
		% reduction of 1-hexanol at the interface	65.00	63.75	62.50	61.25
2:3:5	0.8	Estimate of 1-hexanol at the interface (g)	0.30	0.32	0.34	0.36
		Geometric radius (nm)	5.3	5.1	5.0	4.8
		% reduction of 1-hexanol at the interface	62.50	60.00	57.50	55.00

**Table 4.17|** The percentage reduction of 1-hexanol required to bring the estimated droplet size, as determined using geometric droplet size calculations, into closer correlation with the experimentally determined droplets size using GIFT analysis for the mixed microemulsion systems of the TX-100/1-hexanol surfactant system.

#### 4.6| Single Crystal X-ray Diffraction Experiments

Single crystals grown from both hanging drop vapour diffusion trays and mixed microemulsions were subject to X-ray diffraction experiments. An assessment of the data quality was made for the data collection of each single crystal as a means of comparing the quality of crystals grown from the two different crystallisation mediums. On average, crystals grown from each crystallisation method were the same size, approximately 0.4 mm x 0.3 mm x 0.2 mm as shown in Figure 4.24.



**Figure 4.24|** Single crystal grown from a TX-100/1-hexanol mixed microemulsion composed of a single Lysozyme microemulsion with composition ratio 2:5:3, Lysozyme concentration of  $50 \text{ mgml}^{-1}$ , and of a single anti-solvent microemulsion with composition ratio of 2:3:5. Approximately  $0.4 \text{ mm} \times 0.3 \text{ mm} \times 0.2 \text{ mm}$  in size, the crystal is mounted and centred on the goniometer.

R-merge factors indicate data quality and thus internal consistency of the crystal. Consequently,  $R(\text{int})$  values, the number of independent observations (redundancy) and  $I/\sigma(I)$  values (computed for the entire data set as well as in resolution bins) of different data sets are commonly used to compare the quality of diffraction data.  $R(\text{Int})$ , a linear merging R-value, is the most commonly used data quality indicator used to indicated the general merging on identical, but otherwise unmerged, intensities. Here we discuss some of the quality and validation criteria for data used to solve macromolecular structures in X-ray crystallography for diffraction data obtained from crystals of Lysozyme grown in both standard hanging drop vapour diffusion trays and from mixed microemulsions.

The four single crystals were all found to have a primitive, tetragonal until cell. For the two crystals grown using hanging drop vapour diffusion trays, no statistically significant difference was observed in their unit cell parameters. However, for mixed microemulsion grown crystals, the parameters of their respective unit cells were found to have a statistically significant difference suggesting that the two crystals collected are different. The determination of unit cell parameters from rotation is not extremely accurate as the rotation angle is refined to optimise the quality of the data not the accuracy of the unit cell parameters. Analysis of several high-resolution protein structures<sup>180</sup> revealed that considerable errors in the unit cell parameters were a common occurrence despite refinement during data processing.

	Crystals grown from hanging drop vapour diffusion tray	
	pH 4.8, 2:2	pH 4.4, 3:2
Temperature (K)	100	100
Crystal System	Tetragonal	Tetragonal
Space Group	P4(3)2(1)2	P4(3)2(1)2
a (Å)	78.408	78.814
b (Å)	78.408	78.814
c (Å)	36.880	36.790
$\alpha$ (°)	90.00	90.00
$\beta$ (°)	90.00	90.00
$\gamma$ (°)	90.00	90.00
Volume (Å <sup>3</sup> )	226732.61	228530.00
Resolution (Å <sup>3</sup> )	1.80	1.60
Mean I	25.7	23.7
Mean I/Sigma	35.85	48.55
R(Int)	0.0399	0.0258
R(Sigma)	0.0225	0.0150
Redundancy	8.54	7.64
% Complete	99.3	98.4

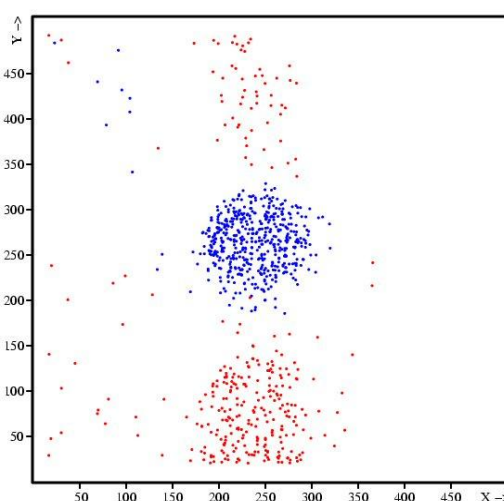
**Table 4.18** | Data statistics for single Lysozyme crystals grown from hanging drop vapour diffusion trays in which the pH of the reservoir buffer solution and the hanging drop ratio (protein solution: reservoir solution) were both varied.

	Crystals grown from mixed microemulsion	
	Crystal 1	Crystal 2
Temperature (K)	100	100
Crystal System	Tetragonal	Tetragonal
Space Group	P4(3)2(1)2	P4(3)2(1)2
a (Å)	76.901	78.049
b (Å)	76.901	78.049
c (Å)	37.249	37.262
$\alpha$ (°)	90.00	90.00
$\beta$ (°)	90.00	90.00
$\gamma$ (°)	90.00	90.00
Volume (Å <sup>3</sup> )	220282.34	226983.38
Resolution (Å <sup>3</sup> )	1.80	1.61
Mean I	22.5	19.3
Mean I/Sigma	28.86	23.36
R(Int)	0.0494	0.0403
R(Sigma)	0.0269	0.0296
Redundancy	8.15	5.56
% Complete	99.3	97.2

**Table 4.19** | Data statistics for two single Lysozyme crystals grown from a TX-100/1-hexanol mixed microemulsion composed of a single Lysozyme microemulsion with composition ratio 2:5:3, Lysozyme concentration of 50 mgml<sup>-1</sup>, and of a single anti-solvent microemulsion with composition ratio, 2:3:5.

Common indicators of data quality for Lysozyme crystals grown in hanging drop vapour diffusion trays and via mixed microemulsions are listed in Tables 4.18 and 4.19 respectively. Similar results were obtained for each data set collected from each of the four Lysozyme crystals. The values obtained were typical for a data collection of a test protein, Lysozyme, from the diffractometer used. For crystals grown in both crystallisation media explored in this thesis, R-values within the expected range were obtained. However, for the crystal grown in a hanging drop of pH 4.4 and hanging drop ratio of 3:2, a slightly low R(Int) value was observed. This may be associated with the slightly lower redundancy of the data set. Alternatively, the low R(Int) value may be an artefact of the freezing of the crystal in the cryo stream which differs for each crystal tested.

The minimal differences observed between each data set may be accounted for by differences in freezing of each Lysozyme crystal in the cryo stream. The setup of the diffractometer should also be considered. Due to the availability of the diffractometer the data sets were not conducted consecutively. Over time, water condensation can build between the Phosphor layer and the glass plate of the detector. This results from the difference in temperature as the CCD chip is cooled to  $-60^{\circ}\text{C}$ . Consequently, the recorded intensity of the X-rays hitting the detector may be above or below the expected intensity. This can be seen using a spatial distribution of  $(I-\langle I \rangle)/\sigma$  plot, Figure 4.25, which indicates in red and blue, intensities that are observed to be above and below the expected intensity respectively.



**Figure 4.25 |** Spatial distribution of  $(I-\langle I \rangle)/\sigma$  from data set collected from crystal grown using hanging drop vapour diffusion, with reservoir solution pH 4.4 and hanging drop ratio, 3:2. Red and blue points respectively indicate intensities that are observed to be above and below the expected intensity.

Over the period of which the four data collections were conducted this was found to be the case. This may contribute to the differences in data quality for each of the four Lysozyme crystals exposed to X-ray diffraction experiments. Subsequently, the diffractometer has been serviced and the condensation between the phosphor layer and glass plate has been addressed.

# Chapter Five

---

## *Conclusions*

In this thesis the crystallisation from microemulsions of a commonly used standard protein, Lysozyme, was compared to its crystallisation using a standard technique, hanging drop vapour diffusion. An assessment of the resultant Lysozyme crystals grown from each crystallisation medium was made with the aid of single crystal X-ray diffraction experiments. Previously, microemulsions have been utilised in the successful crystallisation of small molecules only such as ROY<sup>3</sup> and glycine<sup>4</sup>. Here, it is shown, for the first time that the novel microemulsion methodology can be successfully used for the crystallisation of proteins, extending the methods towards macromolecular crystallography.

Several surfactant systems were explored and variations of the microemulsion method exploited in an attempt to crystallise Lysozyme under thermodynamic control using 3D nano-confinement in microemulsions. The five surfactant systems used include Span80/Brij30, Span80/Tween80, AOT, TX-114 and TX-100/1-hexanol. Three variations of the microemulsion method were made: direct addition of anti-solvent (an aqueous NaCl solution was used), the mixed microemulsion method and evaporation of the continuous phase. SAXS experiments were conducted to confirm the formation of microemulsions through the occurrence of X-ray scattering and subsequent determination of the droplet size using GIFT analysis.

To aid the assessment of the quality of Lysozyme crystals grown using microemulsions a standard hanging drop vapour diffusion tray was utilised to grow Lysozyme crystals of a typically expected quality for single crystal X-ray diffraction experiments. In these standard trays the pH of the reservoir solutions and the ratio of the 50 mgml<sup>-1</sup> Lysozyme solution and reservoir solution within the hanging drop were varied.

A Bruker MicroStar diffractometer was used for the screening of crystals and for data collection of crystals grown from both hanging drop vapour diffusion and microemulsions. An evaluation of the collected data sets was made through comparison of key indicators of data quality commonly published within the crystallographic “table 1”. From the quality of each data set a comparative assessment of crystal quality was made for crystals grown by both protein crystallisation mediums explored within this thesis.

Demonstrating the success of a commonly used crystallisation technique, Lysozyme crystals were grown using a hanging drop vapour diffusion tray. Crystals of a high quality

used for X-ray diffraction experiments were grown from a reservoir solution of pH 4.8 and 4.4 with hanging drop ratio 2:2 and 3:2, respectively. Not all crystallisation conditions in the individual wells were successful and the quality (as judged by eye) and number of crystals present in successful wells varied across the tray (Table 4.1). Crystallisation may not have occurred because of several influencing factors; most likely, supersaturation was not reached. The growth of several smaller crystals within the same drop may be a result of nucleation occurring later on in the supersaturated metastable region resulting in the formation of numerous critical nuclei and thus growth of several small crystals (as shown in the crystallisation phase diagram, Figure 2.15). As expected, in light of extensive previous work on the crystallisation of Lysozyme<sup>13</sup>, single Lysozyme crystals of a good quality could be successfully and reliably grown using the hanging drop vapour diffusion trays.

Of the several surfactant systems explored, not all were successful in supporting the crystallisation of Lysozyme despite being shown to form microemulsions by SAXS experiments and subsequent droplet size determination. Unsuccessful systems typically incorporated either or both a small Lysozyme concentration (less than 3 mgml<sup>-1</sup>) and/or a small volume of aqueous phase. In these circumstances, crystallisation may not occur due to supersaturation not being obtained within the microemulsion droplets on account of the low Lysozyme concentrations. In cases where supersaturation may have been reached and nucleation within the droplets has taken place, the slow rate of droplet collision due the limited amount of aqueous phase incorporated in the microemulsion system may inhibit crystal growth.

The TX-100/1-hexanol surfactant system was found to be most successful system, and therefore the system of choice, successfully crystallising Lysozyme when the mixed microemulsion methodology was applied. The quality, morphology and quantity of Lysozyme crystals were found to vary with the composition ratio of the single anti-solvent (5% (wt) NaCl solution) microemulsions and the concentration of Lysozyme in the single protein microemulsion of composition ratio 2:5:3. Lysozyme crystals of the most suitable quality, as judged by eye and later shown through diffraction experiments, for single crystal X-ray diffraction experiments were obtained from a mixed microemulsion with a Lysozyme microemulsion of concentration 50 mgml<sup>-1</sup> and a NaCl, anti-solvent microemulsion of composition ration 2:3:5. Crystallisation from this mixed microemulsion gave numerous, good quality crystals in one sample. This result was successfully repeated.

The use of SAXS experiments on microemulsion samples proved highly valuable, confirming the formation of microemulsions through the occurrence of X-ray scattering and

the subsequent determination of droplet sizes using GIFT analysis, all of which fell within the expected 1-100 nm range for microemulsions. Interestingly for both the TX-114 and TX-100/1-hexanol surfactant system it was found that to bring the geometrically calculated droplet size and the GIFT calculated droplet size into correlation a reduced amount of 1-hexanol thought to partition at the oil/water interface was required in the geometric calculations.

Key indicators of data quality, including R-values and redundancy, were similar for each data set collected from single Lysozyme crystals grown from both hanging drop vapour diffusion trays and microemulsions, a new methodology for protein crystallisation presented in this thesis. Using the Bruker MicroStar diffractometer, data sets of an equally good quality can be collected from single Lysozyme crystals grown from the two crystallisation mediums discussed in Sections 4.2 and 4.4.8. The data sets collected are of a publishable quality, with the values of common data quality indicators being within the ranges found and expected within literature<sup>181-183</sup>. This demonstrates that microemulsions provide a novel methodology for protein crystallisation producing crystals of a quality commonly found using standard techniques.

Crystallisation remains the bottle neck for structural analysis of proteins<sup>1</sup>, particularly proteins for which structural information is vital for structure based drug design of these key targets. While structures of some targets are known<sup>184-187</sup>, many remain to be determined. Ideally, the development of a generic methodology for protein crystallisation will help relieve the bottle neck in crystallisation, particularly for proteins which display polymorphism. This would be advantageous for pharmaceutical companies which may require the most thermodynamically stable form of a peptide drug, a type of drug which is being increasingly being developed as therapeutic mediums<sup>188</sup>. To this end, further work should be carried out in which the microemulsion method, used for the crystallisation of Lysozyme in this thesis, should be applied to the crystallisation of different model proteins. Proteins such as Insulin, glucose isomerase and albumin would be well suited for this task. Alternative surfactant systems may be required and their crystallisation may or may not require the use of mixed microemulsions as was seen for Lysozyme crystallisation.

Expanding the microemulsion technique to the crystallisation of membrane proteins may require the development of an oil in water microemulsion system as a result of the hydrophobic nature of membrane proteins. Complications may arise for transmembrane proteins which consist of both hydrophobic and hydrophilic moieties. The isolation and purification of membrane proteins through the use of detergent/surfactant



molecules often leads to protein/detergent complexes. The incorporation of these complexes into a microemulsion system may see the complex residing at the interface of the dispersed and continuous phases due to the presence of detergent molecules. SAXS and subsequent GIFT analysis may be used to confirm formation of microemulsions and determine droplets size, it may also be possible to decipher where the membrane protein partitions within the microemulsion structure, either in the oil or water phases or at their interface.

Several potential membrane proteins and membrane spanning peptides could be utilised in order to explore the use of microemulsions for their crystallisation. In particular the 25 residue, membrane-spanning part of the M2 protein of the influenza virus would be an interesting starting point due to its biological importance as a target of anti-influenza drugs, amantadine and rimantadine<sup>189</sup>. The M2 peptide is well suited for systematic crystallisation studies as the crystallisation conditions for the wild-type peptide are known, thus serving as a benchmark for crystal quality. Also, although the peptide is soluble in aqueous solution it inserts itself into biological membranes and therefore behaves like a small integral membrane protein. Through the use of microemulsions for the crystallisation of resistant determining variants of the M2 peptide there is prospect in gaining further insight into one of the resistance mechanisms of the influenza virus. Further still, microemulsions could be applied to the crystallisation of bacteriorhodopsin for which crystallisation conditions are known, again serving as a benchmark for crystal quality.

Microemulsions had previously only been applied to the crystallisation of small molecules, glycine and ROY; in this thesis microemulsions have been successfully used as a novel technique for crystallising the model protein, Lysozyme. The use of microemulsions to crystallise Lysozyme opens up a new avenue for macromolecular crystallography in attempts to relieve the “bottle neck” in crystallisation currently experienced within research concerning the structural exploration of proteins and membrane proteins.

## Appendix

### A1| Crystallisation Conditions for Different Crystal Forms of Lysozyme and Lysozyme Nitrate

	Crystal form	Crystallisation conditions
Lysozyme	Monoclinic	1) 1.0 g HEWL dissolved in 10 ml aqueous solution containing 10% NaCl and 5% 1-propanol. The pH of the solution was adjusted to 7.6 with 0.1 M HCl at 313K <sup>125</sup> .
	Triclinic	1) Sitting drop, vapour diffusion. 30 mgml <sup>-1</sup> protein, 20 nM sodium acetate buffer, pH4.7. Well solution = 0.5 M NaNO <sub>3</sub> , 0.1 M sodium acetate buffer, pH4.7, 20% ethylene glycol. 1.5 µl drops of protein and well solutions were micro-seeded with crushed crystals of triclinic Lysozyme. Crystals grew at 292K over 5days <sup>190</sup> . 2) D <sub>2</sub> O solution containing 1% (w/v) protein, 2% (w,v) NaNO <sub>3</sub> and 10 nM sodium acetate. Seed crystals were added to the protein solution and was allowed to stand at 313K <sup>191</sup> . 3) Triclinic form II was formed by transformation of form I by its exposure to a dry nitrogen gas stream at 263K <sup>191</sup> .
	Hexagonal	1) Solid sodium bicarbonate added to 10% (v/v) aqueous acetone solution until pH8.4. Solution saturated with NaNO <sub>3</sub> , final protein concentration of 25 mgml <sup>-1</sup> at 293K <sup>13</sup> .
	Orthorhombic	1) Batch method. 500 mg HEWL in 5 ml water. 0.625 ml of 0.3M acetate buffer, pH4.7 and 1.875 ml of water. 7.5 ml of 100 mgml <sup>-1</sup> NaCl solution. Crystals obtained in two days <sup>192</sup> . 2) Hanging drop, vapour diffusion. Droplet solution = 40 mgml <sup>-1</sup> protein, phosphate buffer, pH6.5, 5% (w,v) NaCl. Well solution = phosphate buffer, pH6.5, 20% (w,v) NaCl. Crystals took approximately two weeks to grow <sup>193</sup> .
	Tetragonal	1) Yeast extracts, Marmite, Promite and Vegimite using counter diffusion crystallisation <sup>194</sup> . 2) Batch method. Equal volumes of protein solution (50 mgml <sup>-1</sup> Lysozyme solution in 50 mM sodium acetate at pH4.5) and of the precipitating agent (precipitant NaCl in the same buffer, which concentration varied: 0.6, 0.8, 1.0, and 2.0 M), both prepared at room temperature. Prior to crystallization, all solutions were filtered through 0.22 µm syringe filters (Millipore). Quasi two-dimensional glass cells used <sup>195</sup> .

Lysozyme nitrate	Monoclinic	<ol style="list-style-type: none"> <li>1) Generally obtained in the absence of acetate buffer<sup>196</sup>.</li> <li>2) 1% protein solution adjusted to pH4.5 by addition of nitric acid, and 0.35 M sodium nitrate at room temperature<sup>196</sup>.</li> <li>3) 3% protein solution in 0.23 M sodium nitrate at pH4.5 at 4°C and 23°C. Nature of buffer missing but thought most likely to be acetate to fix pH4.5<sup>196</sup>.</li> <li>4) 0.2 M NaNO<sub>3</sub>, 50 mM acetate buffer, pH4.5 in light and heavy water solutions<sup>196, 197</sup>.</li> </ol>
	Triclinic	<ol style="list-style-type: none"> <li>1) 0.2 M NaNO<sub>3</sub>, 50 mM acetate buffered solution, pH4.5, light water<sup>196</sup>.</li> <li>2) 30 mgml<sup>-1</sup> of protein, acetate buffer, pH4.5. Monoclinic forms initially at 23°C, stable for weeks-months. Monoclinic crystals dissolve slowly as triclinic begin to form<sup>196</sup>.</li> <li>3) 7 mgml<sup>-1</sup> of protein, 0.2-0.3 M NaNO<sub>3</sub>, 50 mM acetic acid/Na acetate buffer, pH4.5, stored overnight at 4°C (precipitation step), triclinic crystals begin to form over a few days at 18°C<sup>196</sup>.</li> <li>4) &lt;5 mgml<sup>-1</sup> (3.4 and 3.0 mgml<sup>-1</sup>) protein, 4°C precipitation step, seeded at 18.5°C with triclinic crystals, kept at 18.5°C for four weeks<sup>196</sup>.</li> </ol>

## A2| Preparation of Compounds Subjected to Chemical Crystallisation

Compound	Amino acid sequence	Preparation
ASH81/87	Boc-SerArF-OBn	Made from Boc-L-Ser-OBn with pentafluoropyridine and K <sub>2</sub> CO <sub>3</sub> (Base)
ASH91	Fmoc-Ser(tbu)-SerArF-OBn	Boc-SerArF-OBn (ASH 81/87) was treated with trifluoroacetic acid (TFA) to remove Boc protection to yield: H-SerArF-OBn which was coupled to Fmoc-Ser(tBu)-OH with PyBOP (activator) and NMM (base)
ASH93	Fmoc-Cys(trt)-SerArF-OBn	Boc-SerArF-OBn (ASH 81/87) was treated with TFA to remove Boc protection to yield: H-SerArF-OBn which was coupled to Fmoc-Cys(trt)-OH with PyBOP (activator) and NMM (base) to yield: Fmoc-Cys(trt)-SerArF-OBn (ASH 74). (ASH 74) was then treated with TFA to remove the trt protection from the cysteine.
ASH59		ASH 59 was a side product formed in the preparation of ASH81/87
ASH82	Boc-SerArF-Ala-OBn	Boc-SerArF-OBn was hydrogenated to deprotect the benzyl protection to yield Boc-SerArF-OH (ASH 80) Boc-Ala-OH was treated with benzyl bromide to yield Boc-Ala-OBn (ASH 79), ASH 79 was treated with TFA to remove the Boc protection and yield H-Ala-OBn (H-L-Ala-OBzl.HCl). This H-Ala-OBn (H-L-Ala-OBzl.HCl) was coupled to Boc-SerArF-OH (ASH 80)
AH89	Boc-Ala-SerArF-Ala-OBn	ASH 82 was treated with TFA to yield H-SerArF-Ala-OBn, this was coupled to Boc-Ala-OH to yeild ASH 89

## References

1. N. E. Chayen, *Current Opinion in Structural Biology*, 2004, **14**, 577-583.
2. N. E. Chayen, in *Structural Genomics, Part C*, Elsevier Academic Press Inc, San Diego, Editon edn., 2009, vol. 77, pp. 1-22.
3. C. E. Nicholson, C. Chen, B. Mendis and S. J. Cooper, *Crystal Growth & Design*, 2010, **11**, 363-366.
4. C. Chen, O. Cook, C. E. Nicholson and S. J. Cooper, *Crystal Growth & Design*, 2011, **11**, 2228-2237.
5. T. Werner, M. B. Morris, S. Dastmalchi and W. B. Church, *Adv. Drug Deliv. Rev.*, 2012, **64**, 323-343.
6. S. Y. Huang and X. Q. Zou, *Int. J. Mol. Sci.*, 2010, **11**, 3016-3034.
7. Y. Y. Li, T. J. Hou and W. A. Goddard, *Curr. Med. Chem.*, 2010, **17**, 1167-1180.
8. <http://www.iycr2014.org/>.
9. J. Bauer, S. Spanton, R. Henry, J. Quick, W. Dziki, W. Porter and J. Morris, *Pharmaceutical Research*, 2001, **18**, 859-866.
10. S. R. Chemburkar, J. Bauer, K. Deming, H. Spiwek, K. Patel, J. Morris, R. Henry, S. Spanton, W. Dziki, W. Porter, J. Quick, P. Bauer, J. Donaubauer, B. A. Narayanan, M. Soldani, D. Riley and K. McFarland, *Organic Process Research & Development*, 2000, **4**, 413-417.
11. W. Ostwald, *Physical Chemistry*, 1897, **22**, 289-330.
12. S. Y. Chung, Y. M. Kim, J. G. Kim and Y. J. Kim, *Nat. Phys.*, 2009, **5**, 68-73.
13. C. Brinkmann, M. S. Weiss and E. Weckert, *Acta Crystallographica Section D-Biological Crystallography*, 2006, **62**, 349-355.
14. C. C. West and J. H. Harwell, *Environmental Science & Technology*, 1992, **26**, 2324-2330.
15. T. Cosgrove, *Colloid Science: Principles, Methods and Applications*, John Wiley & Sons, 2010.
16. M. J. Rosen, *Surfactants and Interfacial Phenomena*, 1 edn., Wiley, New York, 1978.
17. R. Kumar, G. C. Kalur, L. Ziserman, D. Danino and S. R. Raghavan, *Langmuir*, 2007, **23**, 12849-12856.
18. M. J. Rosen, *J. Am. Oil Chem. Soc.*, 1972, **49**, 293-&.
19. W. Norde, *Colloids and Interfaces in Life Sciences*, CRC Press, 2003.
20. B. Smit, A. G. Schlijper, L. A. M. Rupert and N. M. Vanos, *J. Phys. Chem.*, 1990, **94**, 6933-6935.
21. B. Smit, *Phys. Rev. A*, 1988, **37**, 3431-3433.
22. R. Varadaraj, J. Bock, P. Valint, S. Zushma and R. Thomas, *J. Phys. Chem.*, 1991, **95**, 1671-1676.
23. A. R. Pitt, S. D. Morley, N. J. Burbidge and E. L. Quickenden, *Colloids and Surfaces a-Physicochemical and Engineering Aspects*, 1996, **114**, 321-335.
24. K. R. Wormuth and S. Zushma, *Langmuir*, 1991, **7**, 2048-2053.
25. A. Aspee and E. Lissi, *Journal of Colloid and Interface Science*, 1996, **178**, 298-302.
26. M. J. Rosen, *J. Am. Oil Chem. Soc.*, 1974, **51**, A518-A518.
27. Y. Moroi, *Micelles: Theoretical and Applied Aspects*, Springer, 1992.
28. P. Mukerjee and K. J. Mysels, *Critical micelle concentrations of aqueous surfactant systems*, U.S. National Bureau of Standards, Washington, D.C., 1971.
29. I. Reich, *The Journal of Physical Chemistry*, 1956, **60**, 257-262.
30. G. S. Hartley, *Aqueous Solutions of Paraffin Chain Salts: A Study in Micelle Formation*, Hermann & Cie., 1936.

31. B. Jonsson, B. Lindman, K. Holmberg and B. Kronberg, *Surfactants and Polymers in Aqueous Solution*, John Wiley & Sons, 1998.
32. H. Hoffmann and G. Ebert, *Angewandte Chemie International Edition in English*, 1988, **27**, 902-912.
33. J. N. Israelachvili, *Intermolecular and Surface Forces: Revised Third Edition*, Elsevier Science.
34. S. Paula, W. Sues, J. Tuchtenhagen and A. Blume, *The Journal of Physical Chemistry*, 1995, **99**, 11742-11751.
35. M. J. Blandamer, P. M. Cullis, L. G. Soldi, J. B. F. N. Engberts, A. Kacperska, N. M. Van Os and M. C. S. Subha, *Advances in Colloid and Interface Science*, 1995, **58**, 171-209.
36. S. H. Tolbert, C. C. Landry, G. D. Stucky, B. F. Chmelka, P. Norby, J. C. Hanson and A. Monnier, *Chemistry of Materials*, 2001, **13**, 2247-2256.
37. N. K. Pandit, J. Kanjia, K. Patel and D. G. Pontikes, *International Journal of Pharmaceutics*, 1995, **122**, 27-33.
38. J. N. Phillips, *Transactions of the Faraday Society*, 1955, **51**, 561-569.
39. Z. L. Wang, H. H. Xu, W. Z. Zhang, B. H. Zhuang and H. S. Qi, *Colloids and Surfaces B-Biointerfaces*, 2008, **61**, 118-122.
40. K. Shinoda, Y. Minegishi and H. Arai, *The Journal of Physical Chemistry*, 1976, **80**, 1987-1988.
41. S. R. Raghavan, H. k. Edlund and E. W. Kaler, *Langmuir*, 2002, **18**, 1056-1064.
42. S. Kumar, D. Sharma and D. Kabir ud, *Langmuir*, 2000, **16**, 6821-6824.
43. P. Mukherjee, S. K. Padhan, S. Dash, S. Patel and B. K. Mishra, *Advances in Colloid and Interface Science*, 2011, **162**, 59-79.
44. C. Manohar, in *Adsorption and Aggregation of Surfactants in Solution*, Editon edn., 2003, vol. 109, pp. 211-217.
45. M. Corti, C. Minero and V. Degiorgio, *J. Phys. Chem.*, 1984, **88**, 309-317.
46. A. Zilman, S. A. Safran, T. Sottmann and R. Strey, *Langmuir*, 2004, **20**, 2199-2207.
47. H. Bock and K. E. Gubbins, *Physical Review Letters*, 2004, **92**, 4.
48. G. Fritz, G. n. Scherf and O. Glatter, *The Journal of Physical Chemistry B*, 2000, **104**, 3463-3470.
49. J. P. Hanrahan, K. J. Ziegler, J. D. Glennon, D. C. Steytler, J. Eastoe, A. Dupont and J. D. Holmes, *Langmuir*, 2003, **19**, 3145-3150.
50. C. D. Ablan, D. Sheppard, E. J. Beckman, M. M. Olmstead and P. G. Jessop, *Green Chemistry*, 2005, **7**, 590-594.
51. C. Rodriguez-Abreu and M. Lazzari, *Current Opinion in Colloid & Interface Science*, 2008, **13**, 198-205.
52. C. Solans and H. Kunieda, *Industrial Applications of Microemulsions*, M. Dekker, 1997.
53. T. Tadros, R. Izquierdo, J. Esquena and C. Solans, *Advances in Colloid and Interface Science*, 2004, **108**, 303-318.
54. I. Danielsson and B. Lindman, *Colloids and Surfaces*, 1981, **3**, 391-392.
55. I. Capek, *Advances in Colloid and Interface Science*, 2004, **107**, 125-155.
56. P. Taylor, *Advances in Colloid and Interface Science*, 1998, **75**, 107-163.
57. L. J. Wei, G. Li, Y. D. Yan, R. Pradhan, J. O. Kim and Q. Z. Quan, *Archives of Pharmacal Research*, 2012, **35**, 1037-1043.
58. S. S. Davis, C. Washington, P. West, L. Illum, G. Liversidge, L. Sternson and R. Kirsh, *Ann. N.Y. Acad. Sci.*, 1987, **507**, 75-88.
59. G. S. Hartley, *Chem. Ind.*, 1967, 575-&.
60. W. C. Griffin, *Journal of Cosmetic Science*, 1949, **1**, 311-326.
61. P. M. Kruglyakov, *Hydrophile - Lipophile Balance of Surfactants and Solid Particles: Physicochemical aspects and applications*, Elsevier Science, 2000.

62. J. T. Davies and E. K. Rideal, *Interfacial phenomena*, Academic Press, 1963.
63. C. Solans, P. Izquierdo, J. Nolla, N. Azemar and M. J. Garcia-Celma, *Current Opinion in Colloid & Interface Science*, 2005, **10**, 102-110.
64. M. S. El-Aasser and E. D. Sudol, *Jct Research*, 2004, **1**, 21-31.
65. J. Y. Fang, P. C. Wu, C. L. Fang and C. H. Chen, *J. Pharm. Sci.*, 2010, **99**, 2375-2385.
66. P. Becher, *Encyclopedia of Emulsion Technology*, M. Dekker, 1996.
67. F. Donsi, M. Annunziata, M. Vincensi and G. Ferrari, *Journal of Biotechnology*, 2012, **159**, 342-350.
68. M. Antonietti and K. Landfester, *Progress in Polymer Science*, 2002, **27**, 689-757.
69. J. L. Chai, Y. H. Gao, K. S. Zhao, G. Z. Li and G. Y. Zhang, *Chinese Chemical Letters*, 2005, **16**, 1263-1266.
70. R. Strey, *Colloid and Polymer Science*, 1994, **272**, 1005-1019.
71. T. Tadros and B. Vincent, in *Encyclopaedia of Emulsion Technology*, ed. P. Becher, Marcel Dekker, New York, Editon edn., 1980, vol. 1.
72. J. H. Schulman, W. Stoeckenius and L. M. Prince, *J. Phys. Chem.*, 1959, **63**, 1677-1680.
73. D. P. Acharya and P. G. Hartley, *Current Opinion in Colloid & Interface Science*, 2012, **17**, 274-280.
74. B. K. Paul and S. P. Moulik, *Current Science*, 2001, **80**, 990-1001.
75. P. A. Winsor, *Transactions of the Faraday Society*, 1948, **44**, 376-398.
76. C. R. B. Mendonca, Y. P. Silva, W. J. Bockel, E. F. Simo-Alfonso, G. Ramis-Ramos, C. M. S. Piatnicki and C. I. D. Bica, *Journal of Colloid and Interface Science*, 2009, **337**, 579-585.
77. G. Palazzo, F. Lopez, M. Giustini, G. Colafemmina and A. Ceglie, *J. Phys. Chem. B*, 2003, **107**, 1924-1931.
78. D. Langevin, *Annual Review of Physical Chemistry*, 1992, **43**, 341-369.
79. M. Gradzielski, D. Langevin and B. Farago, *Physical Review E*, 1996, **53**, 3900-3919.
80. U. Olsson and P. Schurtenberger, *Langmuir*, 1993, **9**, 3389-3394.
81. M. Kahlweit and R. Strey, *Angewandte Chemie International Edition in English*, 1985, **24**, 654-668.
82. J. Balogh, *Advances in Colloid and Interface Science*, 2010, **159**, 22-31.
83. E. van der Linden, S. Geiger and D. Bedaux, *Physica A*, 1989, **156**, 130-143.
84. P. Guering, A. M. Cazabat and M. Paillette, *Europhysics Letters*, 1986, **2**, 953-960.
85. M. A. Arandia, A. M. Forgiarini and J. L. Salager, *J. Surfactants Deterg.*, 2010, **13**, 119-126.
86. S. Iglaue, Y. F. Wu, P. Shuler, Y. C. Tang and W. A. Goddard, *Journal of Petroleum Science and Engineering*, 2010, **71**, 23-29.
87. L. Bemert, S. Engelskirchen, C. Simon and R. Strey, *Abstr. Pap. Am. Chem. Soc.*, 2009, **237**, 1.
88. K. Shinoda, Y. Shibata and B. Lindman, *Langmuir*, 1993, **9**, 1254-1257.
89. F. M. Menger, J. A. Donohue and R. F. Williams, *Journal of the American Chemical Society*, 1973, **95**, 286-288.
90. P. G. Jones, *Chemistry in Britain*, 1981, **17**, 222-&.
91. A. Kuo, M. W. Bowler, J. Zimmer, J. F. Antcliff and D. A. Doyle, *Journal of Structural Biology*, 2003, **141**, 97-102.
92. H. H. Dieu, in *Algoritmy 2009: 18th Conference on Scientific Computing*, Slovak Univ Tech Bratislava, Bratislava, Editon edn., 2009, pp. 196-201.
93. B. Rupp, *Biomolecular Crystallography: Principles, Practice, and Application to Structural Biology*, Taylor & Francis Group.
94. S. Auer and D. Frenkel, *Nature*, 2001, **409**, 1020-1023.

95. I. V. Markov, *Crystal Growth for Beginners: Fundamentals of Nucleation, Crystal Growth and Epitaxy*, World Scientific, 2003.
96. T. Young, *Philosophical Transactions of the Royal Society of London*, 1805, **95**, 65-87.
97. J. W. Quail, J. Shen, M. J. T. Reaney and R. Sammynaiken, *Acta Crystallographica Section E-Structure Reports Online*, 2009, **65**, O1913-U3450.
98. G. Schatte, S. Labiuk, B. Li, P. G. Burnett, M. Reaney, P. Grochulski, M. Fodje, J. Yang and R. Sammynaiken, *Acta Crystallographica Section E-Structure Reports Online*, 2012, **68**, O50-+.
99. P. Jadhav, G. Schatte, S. Labiuk, P. G. Burnett, B. Li, D. Okinyo-Owiti, M. Reaney, P. Grochulski, M. Fodje and R. Sammynaiken, *Acta Crystallographica Section E-Structure Reports Online*, 2011, **67**, O2360-U2514.
100. E. Benedetti and C. Pedone, *Journal of Peptide Science*, 2005, **11**, 268-272.
101. <http://www.ccdc.cam.ac.uk/products/csd/>.
102. A. Darcy, *Acta Crystallographica Section D-Biological Crystallography*, 1994, **50**, 469-471.
103. <http://www.thesgc.org/scientists/groups/oxford/biotechnology>.
104. B. Rupp, B. W. Segelke, H. I. Krupka, T. P. Lakin, J. Schafer, A. Zemla, D. Toppani, G. Snell and T. Earnest, *Acta Crystallographica Section D-Biological Crystallography*, 2002, **58**, 1514-1518.
105. B. W. Segelke, J. Schafer, M. A. Coleman, T. P. Lakin, D. Toppani, J. K. Skowronek, J. A. Kantardjieff and B. Rupp, *Journal of Structural and Functional Genomics*, 2004, **5**, 147-157.
106. A. Ben-Shem, N. G. de Loubresse, S. Melnikov, L. Jenner, G. Yusupova and M. Yusupov, *Science*, 2011, **334**, 1524-1529.
107. [http://www.nobelprize.org/nobel\\_prizes/chemistry/laureates/2012/](http://www.nobelprize.org/nobel_prizes/chemistry/laureates/2012/).
108. K. V. Dunlop and B. Hazes, *Acta Crystallographica Section D-Biological Crystallography*, 2003, **59**, 1797-1800.
109. N. E. Chayen, P. D. S. Stewart and D. M. Blow, *Journal of Crystal Growth*, 1992, **122**, 176-180.
110. E. Conti, N. P. Franks and P. Brick, *Structure*, 1996, **4**, 287-298.
111. E. Conti, L. F. Lloyd, J. Akins, N. P. Franks and P. Brick, *Acta Crystallographica Section D-Biological Crystallography*, 1996, **52**, 876-878.
112. E. V. Boldyreva, T. N. Drebuschak, T. P. Shakhshneider, H. Sowa, H. Ahsbahs, S. V. Goryainov, S. N. Ivashevskaya, E. N. Kolesnik, V. A. Drebuschak and E. B. Burgina, *Arkivoc*, 2004, 128-155.
113. A. Fleming, *Proceedings of the Royal Society of London Series B-Containing Papers of a Biological Character*, 1922, **93**, 306-317.
114. K. Meyer, J. W. Palmer, R. Thompson and D. Khorazo, *Journal of Biological Chemistry*, 1936, **113**, 479-486.
115. D. M. Chipman and N. Sharon, *Science*, 1969, **165**, 454-&.
116. R. R. Feiner, K. Meyer and A. Steinberg, *Journal of Bacteriology*, 1946, **52**, 375-384.
117. E. P. Abraham, *Biochemical Journal*, 1939, **33**, 622-630.
118. M. C. Vaney, S. Maignan, M. RiesKautt and A. Ducruix, *Acta Crystallographica Section D-Biological Crystallography*, 1996, **52**, 505-517.
119. F. Rosenberger, *Journal of Crystal Growth*, 1996, **166**, 40-54.
120. S. Talreja, D. Y. Kim, A. Y. Mirarefi, C. F. Zukoski and P. J. A. Kenis, *Journal of Applied Crystallography*, 2005, **38**, 988-995.
121. P. G. Vekilov, *Journal of Crystal Growth*, 2005, **275**, 65-76.
122. L. K. Steinrauf, *Acta Crystallographica*, 1959, **12**, 77-79.



123. E. Petrova, P. Dold and K. Tsukamoto, *Journal of Crystal Growth*, 2007, **304**, 141-149.
124. C. C. F. Blake, D. F. Koenig, G. A. Mair, A. C. T. North, D. C. Phillips and V. R. Sarma, *Nature*, 1965, **206**, 757-&.
125. K. Harata, *Acta Crystallographica Section D-Biological Crystallography*, 1994, **50**, 250-257.
126. F. H. C. Crick, *Acta Crystallographica*, 1953, **6**, 221-222.
127. M. C. Vaney, I. Broutin, P. Retailleau, A. Douangamath, S. Lafont, C. Hamiaux, T. Prange, A. Ducruix and M. Ries-Kautt, *Acta Crystallographica Section D-Biological Crystallography*, 2001, **57**, 929-940.
128. D. J. Haas, *Acta Crystallographica*, 1967, **23**, 666-&.
129. P. L. Howell, S. C. Almo, M. R. Parsons, J. Hajdu and G. A. Petsko, *Acta Crystallographica Section B-Structural Science*, 1992, **48**, 200-207.
130. P. L. Howell, *Acta Crystallographica Section D-Biological Crystallography*, 1995, **51**, 654-662.
131. J. Lescar, H. Souchon and P. M. Alzari, *Protein Science*, 1994, **3**, 788-798.
132. C. Giles, *Wellcome News*, Winter 2011, 30-31.
133. E. Wallin and G. von Heijne, *Protein Science*, 1998, **7**, 1029-1038.
134. <http://www.rcsb.org/pdb/home/home.do>.
135. R. M. Garavito and S. Ferguson-Miller, *Journal of Biological Chemistry*, 2001, **276**, 32403-32406.
136. C. Ostermeier and H. Michel, *Current Opinion in Structural Biology*, 1997, **7**, 697-701.
137. H. Michel, *Trends in Biochemical Sciences*, 1983, **8**, 56-59.
138. S. Newstead, S. Ferrandon and S. Iwata, *Protein Science*, 2008, **17**, 466-472.
139. L. C. Johansson, A. B. Wohri, G. Katona, S. Engstrom and R. Neutze, *Current Opinion in Structural Biology*, 2009, **19**, 372-378.
140. C. Hunte and H. Michel, *Current Opinion in Structural Biology*, 2002, **12**, 503-508.
141. C. Ostermeier, S. Iwata, B. Ludwig and H. Michel, *Nature Structural Biology*, 1995, **2**, 842-846.
142. S. Iwata, C. Ostermeier, B. Ludwig and H. Michel, *Nature*, 1995, **376**, 660-669.
143. D. M. Rosenbaum, V. Cherezov, M. A. Hanson, S. G. F. Rasmussen, F. S. Thian, T. S. Kobilka, H. J. Choi, X. J. Yao, W. I. Weis, R. C. Stevens and B. K. Kobilka, *Science*, 2007, **318**, 1266-1273.
144. E. M. Landau and J. P. Rosenbusch, *Proc. Natl. Acad. Sci. U. S. A.*, 1996, **93**, 14532-14535.
145. P. Wadsten, A. B. Wohri, A. Snijder, G. Katona, A. T. Gardiner, R. J. Cogdell, R. Neutze and S. Engstrom, *Journal of Molecular Biology*, 2006, **364**, 44-53.
146. J. Bender, P. Jarvoll, M. Nyden and S. Engstrom, *Journal of Colloid and Interface Science*, 2008, **317**, 577-584.
147. S. Faham, G. L. Boulting, E. A. Massey, S. Yohannan, D. Yang and J. U. Bowie, *Protein Science*, 2005, **14**, 836-840.
148. S. Faham and J. U. Bowie, *Journal of Molecular Biology*, 2002, **316**, 1-6.
149. L. Czerski and C. R. Sanders, *Analytical Biochemistry*, 2000, **284**, 327-333.
150. M. Caffrey, *Current Opinion in Structural Biology*, 2000, **10**, 486-497.
151. M. Caffrey, *Journal of Structural Biology*, 2003, **142**, 108-132.
152. P. Nollert, H. Qiu, M. Caffrey, J. P. Rosenbusch and E. M. Landau, *Febs Letters*, 2001, **504**, 179-186.
153. E. PebayPeyroula, G. Rummel, J. P. Rosenbusch and E. M. Landau, *Science*, 1997, **277**, 1676-1681.
154. H. Luecke, H. T. Richter and J. K. Lanyi, *Science*, 1998, **280**, 1934-1937.

155. M. Caffrey, in *Annual Review of Biophysics*, Editon edn., 2009, vol. 38, pp. 29-51.
156. V. I. Gordeliy, J. Labahn, R. Moukhametzianov, R. Efremov, J. Granzin, R. Schlesinger, G. Buldt, T. Savopol, A. J. Scheidig, J. P. Klare and M. Engelhard, *Nature*, 2002, **419**, 484-487.
157. V. Cherezov, D. M. Rosenbaum, M. A. Hanson, S. G. F. Rasmussen, F. S. Thian, T. S. Kobilka, H. J. Choi, P. Kuhn, W. I. Weis, B. K. Kobilka and R. C. Stevens, *Science*, 2007, **318**, 1258-1265.
158. V. P. Jaakola, M. T. Griffith, M. A. Hanson, V. Cherezov, E. Y. T. Chien, J. R. Lane, A. P. Ijzerman and R. C. Stevens, *Science*, 2008, **322**, 1211-1217.
159. <http://www.rcsb.org/pdb/explore/explore.do?structureId=4AYX>.
160. <http://www.thesgc.org/structures>.
161. J. Kepler, C. G. Hardie, B. J. Mason and L. L. Whyte, *The Six-cornered Snowflake. [Edited and Translated by Colin Hardie. With Essays by L. L. Whyte and B. J. Mason. With Illustrations.] Lat. & Eng*, Oxford, 1966.
162. P. P. Ewald, *Zeitschrift Fur Kristallographie*, 1921, **56**, 129-156.
163. M. M. Woolfson, *Reports on Progress in Physics*, 1971, **34**, 369-&.
164. A. L. Patterson, *Physical Review*, 1934, **46**, 0372-0376.
165. H. Hauptman, *Angewandte Chemie-International Edition in English*, 1986, **25**, 603-613.
166. E. M. Lambert, C. Viravaidya, M. Li and S. Mann, *Angewandte Chemie-International Edition*, **49**, 4100-4103.
167. K. Bergstrom and K. Holmberg, *Colloids and Surfaces*, 1992, **63**, 273-280.
168. B. D. Kelley, D. I. C. Wang and T. A. Hatton, *Biotechnology and Bioengineering*, 1993, **42**, 1199-1208.
169. M. Adachi, M. Harada, A. Shioi and Y. Sato, *The Journal of Physical Chemistry*, 1991, **95**, 7925-7931.
170. C. Y. Lin and L. W. Chen, *Fuel Processing Technology*, 2006, **87**, 309-317.
171. J. Brunner-Popela and O. Glatter, *Journal of Applied Crystallography*, 1997, **30**, 431-442.
172. L. K. Shrestha, T. Sato and K. Aramaki, *Physical Chemistry Chemical Physics*, 2009, **11**, 4251-4259.
173. T. Y. Teng, *Journal of Applied Crystallography*, 1990, **23**, 387-391.
174. H. Hope, *Annual Review of Biophysics and Biophysical Chemistry*, 1990, **19**, 107-126.
175. <http://www.bruker.com/en/products/x-ray-diffraction-and-elemental-analysis/single-crystal-x-ray-diffraction/sc-xrd-software/overview/sc-xrd-software/proteum2/proteum2-software/space-group-determination-and-data-statistics.html>.
176. S. Kosmella and J. Koetz, *Current Opinion in Colloid & Interface Science*, **17**, 261-265.
177. J. L. Chai, J. Liu and H. L. Li, *Colloid J.*, 2009, **71**, 257-262.
178. X. Q. Li, J. L. Chai, S. C. Shang, H. L. Li, J. J. Lu, B. Yang and Y. T. Wu, *J. Chem. Eng. Data*, **55**, 3224-3228.
179. W. R. Krigbaum and F. R. Kugler, *Biochemistry*, 1970, **9**, 1216-&.
180. *Journal of Molecular Biology*, 1998, **276**, 417-436.
181. S. Datta, B. K. Biswal and M. Vijayan, *Acta Crystallographica Section D-Biological Crystallography*, 2001, **57**, 1614-1620.
182. <http://www.rcsb.org/pdb/explore/materialsAndMethods.do?structureId=1JIS>.
183. G. J. Kleywegt, *Acta Crystallographica Section D*, 2000, **56**, 249-265.
184. F. Frenois, A. R. Baulard and V. Villeret, *Tuberculosis*, 2006, **86**, 110-114.
185. F. Frenois, J. Engohang-Ndong, C. Locht, A. R. Baulard and V. Villeret, *Molecular Cell*, 2004, **16**, 301-307.
186. <http://www.rcsb.org/pdb/explore/explore.do?structureId=1U9N>.

187. <http://www.rcsb.org/pdb/explore/explore.do?structureId=1U9O>.
188. N. C. Silva, B. Sarmiento and M. Pintado, *Int. J. Antimicrob. Agents*, 2013, **41**, 5-10.
189. A. L. Stouffer, R. Acharya, D. Salom, A. S. Levine, L. Di Costanzo, C. S. Soto, V. Tereshko, V. Nanda, S. Stayrook and W. F. DeGrado, *Nature*, 2008, **451**, 596-U513.
190. J. W. Wang, M. Dauter, R. Alkire, A. Joachimiak and Z. Dauter, *Acta Crystallographica Section D-Biological Crystallography*, 2007, **63**, 1254-1268.
191. K. Harata and T. Akiba, *Acta Crystallographica Section D-Biological Crystallography*, 2004, **60**, 630-637.
192. H. Oki, Y. Matsuura, H. Komatsu and A. A. Chernov, *Acta Crystallographica Section D-Biological Crystallography*, 1999, **55**, 114-121.
193. J. Hogle, S. T. Rao, M. Mallikarjunan, C. Beddell, R. K. McMullan and M. Sundaralingam, *Acta Crystallographica Section B-Structural Science*, 1981, **37**, 591-597.
194. [http://www.phenix-online.org/newsletter/CCN\\_2011\\_07.pdf](http://www.phenix-online.org/newsletter/CCN_2011_07.pdf).
195. D. S. Tsekova, *Crystal Growth & Design*, 2009, **9**, 1312-1317.
196. L. Legrand, M. Ries-Kautt and M. C. Robert, *Acta Crystallographica Section D-Biological Crystallography*, 2002, **58**, 1564-1567.
197. L. Legrand, I. Rosenman, F. Boue and M. C. Robert, *Journal of Crystal Growth*, 2001, **232**, 244-249.